The Effective Behavior of Thermoelectric Composites

Yang Yang

A dissertation
submitted in partial fulfillment of the
requirements for the degree of

Doctor of Philosophy

University of Washington

2014

Reading Committee:

Jiangyu Li, Chair

Jihui Yang

Dayong Gao

Mamidala Ramulu

Program Authorized to Offer Degree:
Mechanical Engineering

University of Washington

Abstract

The Effective Behavior of Thermoelectric Composites

Yang Yang

Chair of the Supervisory Committee:
Professor Jiangyu Li
Mechanical Engineering

Thermoelectric materials have attracted significant interests recently for their capability in converting heat directly into electricity and vice versa, and thus promise a wide range of applications. Despite their importance, there have been only very limited theoretical effort towards the analysis and understanding of effective behavior of thermoelectric composites.

In this work, we develop

- a rigorous continuum analysis on both bi-layered and core-shell thermoelectric composites, in which the distribution of temperature, electric potential, and heat flux are solved from the governing equations, and the effective thermoelectric properties defined through an equivalency principle;

- a conversion efficiency analysis of thermoelectric composites, using an idealized thermoelectric module;

- a non-linear asymptotic homogenization theory to understand the effective behavior of both one-dimensional and two-dimensional thermoelectric composites without macroscopic heterogeneity. We establish the unit cell problem, for which, the two-dimensional numerical solution are obtained by a Finite Element method. The non-linearly coupled thermoelectric transport equations are further homogenized, from

which the macroscopic field distributions are derived with local fluctuation averaged out, and overall thermoelectric conversion efficiency is established.

Through analysis, we

- demonstrate that higher figure of merit of thermoelectric composite than any of its constituents is indeed possible, excluding size and interfacial effects;

- find out that the thermoelectric conversion efficiency of a composite can be enhanced by its constituents, with the mechanism responsible for the enhancement identified, and the upper bound established;

- discover that the thermoelectric field distributions in the composite are different from those in a homogeneous material, and they are difficult to be fitted by homogeneous solution.

We conclude that thermoelectric conversion efficiency of a composite is not bounded, and can be higher than all its constituents in the absence of size and interface effects. Furthermore, it is noted the effective properties defined by a set of equivalency principle depend on specific boundary conditions, resulting in effective figure of merit that is not correlated with thermoelectric conversion efficiency directly. The analysis thus points toward a new route for developing high-performance thermoelectric materials, and provides considerable insight into the effective behavior of thermoelectric composites in terms of both design and optimization.

TABLE OF CONTENTS

Page

LIST OF FIGURES

LIST OF TABLES

ACKNOWLEDGMENTS

I am deeply thankful to my advisor, Professor Jiangyu Li, for teaching me how to do research, and for all the support and encouragement. I thank other members of my Supervisory Committee, Professor Jihui Yang, Professor Dayong Gao, Professor Ramulu Mamidala for their help and guidance. I also want to thank all my lab-mates, Dr. Liangjun Li, Dr. Yuanming Liu, Dr. Shuhong Xie, Dr. Yunya Liu, Chi Hou Lei, Feiyue Ma, Nataly Chen, Peiqi Wang, Ahmad Eshghinejad, Yun Ou, Kai Pan, Liqian Cheng, for the time spent together.

I especially want to thank my wife Chang Chen and my parents for their unremitting support and love. I thank Cameron for being such a great son.

Chapter 1

INTRODUCTION AND OVERVIEW

1.1 Thermoelectrics

1.1.1 Phenomena

Thermoelectric materials have attracted significant interests in recent years due to their capability to convert heat directly into electricity and vice versa[1]. Back in early 1800s, physicist Thomas Johann Seebeck discovered that if two dissimilar materials are joined together and the junctions are held at different temperatures, a voltage difference proportional to the temperature difference will develop, making it possible to convert heat directly into electricity, a phenomenon known as the Seebeck effect. The proportional constant is called Seebeck coefficient α. Alternatively, if an electric current is passed through the material, heat will be absorbed at one end and released at the other; this is known as the Peltier effect. The thermoelectric conversion efficiency is governed by the figure of merit ZT of materials[2], which is intimately related to electric and thermal transport properties of thermoelectric materials[3],

$$ZT = \frac{\alpha^2 \sigma T}{\kappa}, \tag{1.1}$$

where σ, and κ are electric and thermal conductivities, and T is the temperature.

1.1.2 Applications

Because of the phenomena, thermoelectric materials are promising in a wide range of energy and environmental applications in waste heat recovery[4,5], solid state cooling and thermal management[6], solar energy harvesting[7–9], and carbon reduction[10], among others. As seen in Fig. 1.1a, for a vehicle powered by a typical gasoline-fueled internal combustion engine, vast majority of the fuel energy is lost as waste heat - only 25% of the fuel energy is used for vehicle mobility and accessory power. These waste heat can potentially be recovered

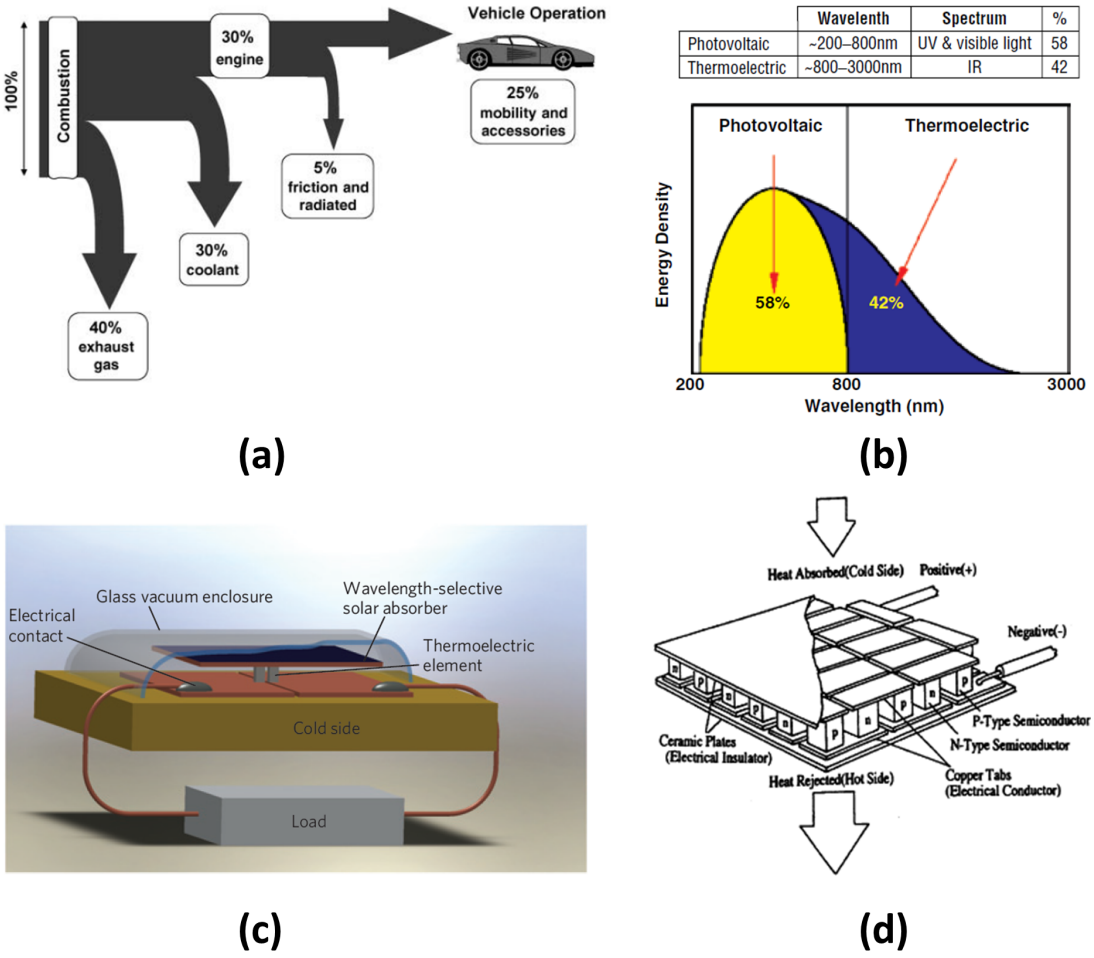

Figure 1.1: Example applications of thermoelectric materials. (a) Typical energy path in gasoline-fueled internal-combustion engine vehicles[4]. (b) Sun radiates energy with part of the energy in the ultraviolet spectrum and part in the infrared spectrum[3]. (c) Illustration of a solar thermoelectric generator made of thermoelectric elements[7]. (d) Schematic description of a single-stage Peltier module[11].

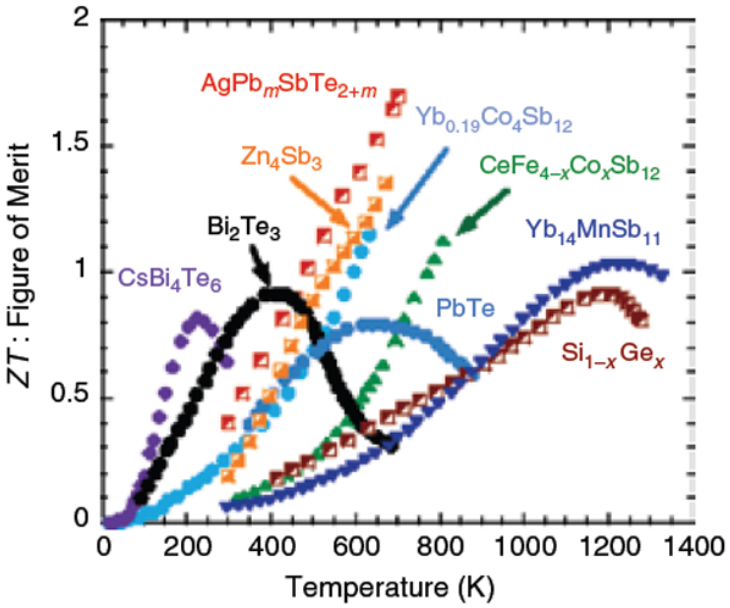

Figure 1.2: Figure of merit as a function of temperature for several high-efficiency bulk thermoelectric materials[3].

using thermoelectric energy conversion. Furthermore, in current solar energy harvesting, photovoltaic solar cells use ultraviolet and visible sun lights that account for 58% of energy radiated from sun, and the infrared spectrum, about 42% of total solar energy, is lost as heat, as shown in Fig. 1.1b, which can be potentially recovered by thermoelectrical materials, see 1.1c. In addition to energy harvesting, thermoelectric materials can also be used for solid-state cooling and thermal management based on the Peltier effect, see 1.1d. As a solid-state technology, thermoelectric energy conversion does not involve moving part, and thus is compact, quiet, more reliable, and environmentally friendly.

1.1.3 Materials

In the past decade, there are mainly two strategies in developing high performance thermoelectric materials, including (1) searching for bulk materials with intrinsically high figure of merit and conversion efficiency, see Fig. 1.2; and (2) engineering hybrid composite materials to enhance and optimize their conversion efficiency. From Eq. (1.1), in order to

have high ZT and thus high conversion efficiency, the thermoelectric material needs to have not only high Seebeck coefficient, but also high electric conductivity and low thermal conductivity. This turns out to be rather difficult, since all these properties are intimately related to each other, making it hard to control them individually in a single-phase material[12–16]. For example, while high electric conductivity requires high concentration of charge carriers, a modest carrier concentration is optimal for high Seebeck coefficient[17]. Furthermore, high electric conductivity is usually accompanied by high thermal conductivity because of Wiedemann-Franz Law[18]. Hybrid materials, especially nanostructured materials, are very attractive for thermoelectric energy conversion[19–31]. By combining different materials together, it is possible to overcome the intrinsic constraints between electric conductivity, thermal conductivity, and Seebeck coefficient in a single-phase material through microstructure engineering and optimization, and thus achieve high electric conductivity, Seebeck coefficient, and low thermal conductivity simultaneously. For example, a large enhancement in thermoelectric power was observed in nanocomposites consisting of bismuth nanowires embedded in porous alumina and porous silica[32], and a ZT value as high as 1.6 has been reported in $K_{1-x}Pb_{m+\delta}Sb_{1+\gamma}Te_{m+2}$ system containing nanoinlcusions, which possesses simultaneously low thermal conductivity and high electrical conductivity[33]. Other high thermoelectric figure of merit heterogeneous systems include La-doped n-type $PbTe - Ag_2Te$ nanocomposites with large nanometer-scale precipitates[34], melt spun $Bi_{0.52}Sb_{1.48}Te_3$ bulk materials with nanocrystals embedded inside the amorphous matrix[35,36], and nanostructured $Ag0.8Pb_{m+x}SbTe_{m+2}$[37], among others.

1.2 Motivation and objectives

While vast amount of experimental works in thermoelectric materials focus on nanostructured composites[38–50], there have been only very limited theoretical efforts toward the analysis and understanding of the effective behavior of heterogeneous thermoelectric materials[51–53], despite their importance. Instead, most previous theoretical studies focused on size and interfacial effects at nanoscale using molecular dynamics and quantum mechanics[54–62]. This motivates us to examine whether the effective thermoelectric figure of merit of a heterogeneous composite can be higher than all its constituents, excluding the effects

of size and interface. If the answer is yes, it will offer us a new route for high figure of merit thermoelectric materials, while the current state of art focuses on nanocomposites that utilize quantum effects at nanoscale and phonon scattering at interfaces, which are much more difficult to process and control than regular composites. The question has actually been visited by a number of investigators before. In 1991, it was claimed that the effective figure of merit of a composite can never exceed the largest figure of merit in any of its component, in the absence of size and interfacial effects[63,64]. This conclusion was drawn from a variational principle similar to Hashin-Strikman bound in elasticity[65]. However, for thermoelectric materials, temperature, which is not uniform in general and varies from point to point, enters into constitutive equations as a coefficient, and thus should not be treated as material constants. Furthermore, heat flux is often assumed to be divergence free[66], and under such assumption, temperature distribution satisfies Laplace equation, as in a regular heat transfer problem uncoupled from electric current. For thermoelectric materials, especially those with high figure of merit, this is also not true.

Because of these difficulties, very few works on the homogenization of thermoelectric composites exist in literature, far less than elastic composites, despite their obvious technological importance in energy harvesting and solid state cooling. We seek to address these issues in this dissertation, by rigorously studying the thermoelectric fields and analyzing the effective thermoelectric properties of heterogeneous medium.

1.3 Organization of the dissertation

This dissertation is organized as follows. In Chapter 2, the definition of thermoelectric effect is introduced and the governing equations deduced from the theory of thermodynamics, laying the foundation for the ensuing chapters. Chapters 3 and 4 study the effective behavior of one-dimensional (1D) bilayered thermoelectric medium, from both thermoelectric figure of merit and conversion efficiency points of view. Core-shell composites are discussed in Chapter 5 as an extension from 1D layered results. For the analysis of composite with macroscopic homogeneity, an asymptotic homogenization method is developed for 1D composite in Chapter 6, and for 2D composite in Chapters 7 and 8, where we first establish the unit cell problem in Chapter 7, and then solve it numerically in Chapter 8. Chapter

9 summaries the main conclusions of the dissertation, and discusses some future work that they could lead to.

Chapter 2

GOVERNING EQUATIONS OF THERMOELECTRICITY

2.1 Thermoelectric effect

Thermoelectric effect is used broadly to refer to the effect of direct conversion of temperature difference to electric voltage, or vice versa. It consists three individually identified yet interrelated effects: Seebeck effect, Peltier effect, and Thomson effect.

2.1.1 Seebeck effect

The Seebeck effect was first discovered (1821) by physicist Thomas Johann Seebeck, who found that a voltage existed between two ends of a metal bar when a temperature gradient existed in the bar, see Fig. 2.1. Perhaps more commonly used for the discussion of Seebeck effect is the model as schematically shown in Fig. 2.2, where two different materials A and B are connected with the junctions subjected to hot and cold temperatures T_h and T_c, and it is found that

$$\Delta V = (\alpha_B - \alpha_A)(T_h - T_c), \tag{2.1}$$

where ΔV is the electric voltage developed, $(\alpha_B - \alpha_A)$ can be regarded as the Seebeck coefficient for the device, of which materials A and B are part of, with their individual Seebeck coefficients α_A and α_B. The subscriptions A and B are to denote the properties pertaining to materials A and B. For the presentation of Seebeck effect for individual material, the counterpart is

$$\Delta V = -\alpha \Delta T. \tag{2.2}$$

The sign convention of ΔV in Eq. 2.1 is set as such that positive value voltage drives the current from A to B at hot end, so that we get consistency in Eqs. 2.1 and 2.2. The physical implication of Seebeck effect is that temperature gradient drives free charge carriers to flow

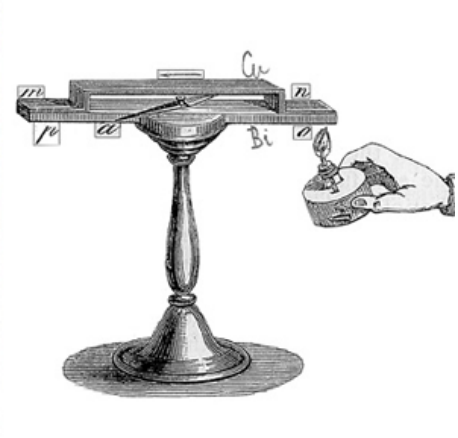

Figure 2.1: The discovery of Seebeck effect [67].

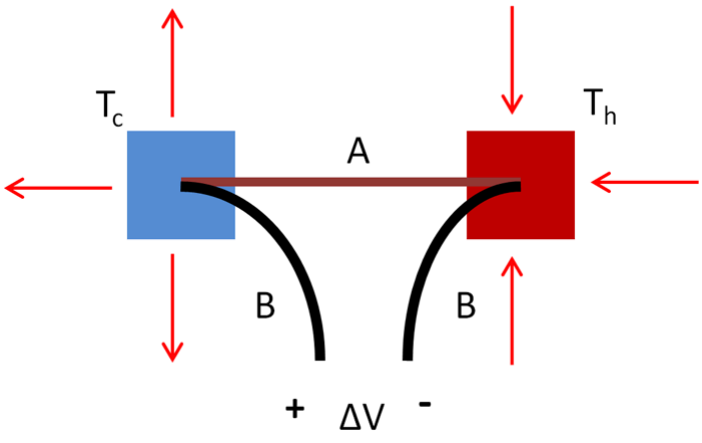

Figure 2.2: Schematics of thermoelectric module with voltage developed by the Seebeck effect.

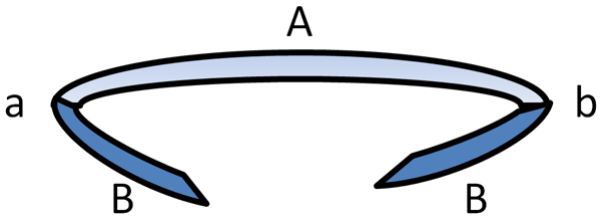

Figure 2.3: Schematics of the Peltier effect.

from high temperature to low temperature, accumulating opposite charges which result in electric field that penalizes further charge carriers migration until equilibrium is reached. So depending on the nature of the charge carrier, electron or hole, the sign of the Seebeck coefficient can be negative or positive.

2.1.2 Peltier effect

In 1834, French physicist Jean Charles Athanase Peltier found that the junctions of dissimilar metals were heated or cooled, depending upon the direction in which an electrical current passed through them, see Fig. 2.3. Heat generated by current flowing in one direction was absorbed if the current was reversed. The Peltier coefficient is defined by

$$\dot{Q} = \Pi_{AB} I = (\Pi_B - \Pi_A) I, \tag{2.3}$$

where I is electric current, $\dot{Q}$ is the rate of heat generated or absorbed. Π_{AB} is the Peltier coefficient for the device, and Π_A, Π_B are values for the individual materials A and B. For the configuration shown in Fig. 2.3, the sign convention stipulates positive Π_{AB} if a is heated and b is cooled with clockwise flowing current I.

2.1.3 Thomson effect

The Thomson effect, predicted and subsequently observed by Lord Kelvin, describes the heating or cooling of a current-carrying conductor with a temperature gradient. Any current-carrying conductor (except for a superconductor) with a temperature difference between two points either absorbs or emits heat, depending on the material. The heat

production q per unit volume is

$$q = \rho J^2 - \mu J \frac{dT}{dx}, \tag{2.4}$$

where J is current density, ρ is the electric resistivity, μ is the Thomson coefficient, $\frac{dT}{dx}$ is the temperature gradient along the wire. It can be recognized that the first term on the right hand side is the Joule heating, and it is irreversible independent of the direction of current density, whereas for Thomson part, which is the second term, trend can be switched from heat absorbtion to generation, or vice versa, by reversing the direction of current density.

Seebeck coefficient, Peltier coefficient and Thomson coefficient are not independent, rather, they are interrelated by the following relations.

$$\mu = T \frac{d\alpha}{dT}, \tag{2.5}$$

$$\Pi = \alpha T, \tag{2.6}$$

which are called the first and second Thomson relations, respectively.

2.2 Thermodynamic considerations and thermoelectric governing equations

The continuum theory of thermoelectrics can be traced back to thermodynamics, where the fundamental relation defines S, the entropy of a system, in terms of its extensive parameters internal energy U, volume V, and the mole numbers of the chemical components N_i,

$$S = S(U, V, N_i). \tag{2.7}$$

We restrict ourself to volume preserving processes, and consider electron as the only type of charge carrier, so that the fundamental relation can be recast as

$$s = s(u, n), \tag{2.8}$$

where s, u, and n are entropy, energy, and mole number of electrons per unit volume. By differentiating this specific fundamental relation, we derive

$$ds = \frac{1}{T} du - \frac{\mu}{T} dn, \tag{2.9}$$

where T is the absolute temperature, and μ is the electrochemical potential of electrons. We are particularly interested in the flows of energy and electrons, for which the rate of entropy production is evaluated as

$$\dot{s} = \nabla\frac{1}{T}\cdot\mathbf{J}_U - \nabla\frac{\mu}{T}\cdot\mathbf{J}_N, \tag{2.10}$$

where $\mathbf{J}_U$ and $\mathbf{J}_N$ are the fluxes of energy and electrons, respectively, while $\nabla\frac{1}{T}$ and $-\nabla\frac{\mu}{T}$ are corresponding affinities that drive such flows. For the Markoffian system[68] where the fluxes depend only on the instantaneous affinities, it was proposed that

$$-\mathbf{J}_N = L'_{11}\nabla\frac{\mu}{T} + L'_{12}\nabla\frac{1}{T}, \tag{2.11}$$

$$\mathbf{J}_U = L'_{12}\nabla\frac{\mu}{T} + L'_{22}\nabla\frac{1}{T}, \tag{2.12}$$

where isotropic symmetry is assumed for simplicity, and L'_{ij} are transport coefficients with $L'_{ij} = L'_{ji}$ due to the Onsager theorem[68]. This set of equation is equivalent to Eq. (2.17) in[69], and it is evident that fluxes of energy and electrons are coupled by L'_{12}.

For the system we are considering, the energy is transported through both heat and electrochemical potential, and thus

$$\mathbf{J}_U = \mathbf{J}_Q + \mu\mathbf{J}_N, \tag{2.13}$$

where $\mathbf{J}_Q$ is the heat flux. This can be used to rewrite the transport equations as

$$-\mathbf{J}_N = L_{11}\frac{1}{T}\nabla\mu + L_{12}\nabla\frac{1}{T}, \tag{2.14}$$

$$\mathbf{J}_Q = L_{12}\frac{1}{T}\nabla\mu + L_{22}\nabla\frac{1}{T}, \tag{2.15}$$

with

$$L_{11} = L'_{11}, \quad L_{12} = \mu L'_{11} + L'_{12}, \quad L_{22} = \mu^2 L'_{11} + 2\mu L'_{12} + L'_{22}.$$

Assume that the chemical potential of electrons is independent of temperature such that

$$\mu = e\phi, \tag{2.16}$$

where e is the charge of electron and ϕ is the electric potential, and notice that the electric current density $\mathbf{J}$ is related to electron flux $\mathbf{J}_N$ as

$$\mathbf{J} = e\mathbf{J}_N, \tag{2.17}$$

we derive the coupled transport equations for electric current density and heat flux

$$\begin{aligned} \mathbf{J} &= -\frac{e^2 L_{11}}{T}\nabla\phi + \frac{eL_{12}}{T^2}\nabla T, \\ \mathbf{J}_Q &= \frac{eL_{12}}{T}\nabla\phi - \frac{L_{22}}{T^2}\nabla T. \end{aligned} \tag{2.18}$$

These allow us to establish connections between transport coefficients L_{ij} with more familiar thermoelectric properties, including electric conductivity σ, Seebeck coefficient, α, and thermal conductivity κ[70]. In particular, notice that electric conductivity is measured under isothermal condition, such that

$$\sigma \equiv -\frac{J|_{\nabla T=0}}{\nabla\phi} = \frac{e^2 L_{11}}{T}. \tag{2.19}$$

Similarly, thermal conductivity is measured under open-circuit condition, resulting in

$$\kappa \equiv -\frac{J_Q|_{J=0}}{\nabla T} = \frac{L_{11}L_{22} - L_{12}^2}{T^2 L_{11}}. \tag{2.20}$$

Furthermore, Seebeck coefficient is measured as electric field induced by unit temperature gradient, under open-circuit condition, leading to

$$\alpha \equiv -\frac{\nabla\phi|_{J=0}}{\nabla T} = -\frac{L_{12}}{eTL_{11}}. \tag{2.21}$$

The thermoelectric transport equations can then be recast into more familiar form as

$$-\mathbf{J} = \sigma\nabla\phi + \sigma\alpha\nabla T, \tag{2.22}$$

$$\mathbf{J}_Q = -T\alpha\sigma\nabla\phi - (T\alpha^2\sigma + \kappa)\nabla T = T\alpha\mathbf{J} - \kappa\nabla T. \tag{2.23}$$

which are nonlinearly coupled. In the absence of thermoelectric effect where $\alpha = 0$, the uncoupled transport equations of electricity and heat are recovered.

It is also evident from energy transport that

$$\mathbf{J}_U = \mathbf{J}_Q + \phi\mathbf{J}. \tag{2.24}$$

For a system wherein both charges and energy are conserved, current density and energy flux are divergence-free,

$$\nabla\cdot\mathbf{J} = 0, \tag{2.25}$$

$$\nabla\cdot\mathbf{J}_U = 0, \tag{2.26}$$

while the heat flux is no longer divergence-free in general,

$$\nabla \cdot \mathbf{J}_Q = -\nabla \cdot (\phi \mathbf{J}) = -\nabla \phi \cdot \mathbf{J}, \tag{2.27}$$

where Joule heat serves as heat source. This is in contrast to a normal heat transfer problem uncoupled from electric conduction.

It is worth comparing the various forms of constitutive equations, (2.11-2.12), (2.14-2.15), and (2.22-2.23). The first two sets of equations, (2.11-2.12) and (2.14-2.15) appear to be linear, if the involved kinetic coefficients L'_{ij} and L_{ij} can be viewed as constants independent of temperature and electrochemical potential; these would make homogenization straightforward. However, under irreversible thermodynamics, these kinetic coefficients are generally functions of local intensive parameters[68], and thus cannot be viewed as constants, making the governing equation intrinsically nonlinear. Indeed these can be better appreciated from Eq. (2.19). If L_{11} would be a constant independent of temperature, then the electric conductivity would vary inversely with respect to temperature. For semiconductors that good thermoelectrics belong to, it is well known that the intrinsic electric conductivity generally increases with respect to temperature. In fact, electric conductivity, thermal conductivity, and Seebeck coefficient all have complicated variation with respect to temperature, and thus thermoelectric transport equations have to be regarded as nonlinear.

Chapter 3

EFFECTIVE THERMOELECTRIC PROPERTIES OF BI-LAYERED COMPOSITES

3.1 Introductory remarks

To investigate whether a thermoelectric composite can have a higher figure of merit than any of its constituents, excluding size and interfacial effects, we consider a one-dimensional (1D) bi-layered thermoelectric medium in this chapter. We assume all the material properties and field variables are only dependent on spatial coordinate x, and independent of y and z. Since the current density is divergence-free, its magnitude J turns out to be a constant in such a 1D configuration,

$$J = |\mathbf{J}| = const, \tag{3.1}$$

which simplifies the governing equation of thermoelectricity considerably, making analytic solutions possible.

In the following sections, we first solve the fields from governing equations for both homogeneous and layered heterogeneous medium. Through equivalency principle, we define effective thermoelectric properties for bi-layered composites in Section 3. Numerical results and discussions are presented in Section 4. In Section 5, the summary for this chapter is provided.

3.2 Field analysis

3.2.1 Analysis of a homogeneous thermoelectric

We first consider a homogeneous material with uniform distribution of material properties, as shown in Fig. 3.1a, and subjected to specified temperatures and electric potentials of (T_0, ϕ_0) and (T_1, ϕ_1) at both ends. All the material properties are assumed to be independent of temperature, and thus Thomson effect is ignored[68]. This allows us to simplify the field

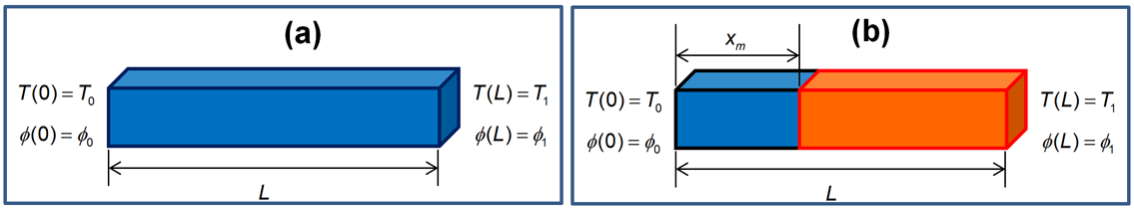

Figure 3.1: Schematics of layered thermoelectric medium; (a) homogeneous thermoelectric; (b) layered heterogeneous thermoelectric[71].

equations governing temperature and electric potential distributions, i.e., Eqs. 2.22∼2.26, as follows,

$$\frac{d^2T}{dx^2} = -\frac{J^2}{\sigma\kappa}, \tag{3.2}$$

$$\frac{d^2\phi}{dx^2} = \alpha\frac{J^2}{\sigma\kappa}. \tag{3.3}$$

Eq. 3.2 can be solved for temperature distribution as

$$T = -\frac{J^2}{2\sigma\kappa}x^2 + c_1x + c_2, \tag{3.4}$$

with integration constants determined from boundary conditions as

$$c_1 = (T_1 - T_0) + \frac{J^2}{2\sigma\kappa}, \qquad c_2 = T_0, \tag{3.5}$$

where all the dimensions are normalized with respect to L, the length of the thermoelectric medium.

To solve for the yet to be determined current density J, we notice from Eq. (2.22) that the distribution of electric potential is govern by

$$\frac{d\phi}{dx} = \frac{\alpha J^2}{\sigma\kappa}x - \frac{\alpha J^2}{2\sigma\kappa} - \frac{J}{\sigma} - (T_1 - T_0)\alpha, \tag{3.6}$$

so that

$$\phi = \frac{\alpha J^2}{2\sigma\kappa}x^2 - [\frac{\alpha J^2}{2\sigma\kappa} + \frac{J}{\sigma} + (T_1 - T_0)\alpha]x + c_3, \tag{3.7}$$

which allows us to solve c_3 and current density from electric boundary conditions as

$$c_3 = \phi_0, \tag{3.8}$$

and

$$J = \sigma\alpha(T_0 - T_1) + \sigma(\phi_0 - \phi_1). \tag{3.9}$$

The heat flux J_Q can then be calculated using Eq. (2.23). This completely solves the distribution of electric potential and temperature in a homogeneous thermoelectric.

3.2.2 Analysis of a bi-layered thermoelectric

We then consider a layered heterogeneous medium consisting of two homogeneous thermoelectric phases A and B, as shown in Fig. 3.1b, and subjected to specified temperatures and electric potentials of (T_0, ϕ_0) and (T_1, ϕ_1) at both ends, identical to those of homogeneous medium considered in the last subsection. Since the layered medium are pieces-wise uniform, equation (3.4) is still applicable to individual segments, with

$$T = \begin{cases} -\frac{J^2}{2\sigma_A\kappa_A}x^2 + a_A x + b_A, & 0 \le x < f, \\ -\frac{J^2}{2\sigma_B\kappa_B}x^2 + a_B x + b_B, & f < x \le 1, \end{cases} \tag{3.10}$$

where $f = x_m/L$ is the volume fraction of phase A. Assume both temperature and electric potential are continuous at interface, $x = f$, and notice that energy flux is a constant, so that the heat flux is also continuous at the interface. Combining these two continuity conditions with two boundary conditions, we derive the following equation that can be solved for the integration constants,

$$\begin{bmatrix} 0 & 1 & 0 & 0 \\ 0 & 0 & 1 & 1 \\ f & 1 & -f & -1 \\ J(\alpha_A - \alpha_B)f - \kappa_A & J(\alpha_A - \alpha_B) & \kappa_B & 0 \end{bmatrix} \begin{bmatrix} a_A \\ b_A \\ a_B \\ b_B \end{bmatrix} = \begin{bmatrix} T_0 \\ T_1 + \frac{J^2}{2\sigma_B\kappa_B} \\ -\frac{J^2}{2\sigma_B\kappa_B}f^2 + \frac{J^2}{2\sigma_A\kappa_A}f^2 \\ \frac{(\alpha_A-\alpha_B)J^3f^2}{2\sigma_A\kappa_A} + \frac{(\sigma_A-\sigma_B)J^2f}{\sigma_A\sigma_B} \end{bmatrix} \tag{3.11}$$

and the results are

$$\begin{aligned}
a_A &= \frac{J^2 f}{2\sigma_A\kappa_A} + \frac{J^2(1-f)}{2\sigma_A\sigma_B}\frac{\sigma_A(1-f)+\sigma_B f}{\Lambda} - \frac{J(1-f)(\alpha_B-\alpha_A)T_0 - \kappa_B(T_1-T_0)}{\Lambda},\\
b_A &= T_0,\\
a_B &= \frac{J^2(1+f)}{2\sigma_B\kappa_B} - \frac{J^2 f}{2\sigma_A\sigma_B}\frac{\sigma_A(1-f)+\sigma_B f}{\Lambda} + \frac{Jf(\alpha_B-\alpha_A)T_1 + \kappa_A(T_1-T_0)}{\Lambda},\\
b_B &= -\frac{J^2 f}{2\sigma_B\kappa_B} + \frac{J^2 f}{2\sigma_A\sigma_B}\frac{\sigma_A(1-f)+\sigma_B f}{\Lambda}\\
&+ \frac{T_1[\kappa_A(1-f)+\kappa_B f - Jf^2(\alpha_B-\alpha_A)] - \kappa_A(T_1-T_0)}{\Lambda},\\
\Lambda &= \kappa_A(1-f)+\kappa_B f + J(\alpha_B-\alpha_A)(1-f)f. \qquad (3.12)
\end{aligned}$$

In a similar manner, the electric potential can be solved from Eq. (3.7) as

$$\phi = \begin{cases} \frac{\alpha_A J^2}{2\sigma_A\kappa_A}x^2 - (\frac{J}{\sigma_A} + \alpha_A a_A)x + c_A, & 0 \le x < f,\\ \frac{\alpha_B J^2}{2\sigma_B\kappa_B}x^2 - (\frac{J}{\sigma_B} + \alpha_B a_B)x + c_B, & f < x \le 1, \end{cases} \qquad (3.13)$$

with the integration constants c_A and c_B determined from the boundary conditions as

$$c_A = \phi_0, \qquad (3.14)$$

$$c_B = \phi_1 + \frac{J}{\sigma_B} + \alpha_B a_B - \frac{\alpha_B J^2}{2\sigma_B\kappa_B}. \qquad (3.15)$$

From the continuity of electric potential at the interface, the current density can then be solved as

$$J = -\frac{1}{(\alpha_B-\alpha_A)f(1-f)(\sigma_A(1-f)+\sigma_B f)}(\Psi_1 + \Psi_3 - \sqrt{\Psi_4}), \qquad (3.16)$$

with

$$\begin{aligned}
\Psi_1 &= [\sigma_A(1-f)+\sigma_B f][\kappa_A(1-f)+\kappa_B f],\\
\Psi_2 &= (\alpha_B-\alpha_A)f(1-f)\sigma_A\sigma_B,\\
\Psi_3 &= \Psi_2(\phi_1-\phi_0+\alpha_B T_1 - \alpha_A T_0),\\
\Psi_4 &= -2\Psi_2\{\Psi_1(\phi_1-\phi_0) + [\sigma_A(1-f)+\sigma_B f][\kappa_A\alpha_B(1-f)+\kappa_B\alpha_A f](T_1-T_0)\}\\
&\quad + (\Psi_1+\Psi_3)^2.
\end{aligned}$$

The heat flux J_Q can then be calculated by using equation (2.23). This completely solves the distribution of electric potential and temperature in a layered heterogeneous thermoelectric.

3.3 Equivalency principle and effective properties

To describe the effective behavior of a heterogeneous thermoelectric, we define its effective thermoelectric properties through the following equivalency principle[71] - given identical boundary conditions of temperature and electric potential, a heterogeneous thermoelectric with a set of effective thermoelectric properties should have identical current density and energy flux as a homogeneous thermoelectric with the same set of properties. With such equivalency, it is clear that the heterogeneous and homogeneous thermoelectrics can be exchanged under the specified boundary conditions. We examine the effective electric conductivity first. Consider a boundary condition of imposed electric potential difference only with $\Delta T = 0$, and compare the current density between homogeneous thermoelectric and layered medium, we conclude that the effective electric conductivity of the layered composite is given by

$$\sigma^*(\Delta\phi, \Delta T = 0) = \frac{J}{\phi_0 - \phi_1} = -\frac{J}{\Delta\phi}, \tag{3.17}$$

with the current density given by equation (3.16). Expanding current density J into Taylor series of $(\alpha_B - \alpha_A)$, we derive the effective conductivity of the layered thermoelectric to the first order of $(\alpha_B - \alpha_A)$,

$$\sigma^*(\Delta\phi) = \frac{\sigma_A\sigma_B}{\sigma_A(1-f)+\sigma_B f} - \frac{f(1-f)\sigma_A^2\sigma_B^2\Delta\phi(\alpha_B-\alpha_A)}{2(\sigma_A(1-f)+\sigma_B f)^2(\kappa_A(1-f)+\kappa_B f)}, \tag{3.18}$$

which clearly depends on the boundary condition in addition to the material constants of the constituents and the volume fraction, a characteristic distinct from linear medium. On the other hand, if we impose open-circuit boundary condition such that $J = 0$, then the effective Seebeck coefficient can be derived as

$$\alpha^* = \frac{\kappa_A(1-f)\alpha_B + \kappa_B f\alpha_A}{\kappa_A(1-f)+\kappa_B f}, \tag{3.19}$$

while the effective thermal conductivity can be derived as

$$\kappa^* = -\frac{J_Q}{T_1 - T_0} = \frac{\kappa_A\kappa_B}{\kappa_A(1-f)+\kappa_B f}. \tag{3.20}$$

Although they do not appear to be dependent on the boundary condition explicitly, open-circuit boundary condition is implied implicitly. From the effective thermoelectric proper-

ties, the effective thermoelectric figure of merit is then defined as

$$Z^* = \frac{\sigma^* \alpha^{*2}}{\kappa^*}, \tag{3.21}$$

and we are interested in whether Z^* of the heterogeneous thermoelectric can be higher than both its constituents.

Table 3.1: Thermoelectric properties of Bi_2Te_3 [72] and $Ag(Pb_{1-y}Sn_y)_mSbTe_{2+m}$ [73].

Material	α ($\times 10^{-6}$V/K)	σ ($\times 10^3$S/m)	κ (W/m/K))
Bi_2Te_3	200	110	1.6
$Ag(Pb_{1-y}Sn_y)_mSbTe_{2+m}$	270	22	0.77

3.4 Numerical results and discussions

3.4.1 Homogeneous thermoelectric

We first consider a homogeneous thermoelectric Bi_2Te_3 of $L = 0.01$m, with its thermoelectric properties listed in Table 3.1. Consider first that only a temperature difference is imposed, with $T_0 = 300$K at cold end and three different temperatures of $T_1 = 800,\ 1000,\ 1500$K at hot end. The distribution of temperature, electric potential, and heat flux are shown in Fig. 3.2, where it is observed that the nonlinearity in temperature distribution is small for small and modest temperature difference, but becomes significant under relatively large temperature difference. For $T_1 = 1500$K, the maximum temperature occurs inside the medium, not at the end, due to Joule heating. Associated with such nonlinear distribution of temperature, substantial variation in heat flux is also observed under large temperature difference, though such variation decreases significantly when temperature difference is reduced. Regardless of the temperature difference, the distribution of electric potential is highly nonlinear, despite that both ends are imposed with same potential, resulting in an current density of $J = -1.1,\ -1.54,\ -2.64 \times 10^6 \mathrm{Am}^{-2}$, respectively. On the other hand,

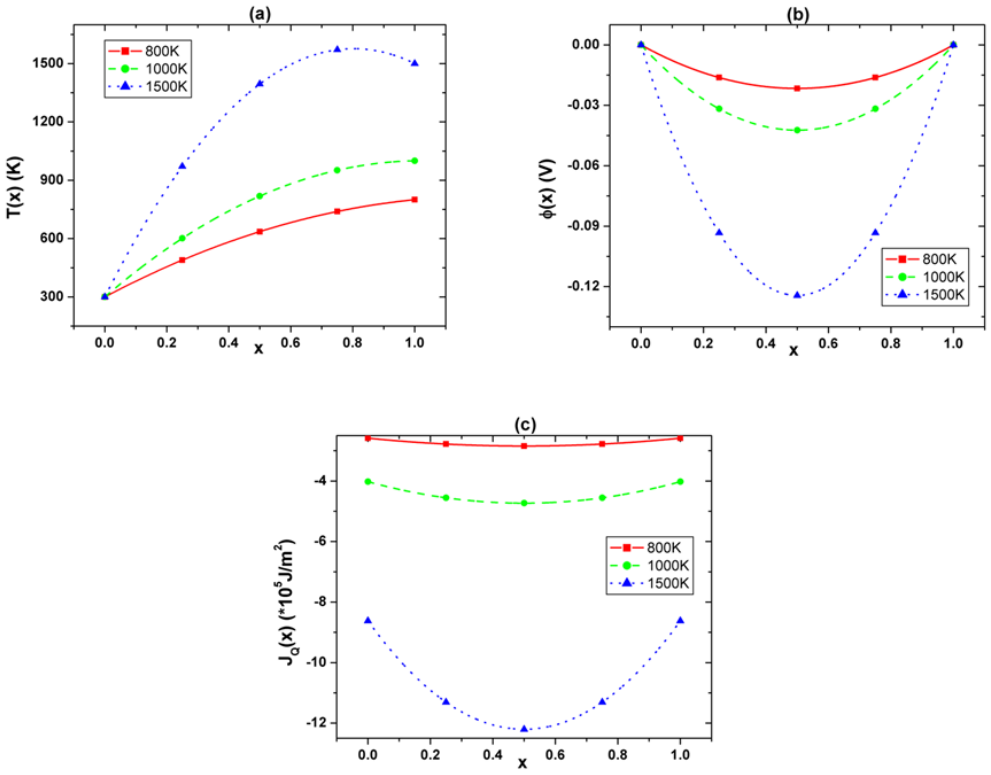

Figure 3.2: The distributions of temperature, electric potential, and heat flux in a homogeneous thermoelectric under an imposed temperature difference[71].

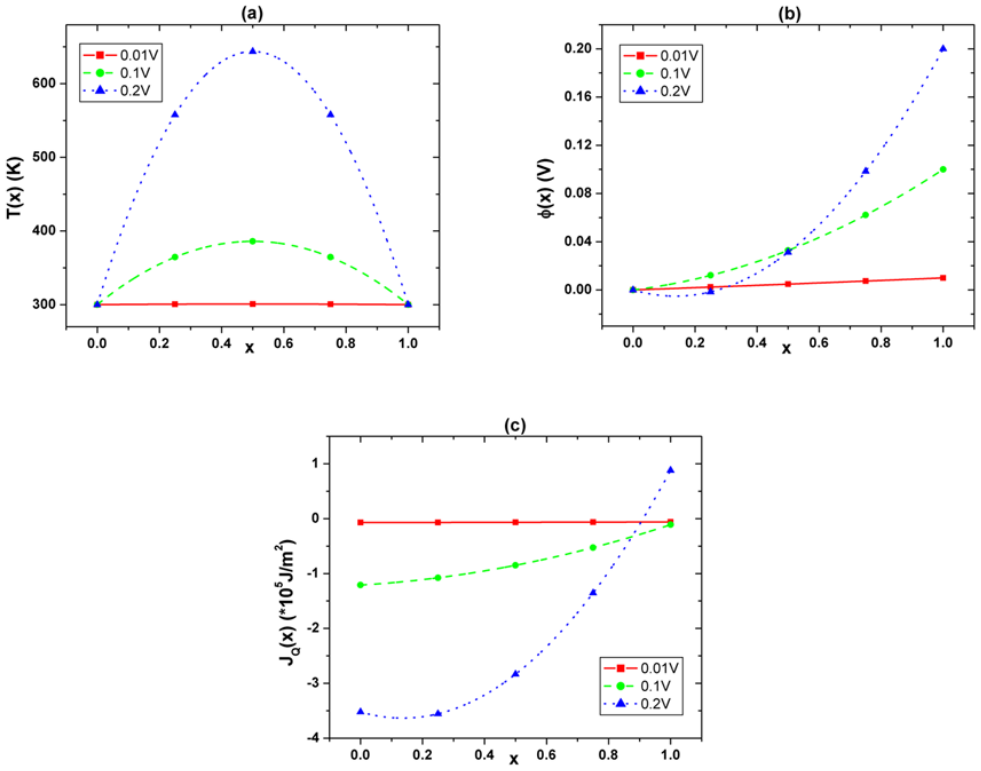

Figure 3.3: The distributions of temperature, electric potential, and heat flux in a homogeneous thermoelectric under an imposed electric potential difference[71].

if only an electric potential difference is imposed with $\phi_0 = 0$ and $\phi_1 = 0.01,\ 0.1,\ 0.2$V, the corresponding results are shown in Fig. 3.3. It is observed that the nonlinearity in the distribution of electric potential becomes substantial under a relatively large potential difference, while the temperature distribution is highly nonlinear regardless of potential difference. Large variation in heat flux is also observed when the potential difference is large, and substantial temperature increase is observed inside the medium. These results suggest that neither temperature nor electric potential of thermoelectric materials satisfies Laplace equation, and the deviation is particularly large under large temperature or potential difference.

3.4.2 Layered thermoelectric

We then consider a layered thermoelectric consisting of Bi_2Te_3 as phase A and $Ag(Pb_{1-y}Sn_y)_m SbTe_{2+m}$ as phase B, with their thermoelectric properties listed in Table 3.1. Notice that both phases have excellent Seebeck coefficient that are comparable to each other, yet Bi_2Te_3 has relatively high thermal conductivity, while $Ag(Pb_{1-y}Sn_y)_mSbTe_{2+m}$ has relatively low electric conductivity, not desirable for high thermoelectric conversion efficiency. We consider the distribution of temperature, electric potential, and heat flux in the layered thermoelectric first, with either temperature difference or electric potential difference imposed, identical to those considered in the last subsection. The volume fraction of Bi_2Te_3 is taken to be $f = 0.42$, and the length remains to be 0.01m. The corresponding results are shown in Figs. 3.4 and 3.5, respectively. The qualitative trends are similar to those observed in homogeneous Bi_2Te_3 under imposed temperature difference. In particular, it is noted that although the thermal conductivity of Bi_2Te_3 is more than 100% higher than that of $Ag(Pb_{1-y}Sn_y)_mSbTe_{2+m}$, temperature drops in these two materials appear to be similar. On the other hand, quite different trends are observed under imposed electric potential difference, where majority of electric potential drop occurs in $Ag(Pb_{1-y}Sn_y)_mSbTe_{2+m}$, which has much smaller electric conductivity.

The effective electric conductivity, Seebeck coefficient, thermal conductivity, and figure of merit of Bi_2Te_3-$Ag(Pb_{1-y}Sn_y)_mSbTe_{2+m}$ layered medium are shown in Fig. 5.7, with the following boundary conditions imposed,

$$T_0 = T_1 = 300K, \quad \phi_0 = 0V, \quad \phi_1 = \{-0.35, -0.2, 0.2, 0.35\}V. \tag{3.22}$$

While the effective Seebeck coefficient and thermal conductivity only show slight deviation from the rule of mixture, as observed in Fig. 5.7ab, the nonlinear dependence of electric conductivity on volume fraction is more significant, and it is sensitive to the voltage difference imposed on the boundaries, as shown in Fig. 5.7c. This results in large difference in the effective thermoelectric figure of merit shown in Fig. 5.7d. What is most interesting is that there is a peak, albeit small, in the effective thermoelectric figure of merit that exceed both constituents, at $f = 0.973$, when the imposed potential difference is $\phi_1 = -0.35$. This is significant, since it demonstrates that the effective thermoelectric figure of merit of

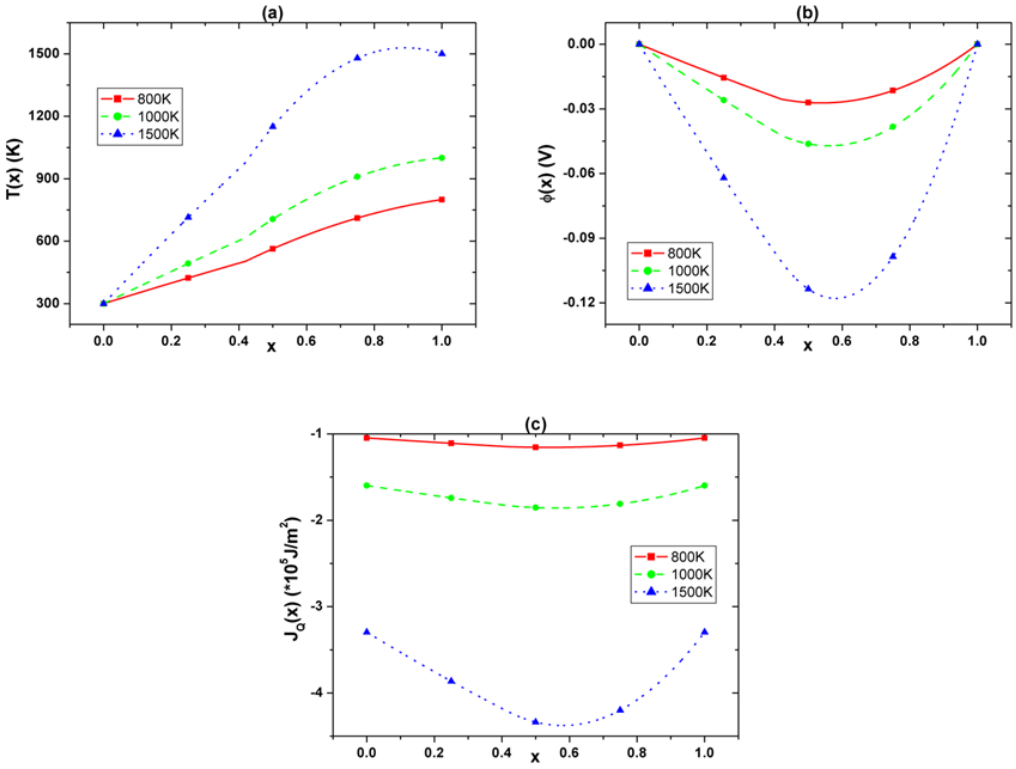

Figure 3.4: The distributions of temperature, electric potential, and heat flux in a layered thermoelectric under an imposed temperature difference[71].

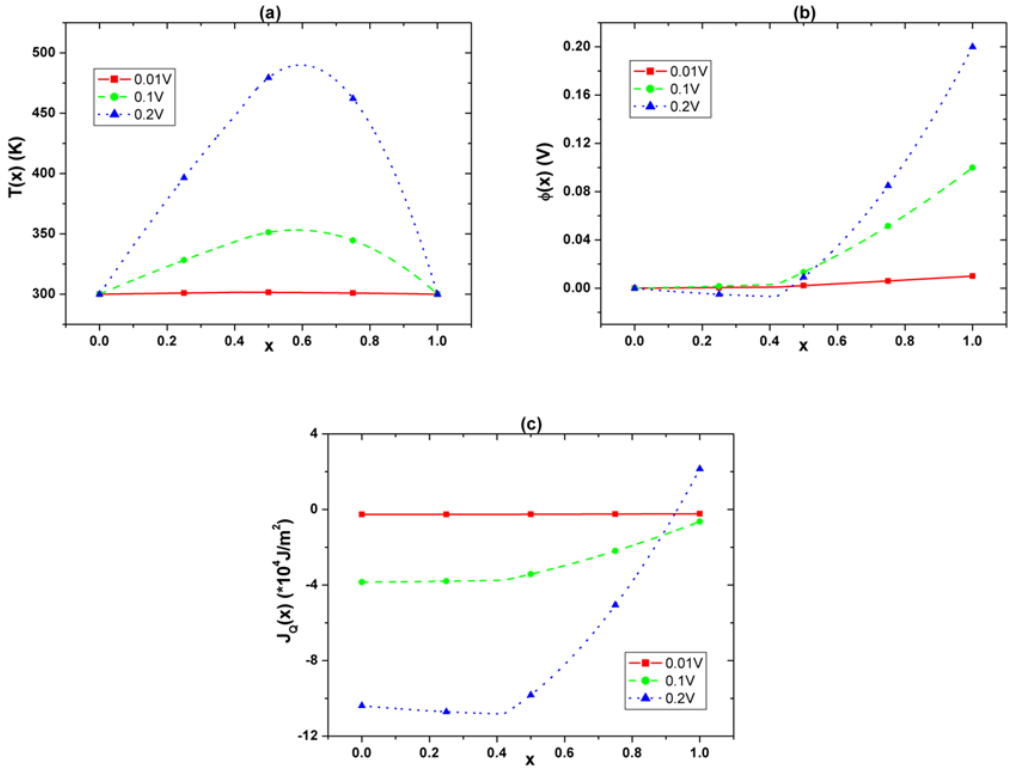

Figure 3.5: The distributions of temperature, electric potential, and heat flux in a layered thermoelectric under an imposed electric potential difference[71].

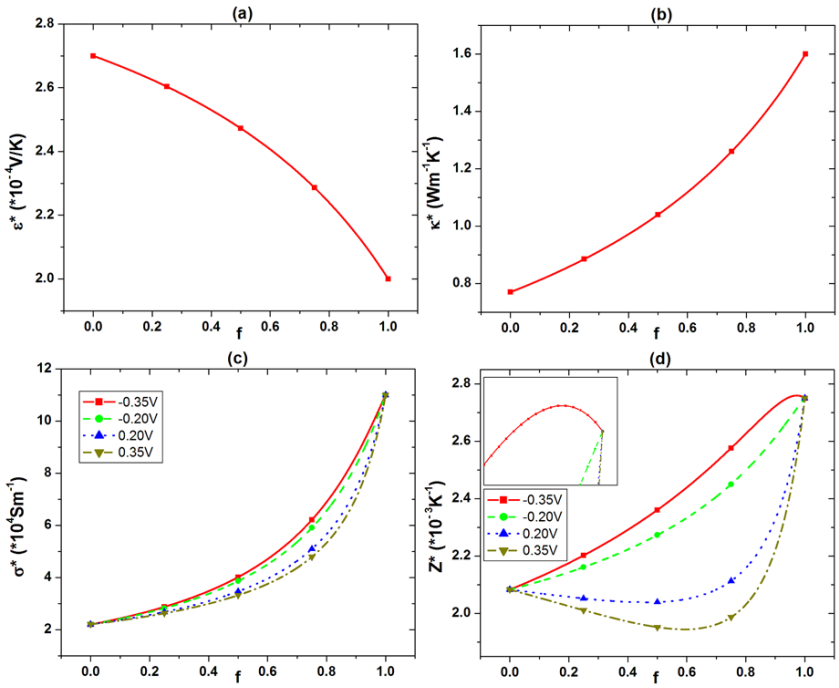

Figure 3.6: The effective Seebeck coefficient, thermal conductivity, electric conductivity, and figure of merit as functions of volume fraction[71].

a heterogeneous medium can be higher than both of its constituents, in contrast to previous studies. The distributions of temperature, electric potential and heat flux for this particular layered structure under imposed boundary condition is given in Fig. (3.7), where substantial temperature increase, though still in the acceptable range, is observed. The distributions of temperature, potential, and heat flux are all highly nonlinear, which is essential for enhanced thermoelectric figure of merit. With higher potential difference imposed at boundary, higher enhancement in thermoelectric figure of merit will be obtained, though it may leads to unrealistic high temperature inside the medium.

3.5 Summary

In this chapter we have developed a rigorous 1D analysis of bi-layered thermoelectric medium, from which the effective thermoelectric properties have been established using an equivalent principle. It is found that the thermoelectric figure of merit of layered medium

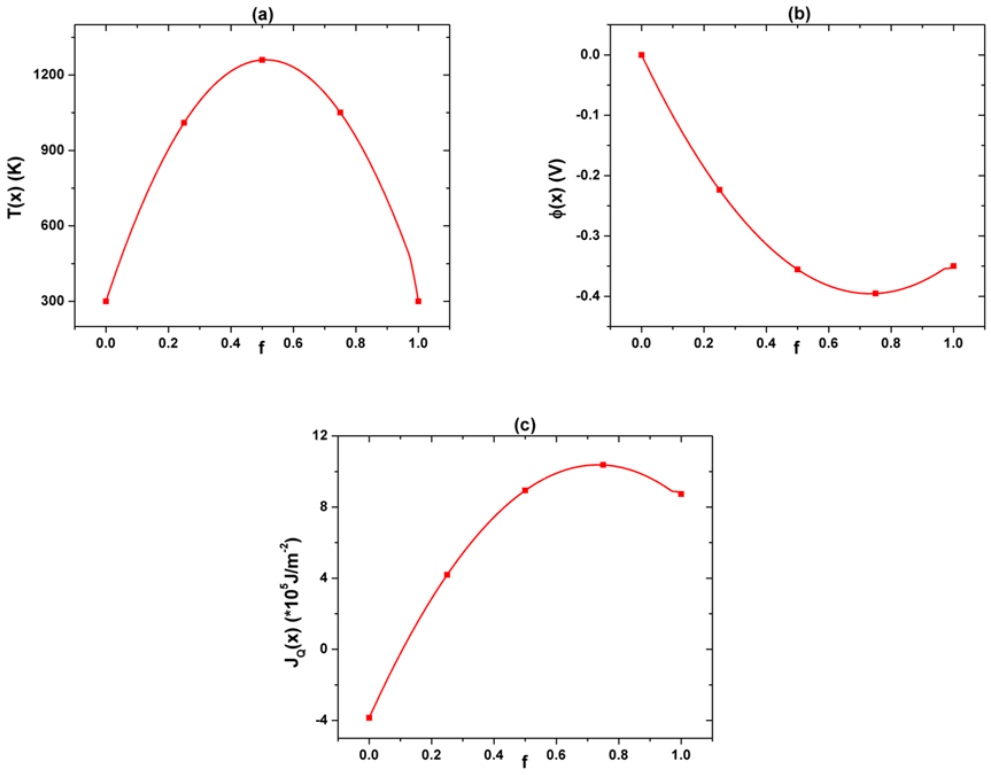

Figure 3.7: The distributions of temperature, electric potential and heat flux at the maximum Z^* with $f = 0.973$[71].

can be higher than both its constituents, and the key is to utilize the nonlinear distribution of temperature and electric potential inherent in thermoelectric transport.

Chapter 4

CONVERSION EFFICIENCY OF BI-LAYERED THERMOELECTRIC COMPOSITE

4.1 Introductory remarks

We have seen from the previous chapter, that the effective thermoelectric properties of composite are not real material constants anymore, rather, they depend on boundary conditions, which is a well known issue for nonlinear composites. Indeed, we have seen from Fig. 5.7 that different $\Delta\phi$ actually leads to very different trends in the effective figure of merit Z^*, as such, the thermoelectric figure of merit ZT as we know it becomes ill-defined for composites. Thus we have to turn to the thermoelectric conversion efficiency directly for a composite material, rather than relying on figure of merit.

We will introduce a hypothesized thermoelectric module for conversion efficiency analysis in Section 2. In Section 3, the conversion efficiency for composites is analyzed. The mechanism responsible for the conversion efficiency enhancement and the way for further optimization are provided in Section 4. Section 5 is the summary of this chapter.

4.2 Thermoelectric module

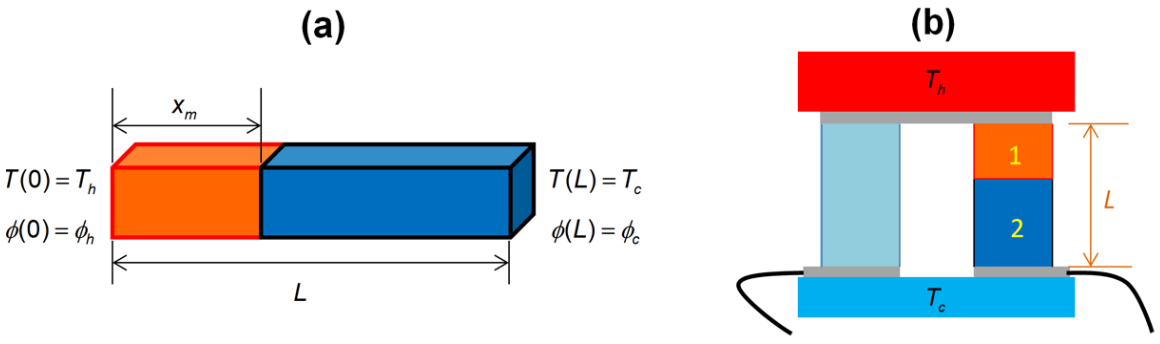

Figure 4.1: Schematics of (a) a bilayered composite and (b) a fictitious thermoelectric module[74].

One difficulty in our analysis of thermoelectric composite is that thermoelectric conversion efficiency is a performance measure for devices instead of materials, depending on both legs of thermoelectric module. In order to evaluate the thermoelectric conversion performance of a material, we propose a thermoelectric module as schematically shown in Fig. 4.1b, with one leg made of material of interest, and the other leg made of fictitious material with zero Seebeck coefficient and thermal conductivity, yet infinite electric conductivity. As such, this fictitious leg only serves as a path for electric current, and is not involved in energy conversion. The conversion efficiency of this idealized thermoelectric module, as a result, measures only the performance of material of interest. With this idealized model, the thermoelectric conversion efficiency H of the material can be derived using standard procedure[2],

$$H = \frac{AJ^2R}{J_U|_{x=0}}, \quad J_U = -\kappa\nabla T + \alpha T J + \phi J, \tag{4.1}$$

where R is the load resistance, A is the cross-section area, and J_U is the energy flux density, which is a constant due to energy conservation. Note that the electric boundary condition for Fig. 4.1b is different from that of Fig. 4.1a, in that the potential difference is not imposed; instead, an electric circuit is formed by the thermoelectric module and the load resistance, and the current density has to be evaluated from line integral $\oint \nabla\phi \cdot d\mathbf{l} = 0$ across the circuit instead of from the imposed potential difference. For a homogeneous material with constant thermoelectric properties, the conversion efficiency H can be evaluated in terms of load resistance R analytically. It can then be optimized with respect to the load resistance R, leading to classical formula relating conversion efficiency to ZT[2],

$$H_{\text{opt}} = \frac{T_h - T_c}{T_h} \frac{\sqrt{1 + Z\frac{T_h+T_c}{2}} - 1}{\sqrt{1 + Z\frac{T_h+T_c}{2}} + \frac{T_c}{T_h}}. \tag{4.2}$$

However, for composite materials with nonuniform thermoelectric properties, H can no longer derived in terms of R analytically, and such simple relationship is no longer available. Instead, we have to evaluate Eq. (4.1) numerically in general.

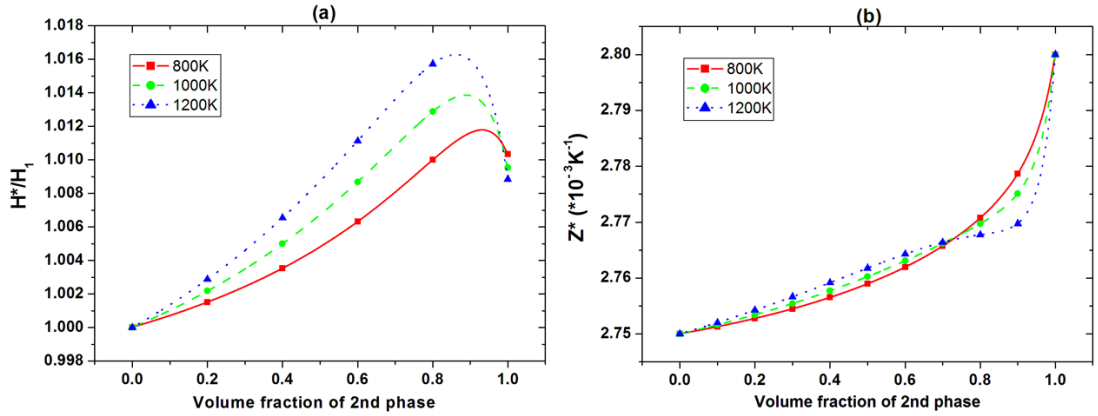

Figure 4.2: Conversion efficiency of the bilayered composite consisting of Bi_2Te_3 and an optimally second phase for different temperatures; (a) enhanced conversion efficiency of the composite versus the volume fraction of the second phase, normalized by the efficiency of the first phase; (b) the effective figure of merit versus the volume fraction calculated from the effective thermoelectric properties[74].

4.3 Optimization of conversion efficiency

To examine if the composite can have higher conversion efficiency than both of its constituent, we calculate efficiency of a bilayered composite consisting of Bi_2Te_3 and a second phase optimally matched (in a sense to be elaborated later) with Bi_2Te_3 under different temperatures, with $T_c = 300K$ and T_h chosen to be $800, 1000, 1200K$, respectively. The material constants used in the calculation are listed in Table 4.1. The results are illustrated as a function of volume fraction of the second phase in Fig. 5.8a, and it is observed that higher efficiency than both constituents is indeed possible. Furthermore, making use of equivalency principle, we evaluate the corresponding effective Z^* with the effective Seebeck coefficient and thermal conductivity calculated under open circuit condition and the effective electric conductivity derived under optimal thermoelectric loading condition. As evident in Fig. 5.8b, it shows no enhancement at all and there appears no correlation between the effective Z^* and the conversion efficiency of the composite. Alternatively, we can define the effective thermoelectric properties using equivalency principle under optimal working condition in

Table 4.1: Thermoelectric properties of Bi_2Te_3 [72] and the optimal constituent 2 under different temperature boundary conditions [74]

Material	α ($\times 10^{-6}$V/K)	σ ($\times 10^3$S/m)	κ (W/m/K))	$Z(\times 10^{-3}K^{-1})$
Bi_2Te_3	200.000	110.000	1.60000	2.75000
800K Optimal	225.322	550.933	9.98962	2.80000
1000K Optimal	232.553	517.242	9.99032	2.80000
1200K Optimal	238.713	490.981	9.99217	2.80000

combination with the requirements of

$$Z = \frac{\alpha^2 \sigma}{\kappa}$$

and Eq. (4.2) instead, and these three conditions allow us to solve for three effective thermoelectric constants simultaneously. Interestingly, this leads to two sets of effective properties, as shown in Fig. 4.3 along with the effective Z^* evaluated from Eq. (4.2). This further demonstrates that the effective thermoelectric properties of composite is ill-defined, and we have to examine the conversion efficiency directly.

4.4 Mechanism and further improvement

In order to understand the enhanced conversion efficiency in bilayered composite, we rewrite the conversion efficiency as

$$H = \frac{\phi_c J}{J_U|_{x=0}} = \frac{\phi_c J}{T_h \alpha J - \frac{J^2 L}{2\sigma} + \frac{\kappa(T_h - T_c)}{L}} \tag{4.3}$$

for a homogeneous material, which can be optimized with respect to current density for given temperatures,

$$J_{\text{opt}} = \frac{\sqrt{2\kappa}\sigma\alpha(T_h - T_c)}{[\sqrt{2\kappa} + \sqrt{2\kappa + \sigma\alpha^2(T_h + T_c)}]L}. \tag{4.4}$$

Since current density is a constant in the layered composite, this points to a need for carefully matching the optimal current density in constituent phases for the optimal overall

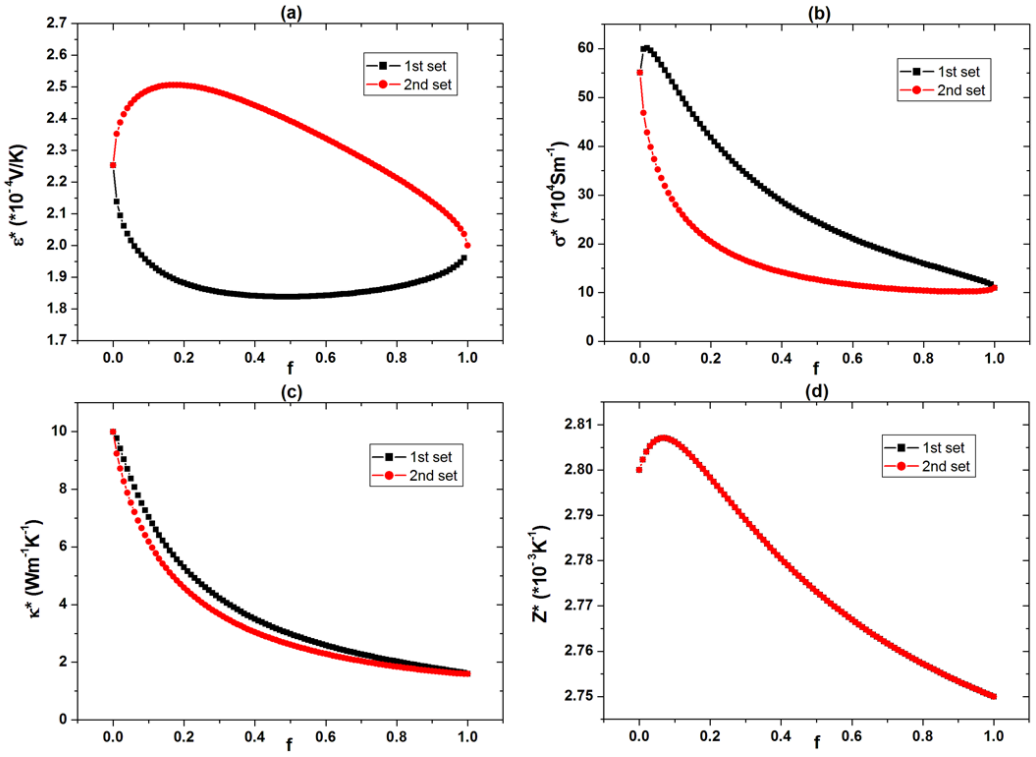

Figure 4.3: Two sets of effective thermoelectric properties corresponding to a given conversion efficiency evaluated at $T_h = 800$K, with the second phase optimally matched with Bi_2Te_3; (a) electric conductivity; (b) Seebeck coefficient; (c) thermal conductivity; and (d) figure of merit [74].

conversion efficiency. Indeed, we can compare the bilayered composite with its homogenous constituents in Fig. 4.4a, all operating at optimal conditions for respective overall conversion efficiency. The temperature at the interface of the bilayer is labeled as T_m, which is also identified in its homogeneous constituents. It is evident that the bilayered composite can have its constituent phases matched for identical optimal current density by tailoring the material properties, which is impossible for homogeneous materials to do. This is clearly illustrated in Fig. 4.4b, where it is observed that the optimal current density for the bilayered composite between T_h and T_c is identical to that for its constituent phases between T_h and T_m as well as between T_m and T_c. For homogeneous material, on the other hand, the optimal current density for the overall structure between T_h and T_c is different from that

for individual segments between T_h and T_m or between T_m and T_c. In other words, both segments of bilayered composite operate at optimal condition, while those of homogeneous materials operate under less optimal ones. This explains higher conversion efficiency in optimally matched bilayered composite.

We can also mathematically prove that optimized layered thermoelectric can achieve higher conversion efficiency than its constituents, we consider the bi-layered composite shown in Fig. 4.4a. Since the various thermoelectric properties of each segment of phase are tailored to match the optimal current density for simultaneous optimization for segments, it is obvious that ($Z_1 = Z_2 = Z$ is assumed for simplicity),

$$H_{U\_i} \leq H_{U\_1-2} = \frac{T_h - T_m}{T_h} \frac{\sqrt{1 + Z\frac{T_h+T_m}{2}} - 1}{\sqrt{1 + Z\frac{T_h+T_m}{2}} + \frac{T_m}{T_h}}, \tag{4.5}$$

$$H_{L\_i} \leq H_{L\_1-2} = \frac{T_m - T_c}{T_m} \frac{\sqrt{1 + Z\frac{T_m+T_c}{2}} - 1}{\sqrt{1 + Z\frac{T_m+T_c}{2}} + \frac{T_c}{T_m}}, \tag{4.6}$$

where Eq. (4.2) is used for optimal efficiency calculation, the subscriptions U and L denote the upper and lower parts separated by $\mathrm{T_m}$, 1-2 the bi-layered structure 1-2, i is to take the value of 1 or 2. The overall efficiency for series structure is thus simply [75],

$$H_i = 1 - (1 - H_{U\_i})(1 - H_{L\_i}) < H_{1-2} = 1 - (1 - H_{U\_1-2})(1 - H_{L\_1-2}), \tag{4.7}$$

in which, the less-than sign is used instead because the simultaneous optimization for homogeneous constituents is not possible due to internal constraint as discussed earlier.

The analysis on bilayered composite points to a direction for optimal conversion efficiency of thermoelectric module, wherein the optimal current density is matched everywhere, resulting in highest conversion efficiency possible. To this end, we reorganize Eq. (4.4) by replace L with dx, leading to a point-wise optimal current density of

$$J_{\mathrm{opt}} = -\kappa \nabla T \frac{\sqrt{1 + ZT} - 1}{\alpha T}, \tag{4.8}$$

which corresponds to maximum local conversion efficiency of

$$dH_{\max} = \frac{\sqrt{1 + ZT} - 1}{\sqrt{1 + ZT} + 1} \frac{dT}{T}. \tag{4.9}$$

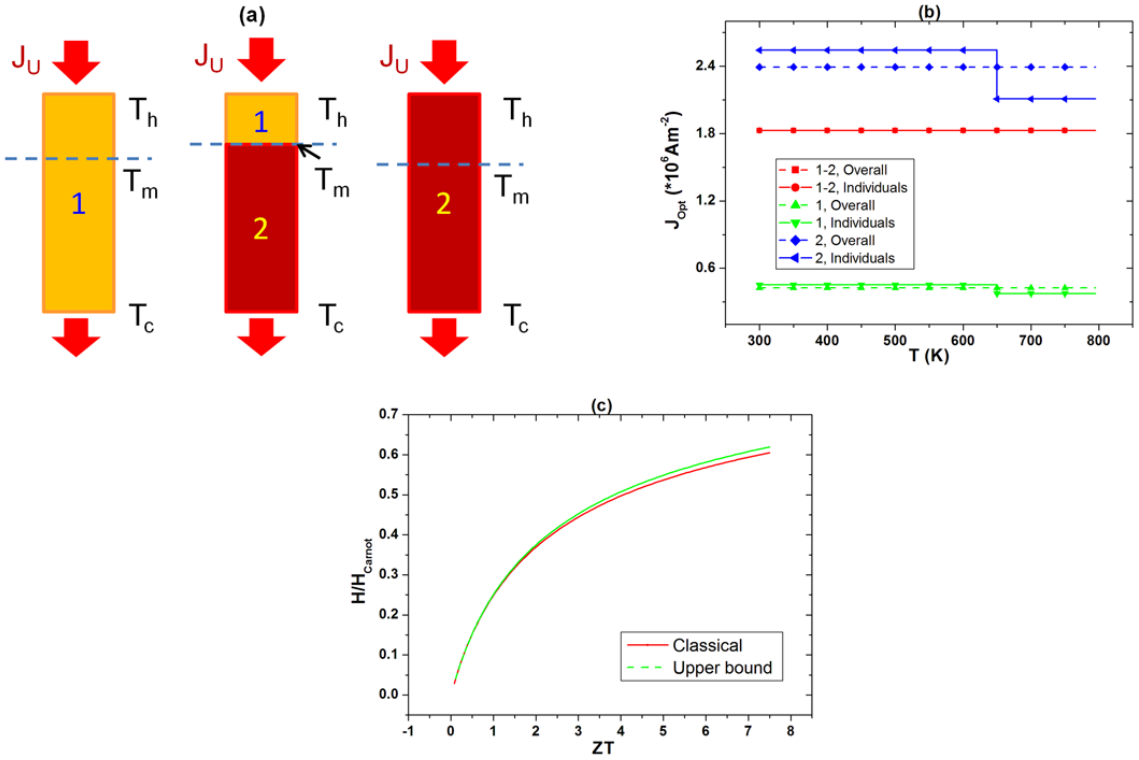

Figure 4.4: Understanding enhanced efficiency in layered composites; (a) schematics for bilayered composite and its homogeneous contituent phases; (b) optimal current density for each segment under respective temperature difference; and (c) upper bound on the conversion efficiency in term of figure of merit ZT, compared with classical formula, evaluated at $T_c = 300\text{K}$ and $T_h = 1200\text{K}$ [74].

This is equivalent to the concept of compatibility factor [75–78]. When the optimality is realized everywhere, maximum overall efficiency is realized as

$$\begin{aligned} H_{\max} &= 1 - \exp\left(-\int_{T_c}^{T_h} \frac{\sqrt{1+ZT}-1}{\sqrt{1+ZT}+1}\frac{dT}{T}\right) \\ &= 1 - \exp\left(\frac{2}{\sqrt{1+ZT_c}+1} - \frac{2}{\sqrt{1+ZT_h}+1} + 2\ln\frac{\sqrt{1+ZT_c}+1}{\sqrt{1+ZT_h}+1}\right), \end{aligned} \tag{4.10}$$

where we have taken Z to be a constant for simpler derivation. This is in fact the upper bound on the conversion efficiency for the layered composite consisting of materials with constant Z, and its comparison with classical conversion efficiency of a homogeneous material with identical Z and boundary condition is shown in Fig. 4.4c, where a small yet definite enhancement is evident.

Finally, we point out that our analysis is related to functionally graded thermoelectrics, where it was suggested that the device figure of merit can be higher than that of materials[79–83].

4.5 Summary

Here, we show that thermoelectric conversion efficiency of a composite is not bounded by its constituents, with the conditions on constituent phases for enhanced conversion efficiency in layered composites identified, and the upper bound on their conversion efficiency established.

Chapter 5

EFFECTIVE PROPERTIES OF THERMOELECTRIC CORE-SHELL COMPOSITES

5.1 Introductory remarks

Built on our earlier analysis of thermoelectic bi-layered structure, here we analyze the effective thermoelectric behavior of core-shell composites, motivated by their potential applications in recovering waste heat from automobile exhaust pipes, among other similar applications. The problem turns out to be axially-symmetric because of geometry, and thus can be reduced to one-dimensional equations, allowing us to simplify the analysis substantially and derive analytic solutions.

In Section 2, we solved the fields for both shell and core-shell materials. In Section 3, the effective thermoelectric properties are determined from equivalency principle. In Section 4, conversion efficiency analysis is carried out on core-shell composites. Numerical results and discussions are presented in Section 5. The final section summarizes this chapter.

5.2 Field analysis of polar symmetry

We consider axially-symmetric thermoelectric problems, as shown in Fig. 5.1, where polar coordinate system is convenient and all the variables are only dependent on its radial coordinate ρ. As such, the transport equations

$$-\mathbf{J} = \sigma\nabla\phi + \sigma\alpha\nabla T, \tag{5.1}$$

$$\mathbf{J}_Q = -T\alpha\sigma\nabla\phi - (T\alpha^2\sigma + \kappa)\nabla T = T\alpha\mathbf{J} - \kappa\nabla T, \tag{5.2}$$

are simplified as

$$-\mathbf{J} = \sigma\frac{d\phi}{d\rho}\widehat{\boldsymbol{\rho}} + \sigma\alpha\frac{dT}{d\rho}\widehat{\boldsymbol{\rho}}, \tag{5.3}$$

$$\mathbf{J}_Q = = T\alpha\mathbf{J} - \kappa\frac{dT}{d\rho}\widehat{\boldsymbol{\rho}}, \tag{5.4}$$

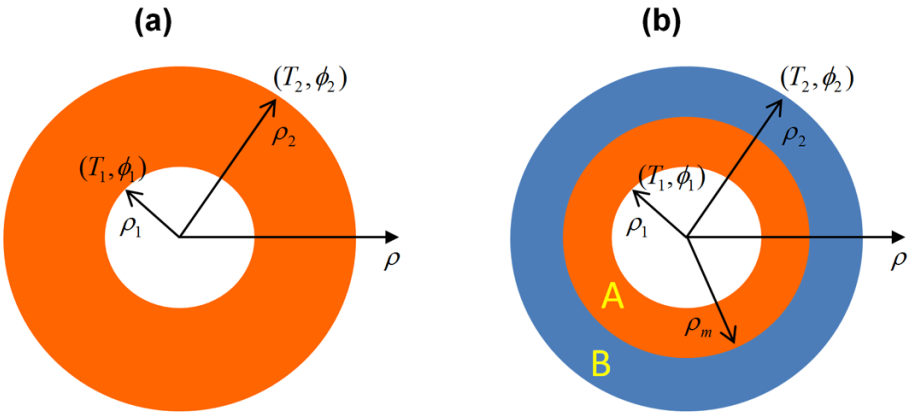

Figure 5.1: The cross-section view of axially-symmetric thermoelectric problems for (a) a homogeneous shell and (b) a core-shell composite[84].

where $\widehat{\boldsymbol{\rho}}$ is the unit vector along radial direction. Furthermore, the field equation

$$\nabla \cdot \mathbf{J} = 0, \tag{5.5}$$

is converted to

$$\frac{dJ}{d\rho} + \frac{J}{\rho} = 0, \tag{5.6}$$

such that

$$J = \frac{c}{\rho}, \tag{5.7}$$

where $J = |\mathbf{J}|$ is the magnitude of current density, and c is an integration constant that needs to be determined by boundary conditions. Note that $c = J\rho = \frac{I}{2\pi d}$ denotes the electric current I per unit length and radian, with d being the length of the material. Similarly, from

$$\nabla \cdot \mathbf{J}_U = 0, \tag{5.8}$$

it can also be shown that $J_U \rho = c_U$, which is the energy transfer per unit length and radian. It is evident that both c and c_U are constant along radial direction.

5.2.1 Analysis of a homogeneous thermoelectric shell

We first consider a thermoelectric shell having homogeneous material properties, with inner and outer radius being ρ_1 and ρ_2, and subjected to specified temperatures and electric potentials of (T_1, ϕ_1) and (T_2, ϕ_2) at inner and outer boundaries, as shown in Fig. 5.1(a). For such an axially-symmetric problem, the governing equations for temperature and electric potential can be simplified as,

$$\frac{d^2T}{d\rho^2} + \frac{1}{\rho}\frac{dT}{d\rho} = -\frac{J^2}{\sigma\kappa}, \tag{5.9}$$

$$\frac{d^2\phi}{d\rho^2} + \frac{1}{\rho}\frac{d\phi}{d\rho} = \frac{\alpha J^2}{\sigma\kappa}. \tag{5.10}$$

Substituting Eq. (5.7) into (5.9) and (5.10), temperature and electric potential can be solved as

$$T(\rho) = -\frac{c^2}{2\sigma\kappa}(\ln\rho)^2 + a\ln\rho + b, \tag{5.11}$$

$$\phi(\rho) = \frac{\alpha c^2}{2\sigma\kappa}(\ln\rho)^2 + g\ln\rho + h, \tag{5.12}$$

where a, b, g, and h are integration constants that will be determined later. By substituting Eqs. (5.7), (5.11), and (5.12) into (5.3), the following relation for the integration constants is obtained,

$$-c = g\sigma + a\sigma\alpha. \tag{5.13}$$

Furthermore, the specified boundary conditions require that

$$T(\rho_1) = -\frac{c^2}{2\sigma\kappa}(\ln\rho_1)^2 + a\ln\rho_1 + b = T_1, \tag{5.14}$$

$$T(\rho_2) = -\frac{c^2}{2\sigma\kappa}(\ln\rho_2)^2 + a\ln\rho_2 + b = T_2, \tag{5.15}$$

$$\phi(\rho_1) = \frac{\alpha c^2}{2\sigma\kappa}(\ln\rho_1)^2 + g\ln\rho_1 + h = \phi_1, \tag{5.16}$$

$$\phi(\rho_2) = \frac{\alpha c^2}{2\sigma\kappa}(\ln\rho_2)^2 + g\ln\rho_2 + h = \phi_2. \tag{5.17}$$

As a result, the five integration constants are derived as

$$c = -\frac{\sigma\alpha(T_2 - T_1) + \sigma(\phi_2 - \phi_1)}{\ln\frac{\rho_2}{\rho_1}}, \tag{5.18}$$

$$a = \frac{T_2 - T_1}{\ln\frac{\rho_2}{\rho_1}} + \frac{c^2\ln(\rho_1\rho_2)}{2\sigma\kappa}, \tag{5.19}$$

$$b = \frac{T_1\ln\rho_2 - T_2\ln\rho_1}{\ln\frac{\rho_2}{\rho_1}} - \frac{c^2\ln\rho_1\ln\rho_2}{2\sigma\kappa}, \tag{5.20}$$

$$g = \frac{\phi_2 - \phi_1}{\ln\frac{\rho_2}{\rho_1}} - \frac{\alpha c^2\ln(\rho_1\rho_2)}{2\sigma\kappa}, \tag{5.21}$$

$$h = \frac{\phi_1\ln\rho_2 - \phi_2\ln\rho_1}{\ln\frac{\rho_2}{\rho_1}} + \frac{\alpha c^2\ln\rho_1\ln\rho_2}{2\sigma\kappa}. \tag{5.22}$$

This solves the temperature and electric potential distributions in the homogeneous thermoelectric shell.

5.2.2 Analysis of thermoelectric core-shell composite

We then consider a core-shell composite consisting of two homogeneous thermoelectric phases A and B, as shown in Fig. 5.1(b), with the interface at ρ_m. The boundary conditions are identical to those of Fig. 5.1(a). Since the core-shell composite is pieces-wise homogeneous, the solutions derived in the last subsection are still applicable to individual phases, such that

$$T = \begin{cases} -\frac{c_A^2}{2\sigma_A\kappa_A}(\ln\rho)^2 + a_A\ln\rho + b_A, & \rho_1 \le \rho < \rho_m, \\ -\frac{c_B^2}{2\sigma_B\kappa_B}(\ln\rho)^2 + a_B\ln\rho + b_B, & \rho_m < \rho \le \rho_2, \end{cases} \tag{5.23}$$

and

$$\phi = \begin{cases} \frac{\alpha_A c_A^2}{2\sigma_A\kappa_A}(\ln\rho)^2 + g_A\ln\rho + h_A, & \rho_1 \le \rho < \rho_m, \\ \frac{\alpha_B c_B^2}{2\sigma_B\kappa_B}(\ln\rho)^2 + g_B\ln\rho + h_B, & \rho_m < \rho \le \rho_2. \end{cases} \tag{5.24}$$

In addition to the specified boundary conditions, it is necessary that both temperature and electric potential are continuous at the interface,

$$-\frac{c_A^2}{2\sigma_A\kappa_A}(\ln\rho_m)^2 + a_A\ln\rho_m + b_A = -\frac{c_B^2}{2\sigma_B\kappa_B}(\ln\rho_m)^2 + a_B\ln\rho_m + b_B, \tag{5.25}$$

$$\frac{\alpha_A c_A^2}{2\sigma_A\kappa_A}(\ln\rho_m)^2 + g_A\ln\rho_m + h_A = \frac{\alpha_B c_B^2}{2\sigma_B\kappa_B}(\ln\rho_m)^2 + g_B\ln\rho_m + h_B. \tag{5.26}$$

so that electric current and energy transfer (per unit length and radian) are continuous as well due to the conservation of charges and energy, resulting in,

$$c_A = c_B = c, \tag{5.27}$$

$$T(\rho_m)J(\rho_m)(\alpha_A - \alpha_B) = \kappa_A(-\frac{c_A^2}{\sigma_A\kappa_A}\frac{\ln\rho_m}{\rho_m} + \frac{a_A}{\rho_m}) - \kappa_B(-\frac{c_B^2}{\sigma_B\kappa_B}\frac{\ln\rho_m}{\rho_m} + \frac{a_B}{\rho_m}) \tag{5.28}$$

From these boundary and continuity conditions, the integration constants can be derived as

$$c = -\frac{\Psi_1 + \Psi_3 - \sqrt{\Psi_4}}{(\alpha_B - \alpha_A)\ln\frac{\rho_m}{\rho_1}\ln\frac{\rho_2}{\rho_m}(\sigma_A\ln\frac{\rho_2}{\rho_m} + \sigma_B\ln\frac{\rho_m}{\rho_1})}, \tag{5.29}$$

with

$$\Psi_1 = (\sigma_A\ln\frac{\rho_2}{\rho_m} + \sigma_B\ln\frac{\rho_m}{\rho_1})(\kappa_A\ln\frac{\rho_2}{\rho_m} + \kappa_B\ln\frac{\rho_m}{\rho_1}),$$

$$\Psi_2 = (\alpha_B - \alpha_A)\sigma_A\sigma_B\ln\frac{\rho_m}{\rho_1}\ln\frac{\rho_2}{\rho_m},$$

$$\Psi_3 = \Psi_2(\alpha_B T_2 - \alpha_A T_1 + \phi_2 - \phi_1),$$

$$\Psi_4 = -2\Psi_2[\Psi_1(\phi_2 - \phi_1) + (\sigma_A\ln\frac{\rho_2}{\rho_m} + \sigma_B\ln\frac{\rho_m}{\rho_1})(\kappa_A\alpha_B\ln\frac{\rho_2}{\rho_m} + \kappa_B\alpha_A\ln\frac{\rho_m}{\rho_1})(T_2 - T_1)]$$
$$+ (\Psi_1 + \Psi_3)^2,$$

and

$$a_A = \frac{c^2 \ln(\rho_m \rho_1)}{2\sigma_A \kappa_A} + \frac{c^2 \ln\frac{\rho_2}{\rho_m} \Lambda}{2\Theta} - \frac{c(\alpha_B - \alpha_A) T_1 \ln\frac{\rho_2}{\rho_m}}{\Theta} + \frac{\kappa_B (T_2 - T_1)}{\Theta}, \tag{5.30}$$

$$b_A = -\frac{c^2 \ln\rho_m \ln\rho_1}{2\sigma_A \kappa_A} - \frac{c^2 \ln\frac{\rho_2}{\rho_m} \ln\rho_1 \Lambda}{2\Theta} + \frac{c(\alpha_B - \alpha_A) T_1 \ln\frac{\rho_2}{\rho_m} \ln\rho_m}{\Theta} + \frac{\kappa_A \ln\frac{\rho_2}{\rho_m} T_1 + \kappa_B (\ln\rho_m T_1 - \ln\rho_1 T_2)}{\Theta}, \tag{5.31}$$

$$g_A = -\frac{c}{\sigma_A} - a_A \alpha_A, \tag{5.32}$$

$$h_A = \phi_1 - \frac{c^2 \alpha_A}{2\sigma_A \kappa_A} (\ln\rho_1)^2 - g_A \ln\rho_1, \tag{5.33}$$

$$a_B = \frac{c^2 \ln(\rho_2 \rho_m)}{2\sigma_B \kappa_B} - \frac{c^2 \ln\frac{\rho_m}{\rho_1} \Lambda}{2\Theta} + \frac{c(\alpha_B - \alpha_A) T_2 \ln\frac{\rho_m}{\rho_1}}{\Theta} + \frac{\kappa_A (T_2 - T_1)}{\Theta}, \tag{5.34}$$

$$b_B = -\frac{c^2 \ln\rho_2 \ln\rho_m}{2\sigma_B \kappa_B} + \frac{c^2 \ln\frac{\rho_m}{\rho_1} \ln\rho_2 \Lambda}{2\Theta} - \frac{c(\alpha_B - \alpha_A) T_2 \ln\frac{\rho_m}{\rho_1} \ln\rho_m}{\Theta} + \frac{\kappa_B \ln\frac{\rho_m}{\rho_1} T_2 + \kappa_A (\ln\rho_2 T_1 - \ln\rho_m T_2)}{\Theta}, \tag{5.35}$$

$$g_B = -\frac{c}{\sigma_B} - a_B \alpha_B, \tag{5.36}$$

$$h_B = \phi_2 - \frac{c^2 \alpha_B}{2\sigma_B \kappa_B} (\ln\rho_2)^2 - g_B \ln\rho_2, \tag{5.37}$$

where

$$\Lambda = \frac{\sigma_A \ln\frac{\rho_2}{\rho_m} + \sigma_B \ln\frac{\rho_m}{\rho_1}}{\sigma_A \sigma_B},$$

$$\Theta = \kappa_A \ln\frac{\rho_2}{\rho_m} + \kappa_B \ln\frac{\rho_m}{\rho_1} + c(\alpha_B - \alpha_A) \ln\frac{\rho_m}{\rho_1} \ln\frac{\rho_2}{\rho_m}.$$

This solves distributions of temperature and electric potential in the core-shell composite.

5.3 The effective thermoelectric properties

To describe the effective behavior of the heterogeneous core-shell thermoelectric, we define its effective thermoelectric properties through the equivalency principle discussed previously. We examine the effective electric conductivity first. Consider a boundary condition of imposed electric potential difference only with $\Delta T = 0$, and compare the electric current (per unit length and radian) between homogeneous and core-shell thermoelectrics. From Eq. (5.18) we conclude that the effective electric conductivity of the core-shell composite is

given by

$$\sigma^*(\Delta\phi, \Delta T = 0) = \frac{c\ln\frac{\rho_2}{\rho_1}}{\phi_1 - \phi_2} = -\frac{c\ln\frac{\rho_2}{\rho_1}}{\Delta\phi}, \tag{5.38}$$

with c given by Eq. (5.29). Expanding c into Taylor series of $(\alpha_B - \alpha_A)$, and using the notation of $f \equiv \ln\frac{\rho_m}{\rho_1}/\ln\frac{\rho_2}{\rho_1}$, we derive the effective electric conductivity of the core-shell thermoelectric to the first order of $(\alpha_B - \alpha_A)$,

$$\sigma^*(\Delta\phi) = \frac{\sigma_A\sigma_B}{\sigma_A(1-f) + \sigma_B f} - \frac{f(1-f)\sigma_A^2\sigma_B^2\Delta\phi(\alpha_B - \alpha_A)}{2[\sigma_A(1-f) + \sigma_B f]^2[\kappa_A(1-f) + \kappa_B f]}, \tag{5.39}$$

which is analog to our earlier result for layered composite, with f denoting volume fraction there instead. Note that the thickness ratio of the core-shell structure is given in term of f by $p \equiv \frac{\rho_m - \rho_1}{\rho_2 - \rho_1} = \frac{\rho_1}{\rho_2 - \rho_1}[(\frac{\rho_2}{\rho_1})^f - 1]$. Eq. (5.39) clearly depends on the boundary condition as well as the material constants of the constituents and f, a characteristic distinct from linear materials. Furthermore, if we impose open-circuit boundary condition such that $c = 0$, then the effective Seebeck coefficient can be derived from Eq. (5.18) as

$$\alpha^* = -\frac{\phi_2 - \phi_1}{T_2 - T_1} = \frac{\kappa_A(1-f)\alpha_B + \kappa_B f\alpha_A}{\kappa_A(1-f) + \kappa_B f}, \tag{5.40}$$

while the effective thermal conductivity can be derived as

$$\kappa^* = -\frac{J_Q}{\frac{dT}{d\rho}} = -\frac{J_Q\rho}{(T_2 - T_1)/\ln\frac{\rho_2}{\rho_1}} = \frac{\kappa_A\kappa_B}{\kappa_A(1-f) + \kappa_B f}. \tag{5.41}$$

Again they are identical to the formula for layered composites, though f has different physical meanings for these two systems. Note that although the effective Seebeck coefficient and thermal conductivity do not appear to be dependent on the boundary condition explicitly, open-circuit boundary condition is implied implicitly in these equations. From the effective thermoelectric properties, the effective thermoelectric figure of merit can be defined as

$$Z^* = \frac{\sigma^*\alpha^{*2}}{\kappa^*}, \tag{5.42}$$

though its relationship with the thermoelectric conversion efficiency remains to be examined.

5.4 Conversion efficiency of core-shell composite

Since the effective thermoelectric properties as defined depend on the boundary condition, the relationship between effective figure of merit and conversion efficiency becomes less clear,

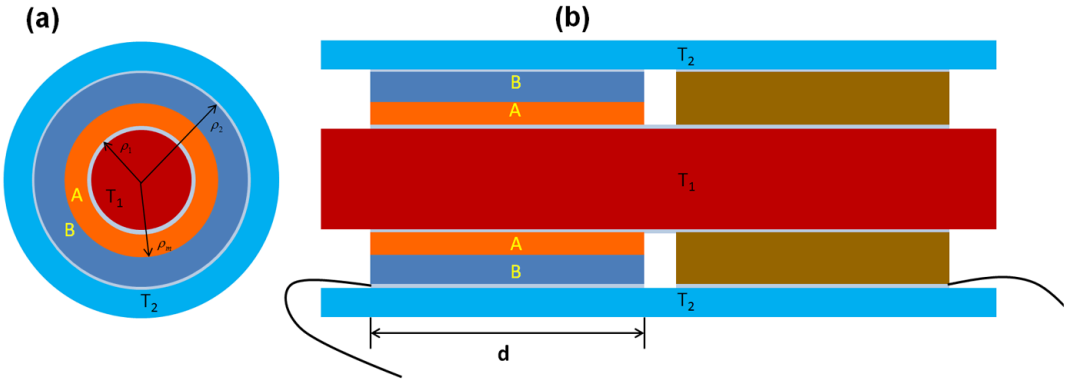

Figure 5.2: Schematics of axially-symmetric thermoelectric generator with (a) cross-section view and (b) side section view, where the left leg consists of materials of interests, and the right leg is a fictitious material with zero Seebeck coefficient and thermoelectric conductivity, yet infinite electric conductivity[84].

and thus we examine the conversion efficiency of the core-shell composite directly. To this end, we consider an idealized thermoelectric module with one of the legs made of fictitious material of zero Seebeck coefficient and thermoelectric conductivity, yet infinite electric conductivity, and the other leg made of thermoelectric material of interests, as shown in Fig. 5.2. The energy conversion efficiency of the thermoelectric generator is calculated as

$$H = \frac{I^2 R}{\dot{E}_1} = \frac{(2\pi dc)^2 R}{2\pi d c_U|_{\rho=\rho_1}}, \quad c_U = -\kappa\rho\nabla T + \alpha T c + \phi c, \tag{5.43}$$

where I is electric current, R is the load resistance, $\dot{E}_1$ denotes the energy flow from high temperature reservoir, d is the length of the materials, and c_U and c are constants related to the transports of energy and electricity, with the latter determined by solving $\oint \nabla\phi \cdot d\mathbf{x} = 0$ around the circuit, as potentials are no longer specified at outer and inner surfaces. For a homogeneous material with constant thermoelectric properties, the conversion efficiency H can be evaluated in terms of load resistance R analytically. It can then be optimized with respect to the load resistance R, leading to classical formula relating conversion efficiency to ZT,

$$H_{\text{opt}} = \frac{T_1 - T_2}{T_1} \frac{\sqrt{1 + Z\frac{T_1+T_2}{2}} - 1}{\sqrt{1 + Z\frac{T_1+T_2}{2}} + \frac{T_2}{T_1}}. \tag{5.44}$$

However, for composite materials with nonuniform thermoelectric properties, H can no longer be derived in terms of R analytically, and such simple relationship is no longer available. Instead, we have to evaluate Eq. (5.43) numerically in general. Nevertheless, by evaluating $\oint \nabla\phi \cdot d\mathbf{x} = 0$ around the circuit, it is derived that

$$c = -\frac{\Gamma_1 + \Gamma_3 - \sqrt{\Gamma_4}}{(\alpha_B - \alpha_A)\ln\frac{\rho_m}{\rho_1}\ln\frac{\rho_2}{\rho_m}(\sigma_A\ln\frac{\rho_2}{\rho_m} + \sigma_B\ln\frac{\rho_m}{\rho_1} + 4\pi d\sigma_A\sigma_B R)}, \tag{5.45}$$

with

$$\begin{aligned}
\Gamma_1 &= (\sigma_A\ln\frac{\rho_2}{\rho_m} + \sigma_B\ln\frac{\rho_m}{\rho_1} + 2\pi d\sigma_A\sigma_B R)(\kappa_A\ln\frac{\rho_2}{\rho_m} + \kappa_B\ln\frac{\rho_m}{\rho_1}),\\
\Gamma_2 &= (\alpha_B - \alpha_A)\sigma_A\sigma_B\ln\frac{\rho_m}{\rho_1}\ln\frac{\rho_2}{\rho_m},\\
\Gamma_3 &= \Gamma_2(\alpha_B T_2 - \alpha_A T_1),\\
\Gamma_4 &= -2\Gamma_2(\sigma_A\ln\frac{\rho_2}{\rho_m} + \sigma_B\ln\frac{\rho_m}{\rho_1} + 4\pi d\sigma_A\sigma_B R)(\kappa_A\alpha_B\ln\frac{\rho_2}{\rho_m} + \kappa_B\alpha_A\ln\frac{\rho_m}{\rho_1})(T_2 - T_1)\\
&\quad + (\Gamma_1 + \Gamma_3)^2.
\end{aligned}$$

5.5 Numerical results and discussions

In this section, numerical results and discussions for thermoelectric behavior of specific material systems are presented. For homogeneous shell we consider Bi_2Te_3 with $\rho_1 =$ 50mm and $\rho_2 =$ 55mm. For core-shell composite, we consider Bi_2Te_3 as phase A and $Ag(Pb_{1-y}Sn_y)_mSbTe_{2+m}$ as phase B, with $\rho_1 =$ 50mm, $\rho_m =$ 53mm, and $\rho_2 =$ 55mm. Materials length is $d = 0.5$m. The thermoelectric properties of both materials are listed in Table 3.1.

5.5.1 Field distributions

We first examine the thermoelectric field distribution under specific boundary condition. Assume that only a temperature difference is imposed, with $T_2 =$ 300K at cold end and three different temperatures of $T_1 =$ 800, 1000, 1200K at the hot end. The distributions of temperature, electric potential, and heat flux in a homogeneous shell are shown in Fig. 5.3, while those in the core-shell composite are shown in Fig. 5.4. Nonlinear temperature distribution is observed in both systems, and internal electric field is induced. Furthermore,

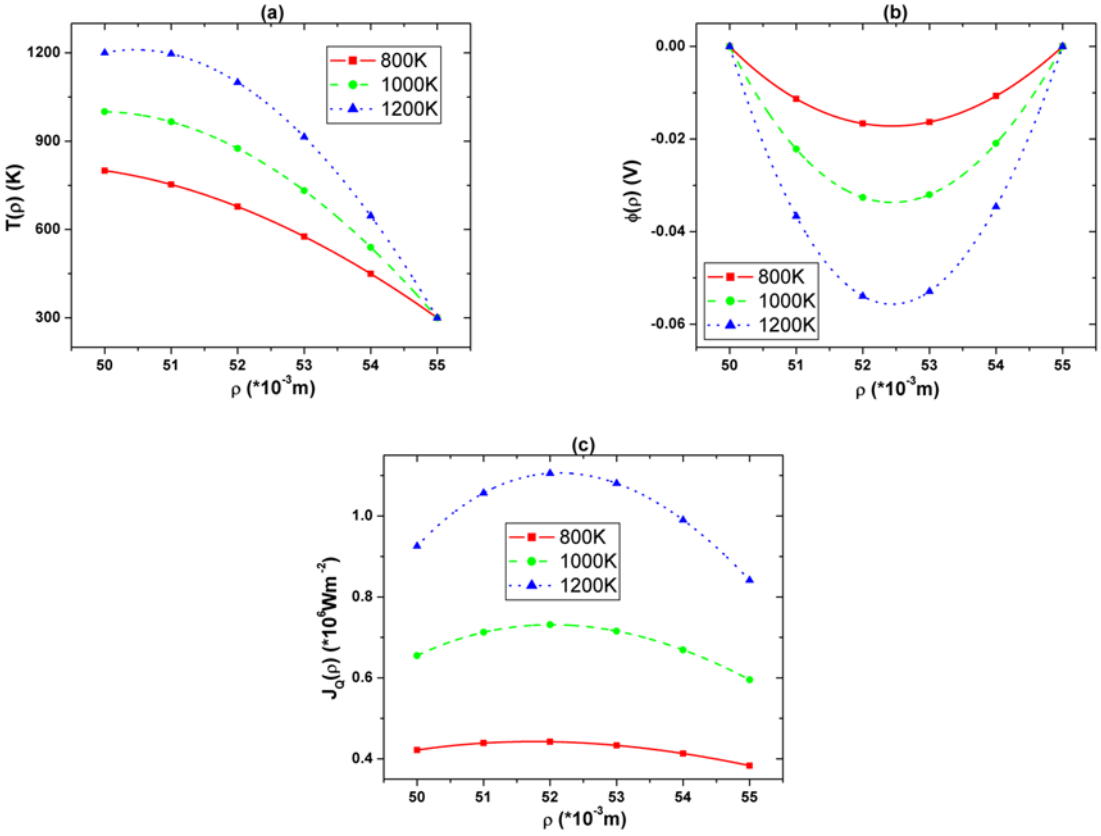

Figure 5.3: The distributions of (a) temperature, (b) electric potential, and (c) heat flux in a homogeneous shell under imposed temperature differences[84],

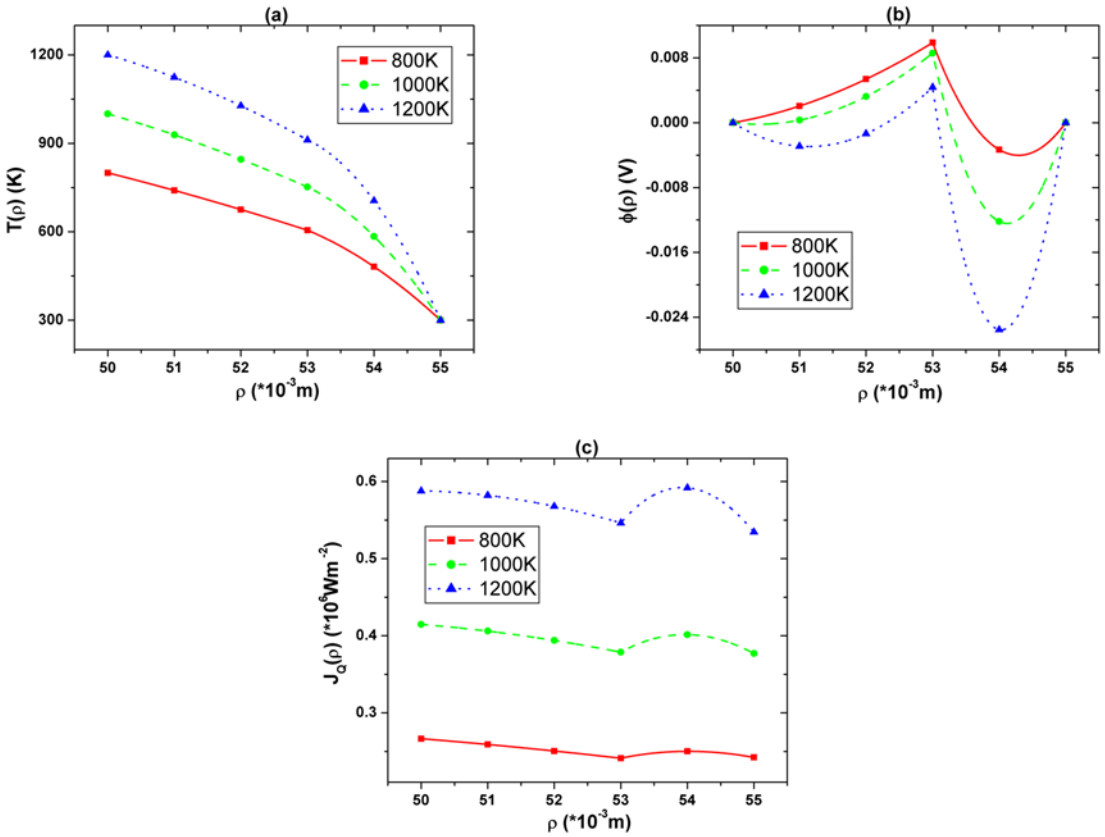

Figure 5.4: The distributions of (a) temperature, (b) electric potential, and (c) heat flux in a core-shell composite under imposed temperature differences[84].

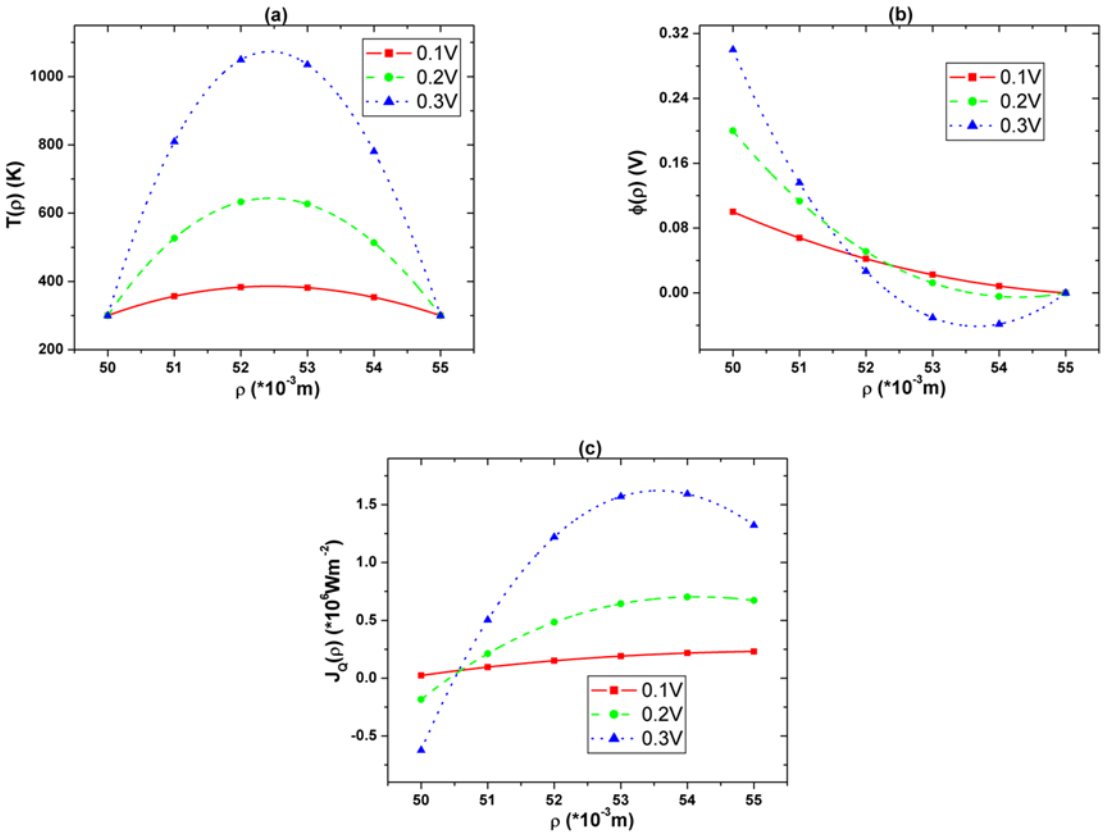

Figure 5.5: The distributions of (a) temperature, (b) electric potential, and (c) heat flux in a homogeneous shell under imposed electric potential differences[84].

heat flux is no longer constant, as we discussed. On the other hand, if only an electric potential difference is imposed with ϕ_2=0.0 and ϕ_1=0.1, 0.2, 0.3V, the corresponding results for homogeneous shell and core-shell composites are shown in Fig. 5.5 and Fig. 5.6. Here substantial temperature rise is observed, due to Joule heating. Inhomogeneous electric field is induced, even for homogeneous shell. Heat flux in the core-shell composite is substantially smaller, due to lower thermal conductivity of the phase B.

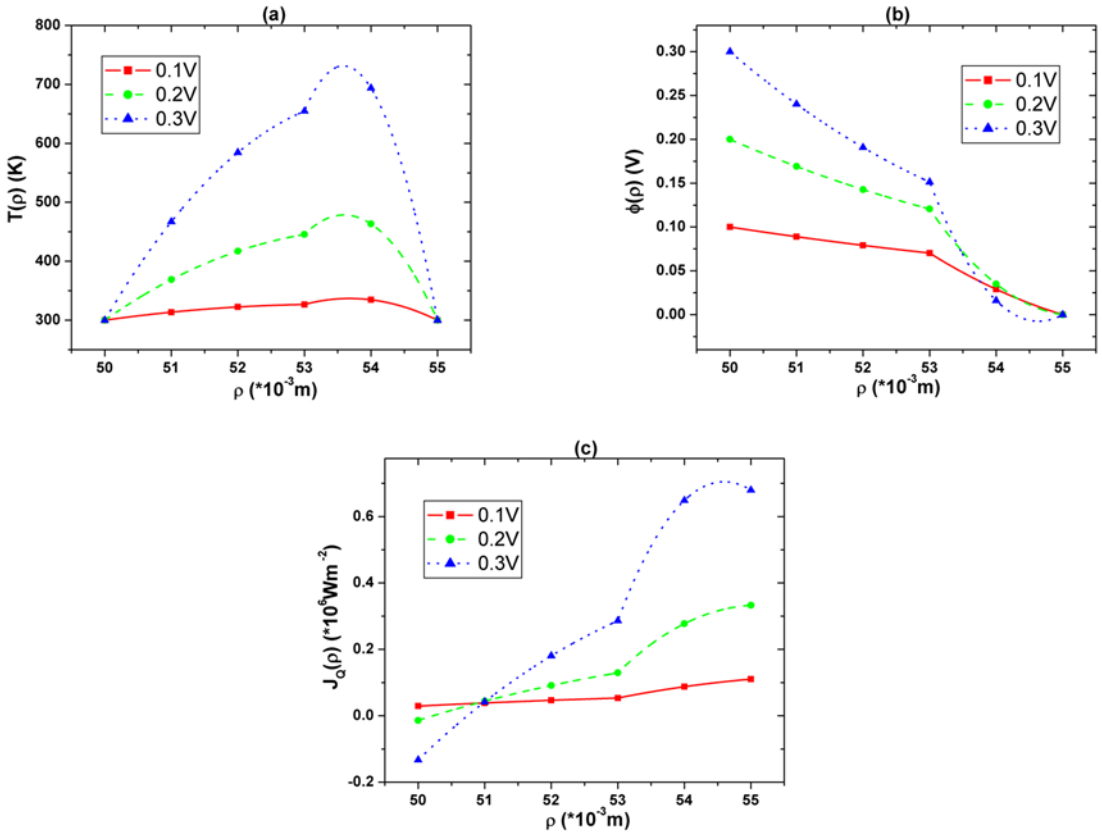

Figure 5.6: The distributions of (a) temperature, (b) electric potential, and (c) heat flux in a core-shell composite under imposed electric potential differences[84].

5.5.2 Effective properties

The effective electric conductivity, Seebeck coefficient, thermal conductivity, and figure of merit of Bi_2Te_3-$Ag(Pb_{1-y}Sn_y)_mSbTe_{2+m}$ core-shell composite are shown in Fig. 5.7, with the following boundary conditions imposed,

$$T_1 = T_2 = 300K, \quad \phi_1 = 0V, \quad \phi_2 = \{-0.5, -0.2, 0.2, 0.5\}V. \tag{5.46}$$

While the effective Seebeck coefficient and thermal conductivity only show slight deviation from the rule of mixture, as observed in Fig. 5.7(a) and 5.7(b), the nonlinear dependence of electric conductivity on thickness ratio is more significant, and it is sensitive to the voltage difference imposed on the boundaries, as shown in Fig. 5.7(c). This results in large difference in the effective thermoelectric figure of merit shown in Fig. 5.7(d). What is most interesting is that there is a peak, albeit small, in the effective thermoelectric figure of merit that exceed both constituents, at $p = 0.939$, when the imposed potential difference is $\phi_2 = -0.5V$. This is significant, since it demonstrates that the effective thermoelectric figure of merit of a heterogeneous medium can be higher than both of its constituents.

Table 5.1: Thermoelectric properties of the optimal constituent B under different temperature boundary conditions[84].

Material	α ($\times 10^{-6}$V/K)	σ ($\times 10^3$S/m)	κ (W/m/K))	$Z(\times 10^{-3}K^{-1})$
800K Optimal	241.668	4.79423	0.1	2.80000
1000K Optimal	246.989	4.58989	0.1	2.80000
1200K Optimal	251.577	4.42401	0.1	2.80000

5.5.3 Conversion efficiency

To examine if the composite can have higher conversion efficiency than both of its constituents, we calculate efficiency of core-shell composites consisting of Bi_2Te_3 and a second phase optimally matched (in a sense to be elaborated later) with Bi_2Te_3 under different

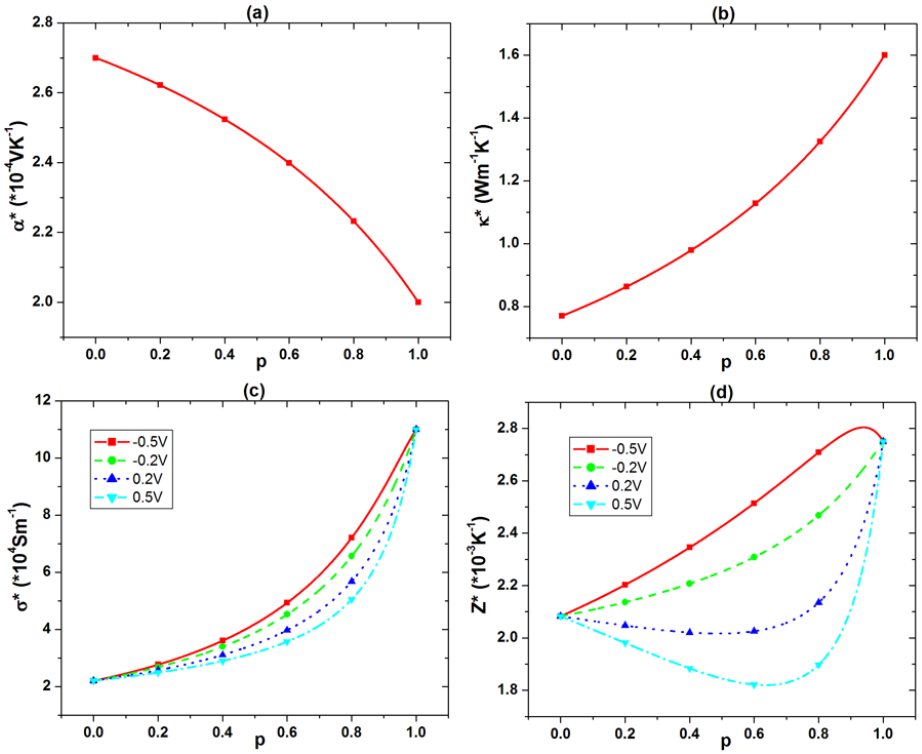

Figure 5.7: The effective (a) Seebeck coefficient, (b) thermal conductivity, (c) electric conductivity, and (d) figure of merit as functions of thickness ratio[84].

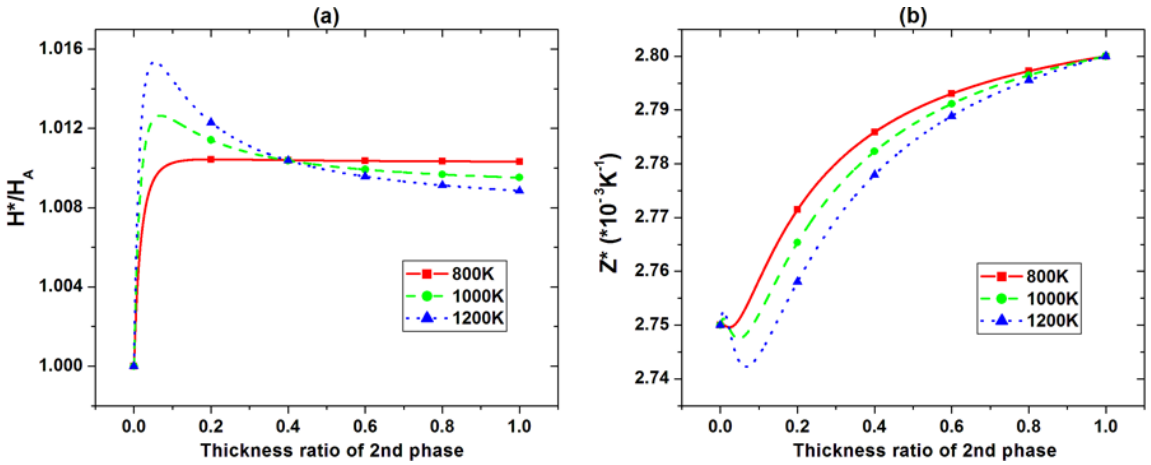

Figure 5.8: Conversion efficiency of the core-shell composite consisting of Bi_2Te_3 and an optimally second phase for different temperatures; (a) enhanced conversion efficiency of the composite, normalized by the efficiency of the first phase, versus the thickness ratio of the second phase; (b) the effective figure of merit calculated from the effective thermoelectric properties versus the thickness ratio of the second phase[84].

temperatures, with $T_2 = 300K$ and T_1 chosen to be $800, 1000, 1200K$, respectively. The material constants used in the calculation are listed in Table 5.1. The results are illustrated as a function of thickness ratio of the second phase in Fig. 5.8(a), and it is observed that higher efficiency than both constituents is indeed possible. Furthermore, we evaluate the corresponding effective Z^* with the effective Seebeck coefficient and thermal conductivity calculated under open circuit condition and the effective electric conductivity derived under optimal thermoelectric loading condition. As evident in Fig. 5.8(b), it shows no enhancement at all and there appears no correlation between the effective Z^* and the conversion efficiency of the composite. This demonstrates that the effective thermoelectric properties of composite are ill-defined, and we have to examine the conversion efficiency directly.

In order to understand the enhanced conversion efficiency in core-shell composite, we rewrite the conversion efficiency as

$$H = \frac{\phi_2 c}{(\rho J_U)|_{\rho=\rho_1}} = \frac{\phi_2 c}{T_1 \alpha c - \frac{c^2}{2\sigma}\ln\frac{\rho_2}{\rho_1} - \kappa(T_2 - T_1)/\ln\frac{\rho_2}{\rho_1}}. \tag{5.47}$$

for a homogeneous material, which can be optimized with respect to c for given tempera-

tures, resulting in

$$c_{\text{opt}} = \frac{\sqrt{2\kappa}\sigma\alpha(T_1 - T_2)}{[\sqrt{2\kappa} + \sqrt{2\kappa + \sigma\alpha^2(T_1 + T_2)}]\ln\frac{\rho_2}{\rho_1}}. \tag{5.48}$$

Since c is a constant in the core-shell composite, this points to a need for carefully matching the c_{opt} in constituent phases for the optimal overall conversion efficiency. It is evident that the core-shell composite can have its constituent phases matched for identical c_{opt} by tailoring the material properties, which is impossible for homogeneous materials to do. In other words, both segments of core-shell composite operate at optimal condition, while the corresponding segments of homogeneous materials operate under less optimal ones. This explains higher conversion efficiency in optimally matched core-shell composite. The analysis on core-shell composite thus points to a direction for optimal conversion efficiency of thermoelectric module, wherein c_{opt} is matched everywhere, resulting in highest conversion efficiency possible. To this end, we reorganize Eq. (5.48) by replacing $(T_2 - T_1)/\ln\frac{\rho_2}{\rho_1}$ with $\rho\nabla T$, leading to a point-wise optimal value of

$$c_{\text{opt}} = -\kappa\rho\nabla T\frac{\sqrt{1 + ZT} - 1}{\alpha T}, \tag{5.49}$$

which corresponds to maximum local conversion efficiency of

$$dH_{\max} = \frac{\sqrt{1 + ZT} - 1}{\sqrt{1 + ZT} + 1}\frac{dT}{T}. \tag{5.50}$$

This is equivalent to the concept of compatibility factor[75], with the value corresponding to reduce current density here being $u = -\frac{c}{\kappa\rho\nabla T}$. When the optimality is realized everywhere, maximum overall efficiency is realized as

$$\begin{aligned} H_{\max} &= 1 - \exp(-\int_{T_2}^{T_1}\frac{\sqrt{1 + ZT} - 1}{\sqrt{1 + ZT} + 1}\frac{dT}{T}) \\ &= 1 - \exp(\frac{2}{\sqrt{1 + ZT_2} + 1} - \frac{2}{\sqrt{1 + ZT_1} + 1} + 2\ln\frac{\sqrt{1 + ZT_2} + 1}{\sqrt{1 + ZT_1} + 1}), \end{aligned} \tag{5.51}$$

where we have taken Z to be a constant for simpler derivation. This is in fact the upper bound on the conversion efficiency for the core-shell composite consisting of materials with constant Z. Compared to classical conversion efficiency of a homogeneous material, it shows a small yet definite enhancement, see Fig. 4.4c.

5.6 Summary

In this chapter, we have analyzed axially-symmetric thermoelectric problems that are particularly relevant for waste heat recovery using automobile exhaust pipe. Building on the field analysis of polar symmetry, we show that higher thermoelectric conversion efficiency can be achieved in core-shell composites, while the effective figure of merit is not well defined.

Chapter 6

ASYMPTOTIC ANALYSIS OF ONE-DIMENSIONAL THERMOELECTRIC MEDIUM

6.1 Introductory remarks

In foregoing chapters, we analyzed bi-layered composites and core-shell composites, however, they are structures without macroscopic homogeneity. In this chapter, we study the thermoelectric composite with periodic microstructure[85]. For that matter, asymptotic homogenization[86–93] is carried out.

We first apply one-dimension asymptotic analysis in Section 2 to derive the homogenized governing equation for thermoelectric composites. From that, we study the effective behavior in Section 3, including solving for the macroscopic fields, defining the effective properties, and analyzing the conversion efficiency. The numerical results and discussions are given in Section 4. The summary for the chapter is in Section 5.

6.2 One-dimensional asymptotic analysis

We confine our scope to one-dimensional (1D) system in this chapter, wherein all the field variables and materials parameters are assumed to be dependent only on coordinate x, and independent of y and z, and the thermoelectric transport equations are simplified as

$$-J = \sigma\frac{d\phi}{dx} + \sigma\alpha\frac{dT}{dx}, \tag{6.1}$$

$$J_Q = \alpha T J - \kappa\frac{dT}{dx}. \tag{6.2}$$

In addition, the divergence-free of current density implies that $J = |\mathbf{J}| = const$ in 1D, and the field equation for heat flux is simplified as

$$\frac{dJ_Q}{dx} = -\frac{d\phi}{dx}J. \tag{6.3}$$

The transport equations can be combined with the field equation, resulting in the following governing equations for temperature and electric potential in a homogeneous medium

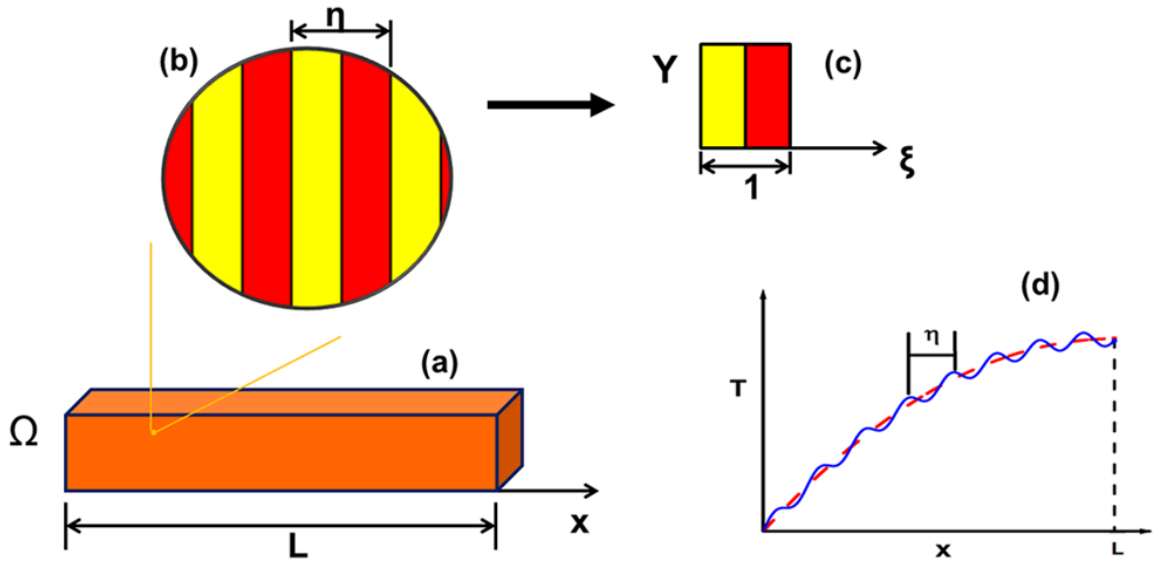

Figure 6.1: Schematics of layered composite in (a) macroscopic, (b) mesoscopic, and (c) microscopic scales, with (d) fast fluctuating actual field (solid blue line) and slow varying homogenized field (dashed red line)[93].

wherein all the thermoelectric properties are constant,

$$\frac{d^2T}{dx^2} + \frac{1}{\sigma\kappa}J^2 = 0, \tag{6.4}$$

$$\frac{d^2\phi}{dx^2} - \frac{\alpha}{\sigma\kappa}J^2 = 0, \tag{6.5}$$

resulting in quadratic distribution of temperature and potential distributions

$$T(x) = -\frac{J^2}{2\sigma\kappa}x^2 + k_1x + k_2, \tag{6.6}$$

$$\phi(x) = \frac{\alpha J^2}{2\sigma\kappa}x^2 - (\frac{J}{\sigma} + \alpha k_1)x + k_3, \tag{6.7}$$

and a constant current density

$$J = \frac{-\sigma\alpha[T(L) - T(0)] - \sigma[\phi(L) - \phi(0)]}{L}, \tag{6.8}$$

with

$$k_1 = \frac{[T(L) - T(0)]}{L} + \frac{J^2L}{2\sigma\kappa}, \quad k_2 = T(0), \quad k_3 = \phi(0), \tag{6.9}$$

where $T(x)$ and $\phi(x)$ at $x = 0, L$ are specified as the boundary conditions. The heat flux is then calculated as

$$J_Q(x) = -\frac{\alpha J^3}{2\sigma\kappa}x^2 + (\frac{J^2}{\sigma} + \alpha J k_1)x - \kappa k_1 + \alpha J k_2. \tag{6.10}$$

We consider a 1D composite consisting of two distinct phases layered periodically, as schematically shown in Fig. 6.1. For such a composite, two different length scales can be identified, one is L, the macroscopic length of the composite associated with the macroscopic coordinate x. The other is η, the characteristic length of the composite unit cell, for which a microscopic coordinate $\xi = x/\eta$ can be introduced. While the material properties $\alpha(\xi)$, $\sigma(\xi)$, and $\kappa(\xi)$ vary fast on the microscopic scale periodically, the field variables such as $T(x,\xi)$, $\phi(x,\xi)$, and $J_Q(x,\xi)$ vary both fast on microscopic scale and slowly on macroscopic scale, as schematically shown in Fig. 6.1(d). What we are interested in is the macroscopic variation of these field variables, for which the fast microscopic fluctuation is averaged out, so that the effective behavior of the composite can be deduced.

To this end, we expand the temperature, potential, and heat flux into polynomials of η

$$T(x,\xi) = T_0(x,\xi) + \eta T_1(x,\xi) + \eta^2 T_2(x,\xi) + ..., \tag{6.11}$$

$$\phi(x,\xi) = \phi_0(x,\xi) + \eta\phi_1(x,\xi) + \eta^2\phi_2(x,\xi) + ..., \tag{6.12}$$

$$J_Q(x,\xi) = J_{Q0}(x,\xi) + \eta J_{Q1}(x,\xi) + \eta^2 J_{Q2}(x,\xi) + ... \tag{6.13}$$

Inserting these into governing equations (6.1) and (6.3) for T and ϕ, and notice that

$$\frac{d}{dx} \to \frac{\partial}{\partial x} + \frac{1}{\eta}\frac{\partial}{\partial \xi}, \tag{6.14}$$

we obtain a series of equations grouped by the orders of η as following,

η^{-2}:

$$\frac{\partial}{\partial \xi}(\kappa\frac{\partial T_0}{\partial \xi}) = 0, \tag{6.15}$$

η^{-1}:

$$\sigma\frac{\partial \phi_0}{\partial \xi} + \sigma\alpha\frac{\partial T_0}{\partial \xi} = 0, \tag{6.16}$$

$$\frac{\partial}{\partial x}(\kappa\frac{\partial T_0}{\partial \xi}) + \frac{\partial}{\partial \xi}(-\alpha J T_0 + \kappa\frac{\partial T_0}{\partial x} + \kappa\frac{\partial T_1}{\partial \xi}) = \frac{\partial \phi_0}{\partial \xi}J, \tag{6.17}$$

η^0:

$$-J = \sigma(\frac{\partial \phi_0}{\partial x} + \frac{\partial \phi_1}{\partial \xi}) + \sigma\alpha(\frac{\partial T_0}{\partial x} + \frac{\partial T_1}{\partial \xi}), \tag{6.18}$$

$$\begin{aligned}(\frac{\partial \phi_0}{\partial x} + \frac{\partial \phi_1}{\partial \xi})J &= \frac{\partial}{\partial x}(-\alpha J T_0 + \kappa\frac{\partial T_0}{\partial x} + \kappa\frac{\partial T_1}{\partial \xi}) \\ &+ \frac{\partial}{\partial \xi}(-\alpha J T_1 + \kappa\frac{\partial T_1}{\partial x} + \kappa\frac{\partial T_2}{\partial \xi}).\end{aligned} \tag{6.19}$$

We first examine $T_0(x,\xi)$ and $\phi_0(x,\xi)$, the lowest order of field variables. By integrating Eq. (6.15) and rearranging the equation, we obtain

$$\frac{\partial T_0}{\partial \xi} = \frac{C_1(x)}{\kappa(\xi)}. \tag{6.20}$$

Since $T_0(x,\xi)$ is periodic in ξ, and the integration of $\frac{\partial T_0}{\partial \xi}$ over the unit cell vanishes, it is concluded that $C_1(x) = 0$, and thus

$$T_0(x,\xi) = T_0(x). \tag{6.21}$$

Combining this with Eq. (6.16), it is also evident that

$$\phi_0(x,\xi) = \phi_0(x). \tag{6.22}$$

In other words, $T_0(x)$ and $\phi_0(x)$ do not vary on microscopic scale, and they represent the macroscopic distributions of temperature and potential when $\eta \to 0$. They thus describe the effective behavior of the layered composite with local fluctuations of temperature and potential averaged out, which we seek to determine.

We then examine $T_1(x,\xi)$ and $\phi_1(x,\xi)$. Making use of Eqs. (6.21) and (6.22), we can integrate Eq. (6.17) with respect to ξ as

$$\frac{\partial T_1}{\partial \xi} = -\frac{dT_0}{dx} + \frac{\alpha(\xi)}{\kappa(\xi)} J T_0(x) + \frac{C_2(x)}{\kappa(\xi)}, \tag{6.23}$$

with

$$C_2 = <\frac{1}{\kappa}>^{-1} (\frac{dT_0}{dx} - <\frac{\alpha}{\kappa}> J T_0) \tag{6.24}$$

determined again from the periodicity of $T_1(x,\xi)$ on the unit cell, where $< \cdot >$ is used to indicate volume averaged quantities over the unit cell. Integrating Eq. (6.23) one more

time, we obtain

$$\begin{aligned} T_1(x,\xi) &= \frac{dT_0}{dx}\int_0^\xi (\kappa^{-1} < \frac{1}{\kappa} >^{-1} -1)d\xi \\ &- JT_0 \int_0^\xi (\kappa^{-1} < \frac{1}{\kappa} >^{-1} < \frac{\alpha}{\kappa} > -\frac{\alpha}{\kappa})d\xi, \end{aligned} \tag{6.25}$$

for which the integration constant $C_3(x)$ is assumed to be zero without loss of generality, since it can be incorporated into $T_0(x)$. Similarly, Eq. (6.18) can be recast as

$$\begin{aligned} \frac{\partial \phi_1}{\partial \xi} &= -\frac{J}{\sigma} - \frac{d\phi_0}{dx} - \frac{\alpha}{\kappa} < \frac{1}{\kappa} >^{-1} \frac{dT_0}{dx} \\ &+ (\frac{\alpha}{\kappa} < \frac{1}{\kappa} >^{-1} < \frac{\alpha}{\kappa} > -\frac{\alpha^2}{\kappa})JT_0, \end{aligned} \tag{6.26}$$

which by integration yields

$$\begin{aligned} \phi_1(x,\xi) &= -J\int_0^\xi \frac{1}{\sigma}d\xi - \frac{d\phi_0}{dx}\xi - \frac{dT_0}{dx}\int_0^\xi \frac{\alpha}{\kappa} < \frac{1}{\kappa} >^{-1} d\xi \\ &+ JT_0 \int_0^\xi (\frac{\alpha}{\kappa} < \frac{1}{\kappa} >^{-1} < \frac{\alpha}{\kappa} > -\frac{\alpha^2}{\kappa})d\xi. \end{aligned} \tag{6.27}$$

As such, Eqs. (6.25) and (6.27) give $T_1(x,\xi)$ and $\phi_1(x,\xi)$ that fluctuate fast on the microscopic scale on the order of η. This will be sufficient for our analysis, and higher order fluctuations will not be considered.

In order to derive the governing equations for $T_0(x)$ and $\phi_0(x)$ that describe the effective behavior of the layered composite, we integrate Eq. (6.19) over the unit cell to obtain

$$\int_0^1 \frac{\partial}{\partial x}(-\alpha JT_0 + \kappa\frac{\partial T_0}{\partial x} + \kappa\frac{\partial T_1}{\partial \xi})d\xi = \int_0^1 (\frac{\partial \phi_0}{\partial x} + \frac{\partial \phi_1}{\partial \xi})Jd\xi, \tag{6.28}$$

which can be simplified by using Eqs. (6.23), (6.24), and (6.26), resulting in

$$\frac{d^2T_0}{dx^2} + < \frac{1}{\sigma} >< \frac{1}{\kappa} > J^2 - (< \frac{\alpha}{\kappa} >^2 - < \frac{\alpha^2}{\kappa} >< \frac{1}{\kappa} >)J^2T_0 = 0. \tag{6.29}$$

This is the governing equation for the macroscopic temperature distribution $T_0(x)$ in the layered composite. Furthermore, we integrate Eq. (6.26) over the unit cell to obtain

$$\begin{aligned} \frac{d\phi_0}{dx} &= - < \frac{1}{\sigma} > J - < \frac{\alpha}{\kappa} >< \frac{1}{\kappa} >^{-1} \frac{dT_0}{dx} \\ &+ (< \frac{1}{\kappa} >^{-1} < \frac{\alpha}{\kappa} >^2 - < \frac{\alpha^2}{\kappa} >)JT_0. \end{aligned} \tag{6.30}$$

By combining Eqs. (6.24) and (6.30), we can rewrite C_2 as

$$C_2 = - < \frac{\alpha}{\kappa} >^{-1} (\frac{d\phi_0}{dx} + < \frac{\alpha^2}{\kappa} > JT_0 + < \frac{1}{\sigma} > J), \tag{6.31}$$

which can be used to recast Eq. (6.28) as

$$\begin{aligned} \frac{d^2\phi_0}{dx^2} &- < \frac{1}{\sigma} >< \frac{\alpha}{\kappa} > J^2 + (< \frac{\alpha^2}{\kappa} > - < \frac{\alpha}{\kappa} >^2 < \frac{1}{\kappa} >^{-1}) J \frac{dT_0}{dx} \\ &- (< \frac{\alpha^2}{\kappa} >< \frac{\alpha}{\kappa} > - < \frac{\alpha}{\kappa} >^3 < \frac{1}{\kappa} >^{-1}) J^2 T_0 = 0. \end{aligned} \tag{6.32}$$

This is the governing equation for the macroscopic potential distribution $\phi_0(x)$ in the layered composite.

Equations (6.29) and (6.32) are homogenized governing equations for temperature and potential distribution in layered periodic composite, one of key results in this work, and the coefficients in these equations can be easily determined from the volume averages of appropriate quantities in the unit cell. These homogenized governing equations are considerably more complicated than those of homogeneous materials, Eqs. (6.4) and(6.5), a consequence of nonlinearly coupled transport equations[94,95], and it is easy to verify that under limiting case of homogeneous materials, the homogeneous governing equations are recovered. With $T_0(x)$ and $\phi_0(x)$ solved from Eqs. (6.29) and (6.32), the macroscopic distribution of heat flux can be derived as

$$J_{Q0} = < \frac{1}{\kappa} >^{-1} (< \frac{\alpha}{\kappa} > T_0 J - \frac{dT_0}{dx}), \tag{6.33}$$

where Eqs. (6.23) and (6.24) have been used. Thus the problem is completely solved, if we can determine the macroscopic temperature and potential distributions along with the constant current density, which we seek to solve in the next section. We can further determine the local fluctuations of temperature and potential from Eqs. (6.25) and (6.27), though we are more interested in the effective behavior, and this line of investigation will not be pursued here.

6.3 The effective behavior

6.3.1 Field analysis

In order to solve for the temperature distribution in the layered composite, we recast Eq. (6.29), a second order ordinary differential equation with constant coefficients, as

$$\frac{d^2T_0}{dx^2} + d_1T_0 + d_2 = 0, \tag{6.34}$$

with

$$d_1 = (< \frac{\alpha^2}{\kappa} >< \frac{1}{\kappa} > - < \frac{\alpha}{\kappa} >^2)J^2, \quad d_2 =< \frac{1}{\sigma} >< \frac{1}{\kappa} > J^2,$$

which can be solved as

$$T_0(x) = q_1\cos(\sqrt{d_1}x) + q_2\sin(\sqrt{d_1}x) - \frac{d_2}{d_1}, \tag{6.35}$$

where q_1 and q_2 are constants that can be determined by boundary conditions as,

$$q_1 = \frac{d_2}{d_1} + T(0), \quad q_2 = \frac{d_2/d_1 + T(L) - q_1\cos(\sqrt{d_1}L)}{\sin(\sqrt{d_1}L)}. \tag{6.36}$$

Not surprisingly, the functional variation of macroscopic temperature distribution of the layered composite is drastically different from the quadratic distribution of homogeneous materials in Eq. (6.6). Having derived $T_0(x)$, we can solve for $\phi_0(x)$ from Eq. (6.30) in a similar manner as,

$$\phi_0 = h_1x + h_2\sin(\sqrt{d_1}x) + h_3\cos(\sqrt{d_1}x) + h_4, \tag{6.37}$$

with

$$\begin{aligned}
h_1 &= - < \frac{1}{\sigma} > J - (< \frac{1}{\kappa} >^{-1} < \frac{\alpha}{\kappa} >^2 - < \frac{\alpha^2}{\kappa} >)J\frac{d_2}{d_1}, \\
h_2 &= - < \frac{1}{\kappa} >^{-1} < \frac{\alpha}{\kappa} > q_2 + (< \frac{1}{\kappa} >^{-1} < \frac{\alpha}{\kappa} >^2 - < \frac{\alpha^2}{\kappa} >)J\frac{q_1}{\sqrt{d_1}}, \\
h_3 &= - < \frac{1}{\kappa} >^{-1} < \frac{\alpha}{\kappa} > q_1 - (< \frac{1}{\kappa} >^{-1} < \frac{\alpha}{\kappa} >^2 - < \frac{\alpha^2}{\kappa} >)J\frac{q_2}{\sqrt{d_1}}, \\
h_4 &= \phi(0) - h_3.
\end{aligned}$$

Note that both temperature and potential distributions are given in terms of yet to be determined current density J, which can be solved from potential boundary condition at $x = L$,

$$\phi(L) = h_1 L + h_2 \sin(\sqrt{d_1} L) + h_3 \cos(\sqrt{d_1} L) + h_4. \tag{6.38}$$

With the current density J determined as such, the heat and energy fluxes can be determined accordingly,

$$\begin{aligned} J_{Q0} &= - < \frac{1}{\kappa} >^{-1} [(-q_1 \sqrt{d_1} - < \frac{\alpha}{\kappa} > J q_2) \sin(\sqrt{d_1} x) \\ &+ (q_2 \sqrt{d_1} - < \frac{\alpha}{\kappa} > J q_1) \cos(\sqrt{d_1} x) + < \frac{\alpha}{\kappa} > J \frac{d_2}{d_1}], \end{aligned} \tag{6.39}$$

and

$$J_U = < \frac{1}{\kappa} >^{-1} (< \frac{\alpha}{\kappa} > T_0 J - \frac{dT_0}{dx}) + \phi_0 J. \tag{6.40}$$

These set of equations completely solved the macroscopic variation of temperature, potential, current density, heat flux, and energy flux in a layered composite, and thus completely describe its effective behavior.

6.3.2 The effective properties

With equivalency principle, we examine the effective electric conductivity first. Consider a boundary condition of imposed electric potential difference only with $\Delta T = 0$, and compare the current density between homogeneous thermoelectric and periodic composite, we conclude that the effective electric conductivity of the periodic composite is given by

$$\sigma^*(\Delta\phi, \Delta T = 0) = -\frac{J}{\Delta\phi / L}, \tag{6.41}$$

with the current density determined by Eq. (6.38). Since $\Delta T = 0$, the current density can be solved analytically, resulting in

$$\sigma^* = \frac{2}{v \Delta\phi} \tan^{-1}\{\frac{< \frac{1}{\kappa} > v \Delta\phi}{2[< \frac{1}{\sigma} >< \frac{1}{\kappa} > + v^2 T(0)]}\}, \tag{6.42}$$

with

$$v = \sqrt{< \frac{\alpha^2}{\kappa} >< \frac{1}{\kappa} > - < \frac{\alpha}{\kappa} >^2}.$$

Clearly, the effective electric conductivity depends on the imposed potential difference at boundary in addition to the material constants of the constituents and the volume fraction f, a characteristic distinct from linear medium. On the other hand, if we impose open-circuit boundary condition where $J = 0$, such that

$$\frac{d\phi_0}{dx} = - < \frac{\alpha}{\kappa} >< \frac{1}{\kappa} >^{-1} \frac{dT_0}{dx}, \tag{6.43}$$

the effective Seebeck coefficient can be derived as

$$\alpha^* = -\frac{\phi(L) - \phi(0)}{T(L) - T(0)} =< \frac{\alpha}{\kappa} >< \frac{1}{\kappa} >^{-1} . \tag{6.44}$$

In addition, under the condition of $J = 0$, we have

$$J_{Q0} = - < \frac{1}{\kappa} >^{-1} \frac{dT_0}{dx}, \tag{6.45}$$

from which the effective thermal conductivity can be derived as

$$\kappa^* = -\frac{J_{Q0}}{[T(L) - T(0)]/L} =< \frac{1}{\kappa} >^{-1} . \tag{6.46}$$

Notice that this effective thermal conductivity is identical to that of a layered linear thermal conductor uncoupled from electric conduction, since open circuit condition is assumed, and different effective Seebeck coefficient and thermal conductivity will be resulted if different electric boundary condition is imposed. From these effective thermoelectric properties, the effective thermoelectric figure of merit is then defined as

$$Z^* = \frac{\sigma^* \alpha^{*2}}{\kappa^*}, \tag{6.47}$$

though its connection with the thermoelectric conversion efficiency remains to be examined, which we analyze in the next subsection.

6.3.3 Thermoelectric conversion efficiency

While the figure of merit is directly related to thermoelectric conversion efficiency for a homogeneous material, our analysis on bilayered thermoelectric composite indicates that it is not well defined for heterogenous thermoelectric. As a result, we analyze the thermoelectric conversion efficiency of the periodic layered composite directly, based on the thermoelectric

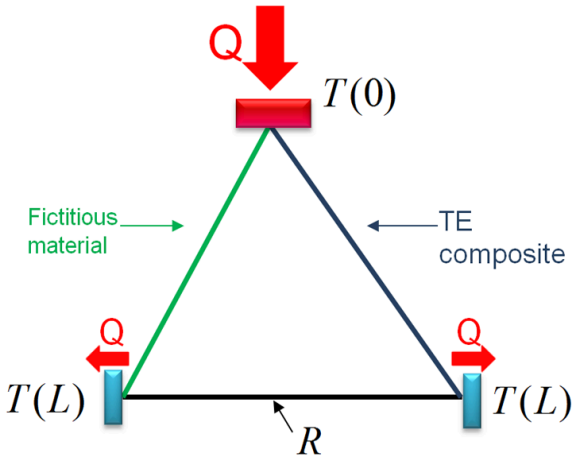

Figure 6.2: Schematics of the fictitious thermoelectric module for conversion efficiency analysis [93].

module schematically shown in Fig. 6.2. One leg of the module is made of material of interest, which is the layered composite with periodic microstructure, and the other leg is made of a fictitious material with zero Seebeck coefficient and thermal conductivity, yet infinite electric conductivity, and thus it only serves as a path for electric current, not involved in energy conversion [93]. The conversion efficiency of this idealized thermoelectric module, as a result, measures only the performance of the composite material of interest, and it can be defined as

$$H = \frac{(JA)^2 R}{\dot{E}_0} = \frac{(JA)^2 R}{A J_U|_{x=0}}, \tag{6.48}$$

where the numerator denotes the electric energy delivered to the load resistance, whereas the denominator denotes the heat (energy) flowing in at the joint from the hot reservoir with temperature $T(0)$. From Eq. (6.40), it is derived that

$$J_U|_{x=0} = <\frac{1}{\kappa}>^{-1} [<\frac{\alpha}{\kappa}> T(0) J - \frac{dT_0}{dx}|_{x=0}], \tag{6.49}$$

and the current density J can be determined from integral of $\nabla\phi$ around the circuit,

$$\oint \nabla\phi \cdot d\mathbf{r} = 0, \tag{6.50}$$

which replaces the imposed potential at boundaries we used earlier. The efficiency can be optimized with respect to the load resistance R, and for homogeneous materials, this lead

to classical equation relating figure of merit ZT to optimal conversion efficiency under given temperature difference,

$$H_{\rm opt} = \frac{T_h - T_c}{T_h} \frac{\sqrt{1 + Z\frac{T_h+T_c}{2}} - 1}{\sqrt{1 + Z\frac{T_h+T_c}{2}} + \frac{T_c}{T_h}}, \tag{6.51}$$

where T_h and T_c refer to temperatures at hot and cold ends. For composite materials, however, such simple relationship is no longer available, and we have to evaluate the optimal conversion efficiency numerically in general. Alternatively, it is sometimes insightful to recast the conversion efficiency as

$$H = \frac{\phi(L)J}{J_U|_{x=0}} = \frac{\phi(L)J}{<\frac{1}{\kappa}>^{-1}(<\frac{\alpha}{\kappa}>T(0)J - \frac{dT_0}{dx}|_{x=0})}, \tag{6.52}$$

with

$$\begin{aligned} \phi(L) &= -<\frac{1}{\sigma}>JL - <\frac{\alpha}{\kappa}><\frac{1}{\kappa}>^{-1}[T(L) - T(0)] \\ &+ (<\frac{1}{\kappa}>^{-1}<\frac{\alpha}{\kappa}>^2 - <\frac{\alpha^2}{\kappa}>)J\int_0^L T_0 dx, \end{aligned} \tag{6.53}$$

where $\phi(0) = 0$ is assumed without loss of generality. The efficiency can then be optimized equivalently with respect to the current density instead, though the current density is upper bounded by the current density achieved without the load resistance. These two approaches for deriving the optimal conversion efficiency are equivalent, and both requires numerical computation in general, yet the one using current density is more efficient numerically.

6.4 Numerical results and discussions

6.4.1 Field distributions

To demonstrate the analysis, we consider a periodic thermoelectric composite consisting of Bi_2Te_3 and $Ag(Pb_{1-y}Sn_y)_mSbTe_{2+m}$, with their thermoelectric properties listed in Table 3.1 and the volume fraction of Bi_2Te_3 being f. Consider either only a temperature difference or an electric potential difference is imposed, and the corresponding distributions of temperature, electric potential, and heat flux are shown in Figs. 6.3 and 6.4, where $f = 0.4$ is assumed, and homogeneous materials with $f = 0, 1$ are also included for comparison. It

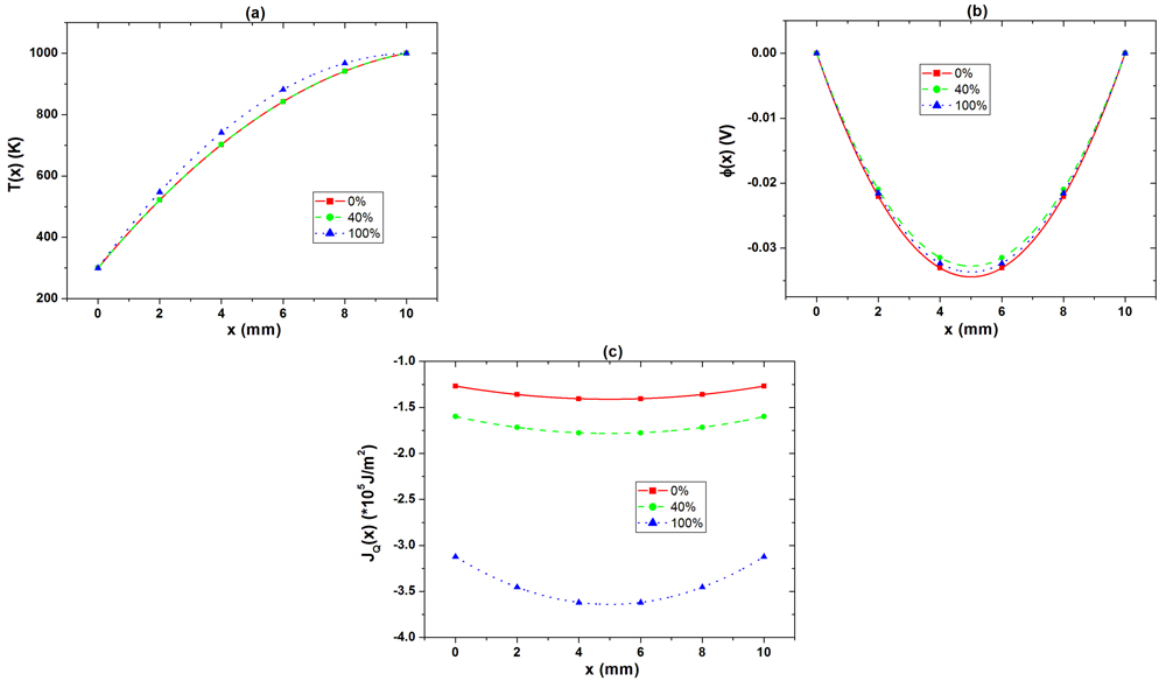

Figure 6.3: The distributions of (a) temperature, (b) electric potential, and (c) heat flux in thermoelectric composite under an imposed temperature difference of $T(0) = 300$K and $T(L) = 1000$K, with $\phi(0) = \phi(L) = 0$ and $f = 0, 0.4, 1$ [93].

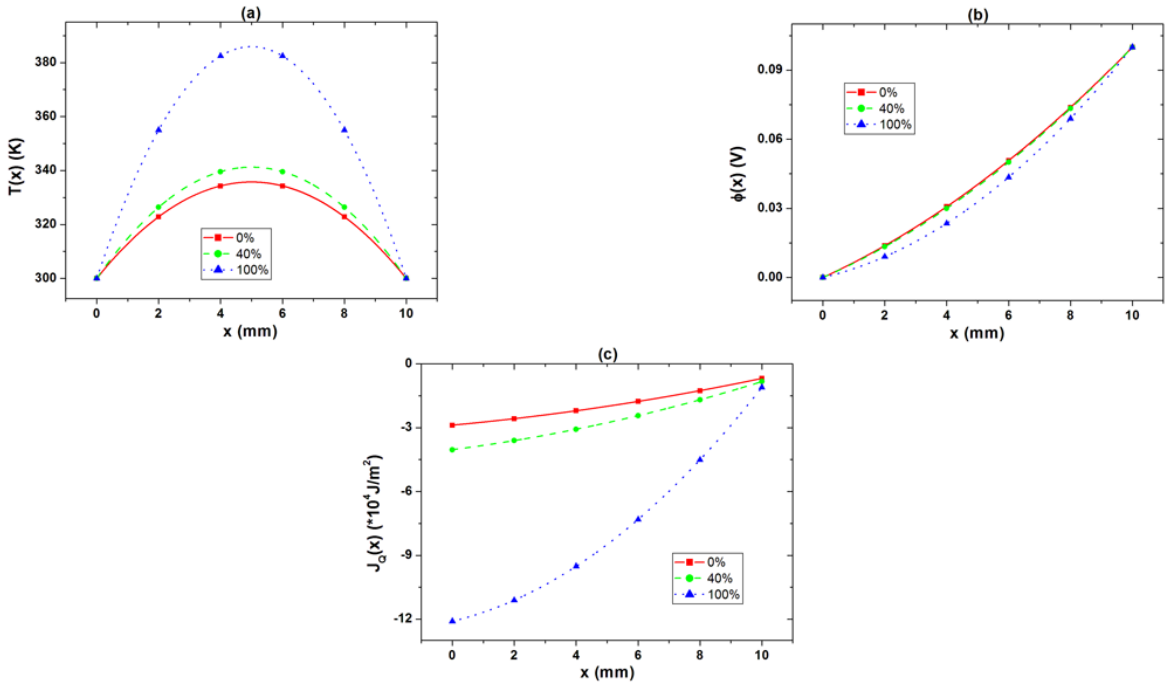

Figure 6.4: The distributions of (a) temperature, (b) electric potential, and (c) heat flux in thermoelectric composite under an imposed electric potential difference of $\phi(0) = 0$ and $\phi(L) = 0.1$V, with $T(0) = T(L) = 300$K and $f = 0, 0.4, 1$ [93].

is observed that under both types of boundary conditions, the field distributions are highly nonlinear, as expected, and the heat flux is not constant. Notable temperature rising is also observed in Fig. 6.4 inside of the composite under imposed potential difference, due to Joule heating, and the increase in temperature is most prominent in Bi_2Te_3, which has higher electric conductivity, and its heat flux is also larger due to higher thermal conductivity.

Table 6.1: By fitting curves of temperature, electric potential, and heat flux of composite to homogeneous results, sets of thermoelectric properties are derived[93].

Under imposed ΔT:			
Curves fitted	α ($\times 10^{-6}$V/K)	σ ($\times 10^{4}$S/m)	κ (W/m/K))
T_0	541	635	890
ϕ_0	467	440	838
J_{Q0}	29077	0.0002	1
Under imposed $\Delta\phi$:			
Curves fitted	α ($\times 10^{-6}$V/K)	σ ($\times 10^{4}$S/m)	κ (W/m/K))
T_0	2424	3156	957
ϕ_0	1016	809	985
J_{Q0}	276	3	620

It is worth noting that the quantitative variations of temperature and electric potential for the layered composite are not much different from those of homogeneous materials, despite drastically different functional forms. This motivates us to fit the distributions of temperature, potential, or the heat flux in the composite using homogeneous solutions, Eqs. (6.6), (6.7), and (6.10). The resulting sets of thermoelectric properties identified from these fittings are listed in Table 6.1, where it is observed that different curves resulting in thermoelectric constants that differ in orders of magnitude, for both types of boundary conditions. In other words, it is impossible to identify a consistent set of effective thermoelectric

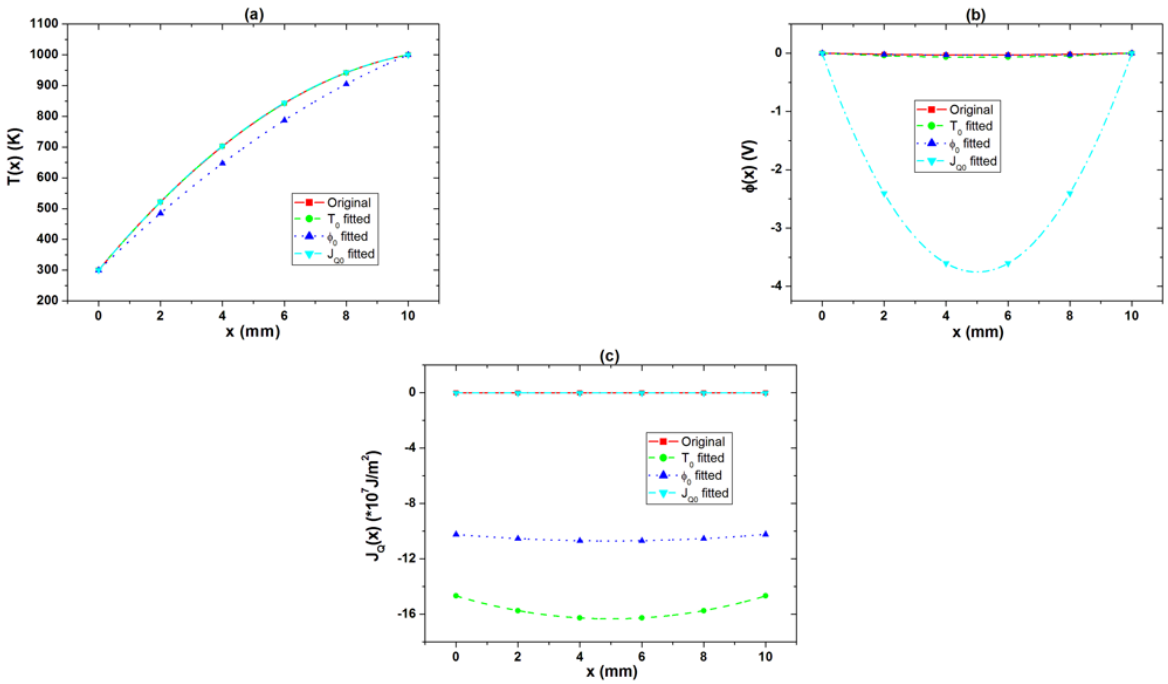

Figure 6.5: Distribution of (a) temperature, (b) electric potential, and (c) heat flux of thermoelectric composite are fitted to the solutions of homogeneous material for $T(0) = 300\text{K}$, $T(L) = 1000\text{K}$, $\phi(0) = \phi(L) = 0$, and f=0.4 [93].

properties that fit the distributions of temperature, potential, and heat flux simultaneously under given boundary conditions. The comparison of original distributions and fitted results shown in Figs. 6.5 and 6.6 also confirm this observation. For example, in Fig. 6.5, it is observed that the data fitted by heat flux leads to good agreement for temperature distribution, yet results in poor agreement for potential. In Fig. 6.6, on the other hand, the data fitted by heat flux results in poor agreement for both temperature and potential. Similar conclusion can be drawn for data fitted by temperature or potential. This highlights the difficulty in homogenizing the effective thermoelectric properties of the composite that would resemble the behavior of homogenous materials.

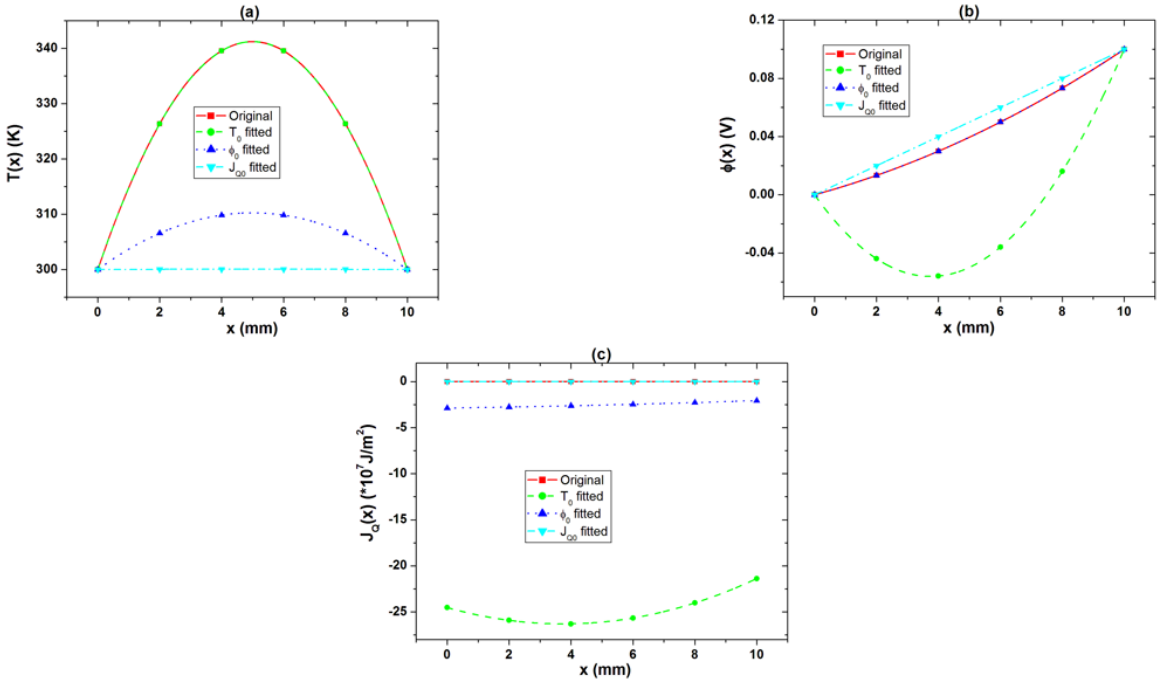

Figure 6.6: Distribution of (a) temperature, (b) electric potential, and (c) heat flux of thermoelectric composite are fitted to the solutions of homogeneous material for $\phi(0) = 0$, $\phi(L) = 0.1$V, $T(0) = T(L) = 300$K, and f=0.4[93].

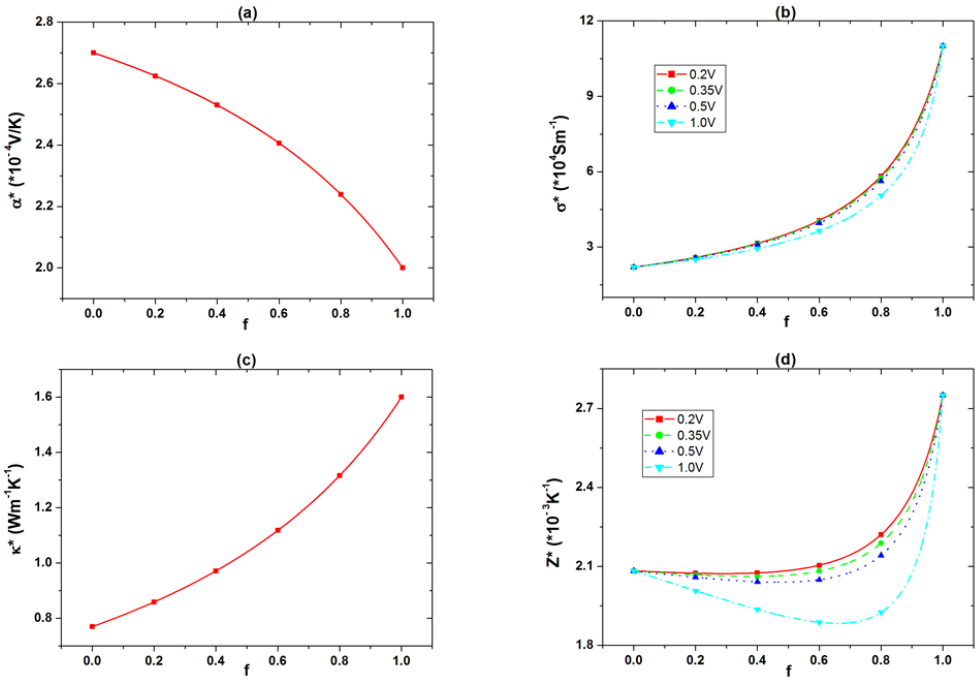

Figure 6.7: The effective thermoelectric properties calculated by equivalency principle; (a) electric conductivity; (b) Seebeck coefficient; (c) thermal conductivity; and (d) figure of merit [93].

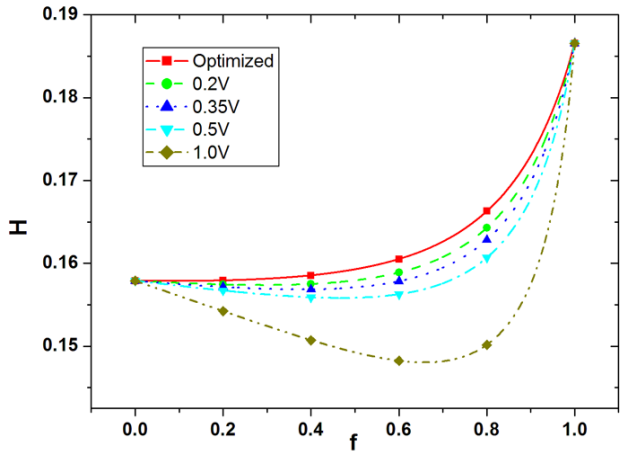

Figure 6.8: Conversion efficiencies of composite versus volume fraction. There is discrepancy between directly optimized value and the results converted from effective figures of merit from different boundary conditions [93].

6.4.2 The effective properties and conversion efficiency

Since it is impossible to find a set of effective thermoelectric properties of composite that will fit its distributions of temperature, potential, and heat flux into homogenous solution, we calculate the effective properties of the composite versus the volume fraction of Bi_2Te_3 using equivalency principle instead, as shown in Fig. 6.7, which ensures the equivalency in current density and energy flux between composite and homogeneous material with the identical set of properties. The effective Seebeck coefficient and thermal conductivity are calculated under open circuit condition, and the effective electric conductivity is evaluated with $T(0) = T(L) = 300\text{K}$ and $\Delta\phi = 0.2, 0.35, 0.5, 1.0\text{K}$. It is observed that there is a noticeable dependence of the effective electric conductivity and figure of merit on boundary condition. We further calculated the optimized conversion efficiency of the composite versus the volume fraction of Bi_2Te_3 with $T(0) = 800\text{K}$ and $T(L) = 300\text{K}$, as shown in Fig. 6.8, along with the conversion efficiency calculated using the effective figure of merit based on Eq. (6.51), and it is clear that there is a large discrepancy between the actual efficiency and the efficiency evaluated from the effective figure of merit, which depends on boundary condition. This suggest that the effective thermoelectric figure of merit of composite is not well defined, and does not correlate with its thermoelectric conversion efficiency.

The lack of correlation between the effective figure of merit and the thermoelectric conversion efficiency can be understood as following. To define the effective Seebeck coefficient, electric conductivity, and thermal conductivity, two sets of boundary conditions are required, making it impossible to match the actual optimal boundary condition under which the conversion efficiency is evaluated. This motivates us to suggest an alternative way to define the effective thermoelectric properties, using equivalency principle under optimal working condition in combination with the requirements of Eqs. (6.47) and (6.51) instead, and interestingly, this leads to two sets of effective properties, as shown in Fig. 6.9 along with the effective Z^*. This again suggests that the effective properties of thermoelectric composites are ill-defined.

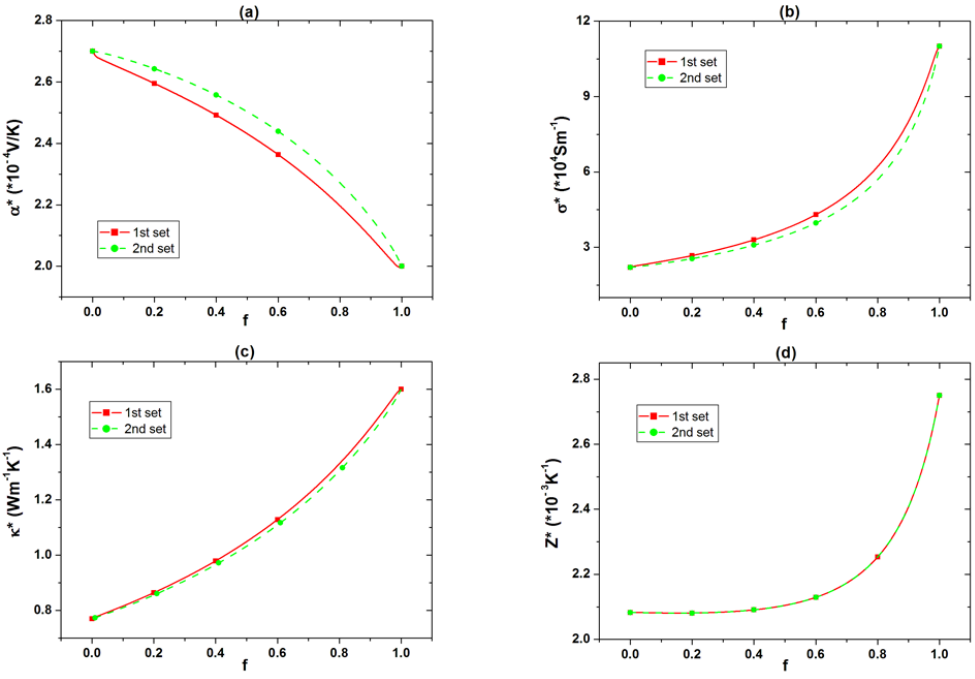

Figure 6.9: Two sets of effective thermoelectric properties corresponding to a given conversion efficiency, evaluated at $T(L) = 300\text{K}$, $T(0) = 1000\text{K}$; (a) electric conductivity; (b) Seebeck coefficient; (c) thermal conductivity; and (d) figure of merit[93].

6.5 Summary

In this chapter, we developed a rigorous nonlinear asymptotic homogenization theory to analyze the coupled transport of electricity and heat in thermoelectric composite materials, with which we solved for the macroscopic field distributions that are drastically different from those in homogeneous materials, analyzed the overall conversion efficiency using an idealized thermoelectric module, and showed that the effective thermoelectric properties are ill-defined, and the effective thermoelectric figure of merit does not directly correlate with the thermoelectric conversion efficiency.

Chapter 7

ASYMPTOTIC ANALYSIS OF TWO-DIMENSIONAL THERMOELECTRIC MEDIUM I: UNIT CELL PROBLEM

7.1 Introductory remarks

Our analysis in the previous chapter shows thermoelectric composite have more complex, yet more interesting field distributions than those of homogeneous materials. Conceivably, with the introduction of 2D or 3D unit cell configuration, and thus the introduction of more parameters, our problem will provide more room for manipulation. As we did in the last chapter, we apply asymptotic analysis on two-dimensional thermoelectric composite in this chapter.

We first establish the unit cell problem for 2D/3D in Section 2, where governing equations, interfacial conditions, boundary conditions for the unit cell problem are identified. In Section 3, we derive the homogenized governing equation for 2D/3D thermoelectric composites. In Section 4, we present an variation of unit cell problem, which has Neumann's boundary condition, making the unit cell isolated laterally. Section 5 summarizes the theory part of the 2D asymptotic analysis of thermoelectric composites.

7.2 Unit cell problem

We consider the three-dimensional coupled transports of heat and electrons in a thermoelectric material, with the respective transport equations given by

$$-\mathbf{J} = \sigma\nabla\phi + \sigma\alpha\nabla T, \tag{7.1}$$

$$\mathbf{J}_Q = -T\alpha\sigma\nabla\phi - (T\alpha^2\sigma + \kappa)\nabla T. \tag{7.2}$$

and conserved system such that

$$\nabla\cdot\mathbf{J} = 0, \tag{7.3}$$

$$\nabla\cdot\mathbf{J}_U = 0, \tag{7.4}$$

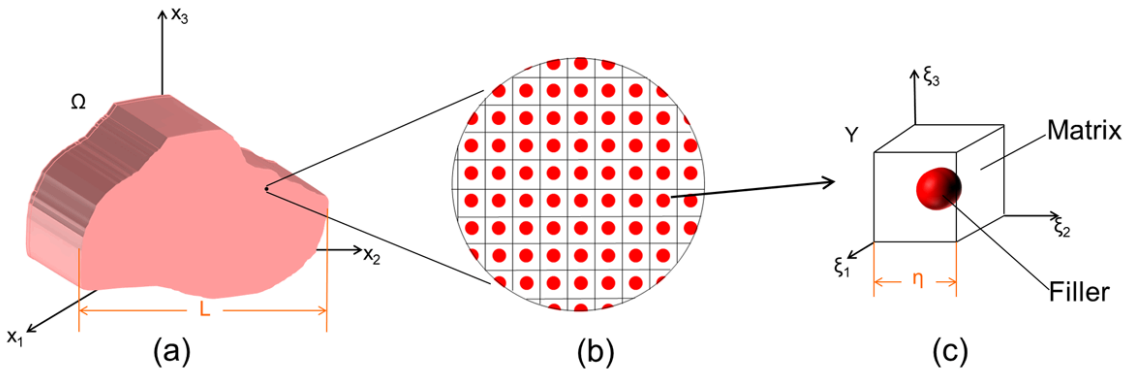

Figure 7.1: Schematics of a 3D composite in (a) macroscopic, (b) mesoscopic, and (c) microscopic scales.

with

$$\mathbf{J}_U = \mathbf{J}_Q + \phi\mathbf{J}. \tag{7.5}$$

As such, the distributions of electric potential and temperature are decided by the following coupled governing equations

$$\nabla \cdot (\sigma\nabla\phi + \sigma\alpha\nabla T) = 0, \tag{7.6}$$

$$\nabla \cdot (\kappa\nabla T + \sigma\phi\nabla\phi + \sigma\alpha\phi\nabla T + \sigma\alpha T\nabla\phi + \sigma\alpha^2 T\nabla T) = 0, \tag{7.7}$$

or

$$\frac{\partial}{\partial x_i}(D_{\rho\theta}\frac{\partial v_\theta}{\partial x_i}) + \frac{\partial}{\partial x_i}(E_{\rho\theta\zeta}v_\theta\frac{\partial v_\zeta}{\partial x_i}) = 0, \tag{7.8}$$

where

$$D_{\rho\theta} = \begin{bmatrix} \sigma & \sigma\alpha \\ 0 & \kappa \end{bmatrix}, \quad v_\theta = \begin{bmatrix} \phi \\ T \end{bmatrix}, \tag{7.9}$$

$$E_{\rho\theta1} = \begin{bmatrix} 0 & 0 \\ \sigma & \sigma\alpha \end{bmatrix}, \quad E_{\rho\theta2} = \begin{bmatrix} 0 & 0 \\ \sigma\alpha & \sigma\alpha^2 \end{bmatrix}. \tag{7.10}$$

The subscripts ρ, θ, ζ take values of 1, 2, while i takes value 1, 2 in two-dimensional space (2D), and 1, 2, 3 in three dimensions (3D). Note that in this tensor form, isotropic material

properties of σ, α, κ are assumed. If more general material properties are used, the material property matrices would be $D_{ij\rho\theta}$ and $E_{ij\rho\theta\zeta}$ to account for the anisotropy.

To apply asymptotic method and establish the unit cell problem, we consider a composite consisting of two distinct phases that are organized periodically, as schematically shown in Figure 7.1. For such a composite, two different length scales can be identified, one is L, the macroscopic length of the composite associated with the macroscopic coordinate x_i. The other is η, the characteristic length of the composite unit cell, for which a microscopic coordinate $\xi_i = x_i/\eta$ can be introduced. While the material properties $\alpha(\xi_i)$, $\sigma(\xi_i)$, and $\kappa(\xi_i)$ vary fast on the microscopic scale periodically, the field variables such as $T(x_i, \xi_i)$, $\phi(x_i, \xi_i)$ vary both fast on microscopic scale and slowly on macroscopic scale. What we are interested in is the macroscopic variation of these field variables, for which the fast microscopic fluctuation is averaged out, so that the effective behavior of the composite can be deduced.

To this end, we expand the temperature, potential into polynomials of η

$$v_\theta(x_i, \xi_i) = v_\theta^{(0)}(x_i, \xi_i) + \eta v_\theta^{(1)}(x_i, \xi_i) + \eta^2 v_\theta^{(2)}(x_i, \xi_i) + ..., \tag{7.11}$$

Inserting this into governing equation (7.8) for v_θ, and notice that

$$\frac{\partial}{\partial x_i} \to \frac{\partial}{\partial x_i} + \frac{1}{\eta}\frac{\partial}{\partial \xi_i}, \tag{7.12}$$

we obtain a series of equations grouped by the orders of η as the following,

η^{-2}:

$$\frac{\partial}{\partial \xi_i}[D_{\rho\theta}\frac{\partial v_\theta^{(0)}}{\partial \xi_i}] + \frac{\partial}{\partial \xi_i}[E_{\rho\theta\zeta} v_\theta^{(0)} \frac{\partial v_\zeta^{(0)}}{\partial \xi_i}] = 0, \tag{7.13}$$

η^{-1}:

$$\frac{\partial}{\partial \xi_i}[D_{\rho\theta}(\frac{\partial v_\theta^{(1)}}{\partial \xi_i} + \frac{\partial v_\theta^{(0)}}{\partial x_i})] + \frac{\partial}{\partial \xi_i}[E_{\rho\theta\zeta} v_\theta^{(1)} \frac{\partial v_\zeta^{(0)}}{\partial \xi_i} + E_{\rho\theta\zeta} v_\theta^{(0)}(\frac{\partial v_\zeta^{(1)}}{\partial \xi_i} + \frac{\partial v_\zeta^{(0)}}{\partial x_i})]$$
$$= -\frac{\partial}{\partial x_i}[D_{\rho\theta}\frac{\partial v_\theta^{(0)}}{\partial \xi_i}] - \frac{\partial}{\partial x_i}[E_{\rho\theta\zeta} v_\theta^{(0)} \frac{\partial v_\zeta^{(0)}}{\partial \xi_i}], \tag{7.14}$$

η^0:

$$\begin{aligned}
&\frac{\partial}{\partial \xi_i}[D_{\rho\theta}(\frac{\partial v_\theta^{(2)}}{\partial \xi_i}+\frac{\partial v_\theta^{(1)}}{\partial x_i})]\\
+\frac{\partial}{\partial \xi_i}[E_{\rho\theta\zeta}v_\theta^{(2)}\frac{\partial v_\zeta^{(0)}}{\partial \xi_i}+E_{\rho\theta\zeta}v_\theta^{(1)}(\frac{\partial v_\zeta^{(1)}}{\partial \xi_i}+\frac{\partial v_\zeta^{(0)}}{\partial x_i})+E_{\rho\theta\zeta}v_\theta^{(0)}(\frac{\partial v_\zeta^{(2)}}{\partial \xi_i}+\frac{\partial v_\zeta^{(1)}}{\partial x_i})]&\\
=-\frac{\partial}{\partial x_i}[D_{\rho\theta}(\frac{\partial v_\theta^{(1)}}{\partial \xi_i}+\frac{\partial v_\theta^{(0)}}{\partial x_i})]&\\
-\frac{\partial}{\partial x_i}[E_{\rho\theta\zeta}v_\theta^{(1)}\frac{\partial v_\zeta^{(0)}}{\partial \xi_i}+E_{\rho\theta\zeta}v_\theta^{(0)}(\frac{\partial v_\zeta^{(1)}}{\partial \xi_i}+\frac{\partial v_\zeta^{(0)}}{\partial x_i})]. &\qquad (7.15)
\end{aligned}$$

From equation (7.13), it can be concluded that $v_\theta^{(0)}=v_\theta^{(0)}(\mathbf{x})$ and does not depend on $\boldsymbol{\xi}$. Thus Eqs. (7.14) and (7.15) can be simplified as

$$\frac{\partial}{\partial \xi_i}[D_{\rho\theta}\frac{\partial v_\theta^{(1)}}{\partial \xi_i}]+\frac{\partial}{\partial \xi_i}[E_{\rho\theta\zeta}v_\theta^{(0)}\frac{\partial v_\zeta^{(1)}}{\partial \xi_i}]=-\frac{\partial D_{\rho\theta}}{\partial \xi_i}\frac{\partial v_\theta^{(0)}}{\partial x_i}-\frac{\partial E_{\rho\theta\zeta}}{\partial \xi_i}v_\theta^{(0)}\frac{\partial v_\zeta^{(0)}}{\partial x_i}, \qquad (7.16)$$

$$\begin{aligned}
&\frac{\partial}{\partial \xi_i}[D_{\rho\theta}\frac{\partial v_\theta^{(2)}}{\partial \xi_i}]+\frac{\partial}{\partial \xi_i}[E_{\rho\theta\zeta}v_\theta^{(0)}\frac{\partial v_\zeta^{(2)}}{\partial \xi_i}]\\
=-\frac{\partial}{\partial \xi_i}[D_{\rho\theta}\frac{\partial v_\theta^{(1)}}{\partial x_i}]-\frac{\partial}{\partial x_i}[D_{\rho\theta}(\frac{\partial v_\theta^{(1)}}{\partial \xi_i}+\frac{\partial v_\theta^{(0)}}{\partial x_i})]&\\
-\frac{\partial}{\partial \xi_i}[E_{\rho\theta\zeta}v_\theta^{(1)}(\frac{\partial v_\zeta^{(1)}}{\partial \xi_i}+\frac{\partial v_\zeta^{(0)}}{\partial x_i})+E_{\rho\theta\zeta}v_\theta^{(0)}\frac{\partial v_\zeta^{(1)}}{\partial x_i}]&\\
-\frac{\partial}{\partial x_i}[E_{\rho\theta\zeta}v_\theta^{(0)}(\frac{\partial v_\zeta^{(1)}}{\partial \xi_i}+\frac{\partial v_\zeta^{(0)}}{\partial x_i})]. &\qquad (7.17)
\end{aligned}$$

Existence and Uniqueness Theorem Before we continue, an existence and uniqueness theorem[86] is introduced here. The validness of all our further procedures rest on this important theorem.

Let $\mathbf{A}_{ij}(\boldsymbol{\xi})$ $(i,j=1,2,3)$ be $n\times n$ matrix-valued functions, $\mathbf{f}_k(\boldsymbol{\xi})$ $(k=0,1,2,3)$ be n-dimensional vector functions, and suppose the elements of $\mathbf{A}_{ij}(\boldsymbol{\xi})$, $\mathbf{f}_k(\boldsymbol{\xi})$ are bounded measurable functions, and are periodic in $\boldsymbol{\xi}$ with period of 1 (1-periodic). Let $\mathbf{A}_{ij}(\boldsymbol{\xi})=\mathbf{A}_{ji}(\boldsymbol{\xi})$ and the inequality

$$\langle(\mathbf{A}_{ij}\frac{\partial \mathbf{u}}{\partial \xi_j},\frac{\partial \mathbf{u}}{\partial \xi_i})\rangle\geq\epsilon\langle(\frac{\partial \mathbf{u}}{\partial \xi_i},\frac{\partial \mathbf{u}}{\partial \xi_i})\rangle,\quad \epsilon>0, \qquad (7.18)$$

hold for any n-dimensional vector function $\mathbf{u}(\boldsymbol{\xi}) \in W^{1,2}(\mathbf{R}^3)$. Here $(\mathbf{a}, \mathbf{b})$ denotes the scalar product of vectors $\mathbf{a}, \mathbf{b} \in \mathbf{R}^n$ and $\langle . \rangle$ is an averaged value evaluated on a unit cell in the following sense

$$\langle f(\xi_1, \xi_2, \xi_3) \rangle = \int_0^1 \int_0^1 \int_0^1 f(\xi_1, \xi_2, \xi_3) d\xi_1 d\xi_2 d\xi_3. \tag{7.19}$$

$W^{1,2}(\mathbf{R}^3)$ is a Sobolev space $W^{k,p}(\mathbf{R}^n)$ [96,97] where $k = 1, p = 2$ and the functions in Sobolev space are defined in 3D real space of $\mathbf{R}^3$. In case $\mathbf{A}_{ij}(\boldsymbol{\xi})$ and $\mathbf{f}_k(\boldsymbol{\xi})$ are smooth functions for $\boldsymbol{\xi} \in \mathbf{R}^3$, then a necessary and sufficient condition for the following system

$$\frac{\partial}{\partial \xi_i}(\mathbf{A}_{ij}(\boldsymbol{\xi}) \frac{\partial \mathbf{u}}{\partial \xi_j}) = \mathbf{f}_0(\boldsymbol{\xi}) + \frac{\partial}{\partial \xi_k} \mathbf{f}_k(\boldsymbol{\xi}) \tag{7.20}$$

to have 1-periodic solution is

$$\langle \mathbf{f}_0(\boldsymbol{\xi}) \rangle = \mathbf{0}. \tag{7.21}$$

The solution is unique up to a constant vector $\mathbf{c}$,

$$\mathbf{u}(\boldsymbol{\xi}) = \mathbf{u}_0(\boldsymbol{\xi}) + \mathbf{c}, \tag{7.22}$$

here $\mathbf{u}_0(\boldsymbol{\xi})$ is a solution of (7.20) satisfying the condition

$$\langle \mathbf{u}_0(\boldsymbol{\xi}) \rangle = \mathbf{0}. \tag{7.23}$$

In cases $\mathbf{A}_{ij}(\boldsymbol{\xi})$ is not perfectly smooth (e.g., piece-wise smooth as in multi-phased composites), the system of (7.20) is modified by multiplying an arbitrary n-dimensional 1-periodic function of $\boldsymbol{\varphi}(\boldsymbol{\xi})$ and integrating over the unit cell Ω to give

$$-\int_\Omega (\mathbf{A}_{ij} \frac{\partial \mathbf{u}}{\partial \xi_j}, \frac{\partial \boldsymbol{\varphi}}{\partial \xi_i}) d\boldsymbol{\xi} = \int_\Omega (\mathbf{f}_0, \boldsymbol{\varphi}) d\boldsymbol{\xi} - \int_\Omega (\mathbf{f}_k, \frac{\partial \boldsymbol{\varphi}}{\partial \xi_k}) d\boldsymbol{\xi}, \tag{7.24}$$

where the Divergence theorem is used, and the terms with area integration disappear because $(\mathbf{A}_{ij} \frac{\partial \mathbf{u}}{\partial \xi_j}, \boldsymbol{\varphi})$ and $(\mathbf{f}_k, \boldsymbol{\varphi})$ are periodic, on boundary the net effect will cancel out. For this system to have a solution $\mathbf{u}(\boldsymbol{\xi}) \in W^{1,2}(\mathbf{R}^3)$ that satisfies (7.24) for any 1-periodic trial vector function $\boldsymbol{\varphi}(\boldsymbol{\xi}) \in W^{1,2}(\mathbf{R}^3)$, the above condition and existence and uniqueness conclusion still apply. The solution $\mathbf{u}(\boldsymbol{\xi})$ in this this case is known as a generalized solution of system (7.20).

Comparing equation (7.16) with (7.20) reveals that (7.16) is an equation of $\boldsymbol{\xi}$ with the structure

$$\frac{\partial}{\partial \xi_i}[\widetilde{\mathbf{D}}\delta_{ij}\frac{\partial \mathbf{v}^{(1)}}{\partial \xi_j}] = \mathbf{f}(\boldsymbol{\xi}), \tag{7.25}$$

where δ_{ij} is the Kronecker delta and

$$\widetilde{D}_{\rho\zeta} = D_{\rho\zeta} + E_{\rho\theta\zeta}v_\theta^{(0)}, \quad f_\rho(\boldsymbol{\xi}) = -\frac{\partial D_{\rho\zeta}}{\partial \xi_i}\frac{\partial v_\zeta^{(0)}}{\partial x_i} - \frac{\partial E_{\rho\theta\zeta}}{\partial \xi_i}v_\theta^{(0)}\frac{\partial v_\zeta^{(0)}}{\partial x_i}.$$

So clearly the Existence and Uniqueness theorem applies here. And because $\langle f_\rho(\boldsymbol{\xi})\rangle = 0$ due to 1-periodic $D_{\rho\zeta}$ and $E_{\rho\theta\zeta}$, we know that (7.16) should have a unique solution (up to a constant vector).

7.2.1 Governing equations for unit cell problem

The first step to find out the solution $\mathbf{v}^{(1)}$ to equation (7.16) is to establish the governing equations for the unit cell problem. To do so, we are going to guess the structure of $\mathbf{v}^{(1)}$. It is hypothesized that

$$\begin{aligned} v_1^{(1)} &= \phi^{(1)} = N_i^{(1)}(\boldsymbol{\xi})\frac{1}{T^{(0)}-X}\frac{\partial \phi^{(0)}}{\partial x_i} + N_i^{(2)}(\boldsymbol{\xi})\frac{1}{T^{(0)}-X}\frac{\partial T^{(0)}}{\partial x_i} \\ &+ N_i^{(3)}(\boldsymbol{\xi})\frac{\partial \phi^{(0)}}{\partial x_i} + N_i^{(4)}(\boldsymbol{\xi})\frac{\partial T^{(0)}}{\partial x_i}, \end{aligned} \tag{7.26}$$

$$\begin{aligned} v_2^{(1)} &= T^{(1)} = M_i^{(1)}(\boldsymbol{\xi})\frac{1}{T^{(0)}-X}\frac{\partial \phi^{(0)}}{\partial x_i} + M_i^{(2)}(\boldsymbol{\xi})\frac{1}{T^{(0)}-X}\frac{\partial T^{(0)}}{\partial x_i} \\ &+ M_i^{(3)}(\boldsymbol{\xi})\frac{\partial \phi^{(0)}}{\partial x_i} + M_i^{(4)}(\boldsymbol{\xi})\frac{\partial T^{(0)}}{\partial x_i}, \end{aligned} \tag{7.27}$$

where $N_i^{(1)}(\boldsymbol{\xi}), N_i^{(2)}(\boldsymbol{\xi}), N_i^{(3)}(\boldsymbol{\xi}), N_i^{(4)}(\boldsymbol{\xi}), M_i^{(1)}(\boldsymbol{\xi}), M_i^{(2)}(\boldsymbol{\xi}), M_i^{(3)}(\boldsymbol{\xi}), M_i^{(4)}(\boldsymbol{\xi})$ are unknown variables of $\boldsymbol{\xi}$, X is a constant that needs to be determined. So by guessing the structure of (7.26-7.27), we are guessing that $\mathbf{v}^{(1)}$ is a function of linear combinations of $f(\boldsymbol{\xi})g(\mathbf{x})$, where $f(\boldsymbol{\xi})$ and $g(\mathbf{x})$ are respectively functions of $\boldsymbol{\xi}$ and $\mathbf{x}$ only. We then substitute (7.26-7.27) into (7.16), and collect terms that have the same factoring $g(\mathbf{x})$ functions. To be specific, we have

$\frac{1}{\widetilde{T}_0}\frac{\partial \phi_0}{\partial x_j}$:

$$\frac{\partial}{\partial \xi_i}[\sigma \frac{\partial N_j^{(1)}}{\partial \xi_i} + \sigma\alpha \frac{\partial M_j^{(1)}}{\partial \xi_i}] = 0, \tag{7.28}$$

$$\frac{\partial}{\partial \xi_i}[X\sigma\alpha \frac{\partial N_j^{(1)}}{\partial \xi_i} + (X\sigma\alpha^2 + \kappa)\frac{\partial M_j^{(1)}}{\partial \xi_i}] = 0, \tag{7.29}$$

$\frac{1}{\widetilde{T}_0}\frac{\partial \widetilde{T}_0}{\partial x_j}$:

$$\frac{\partial}{\partial \xi_i}[\sigma \frac{\partial N_j^{(2)}}{\partial \xi_i} + \sigma\alpha \frac{\partial M_j^{(2)}}{\partial \xi_i}] = 0, \tag{7.30}$$

$$\frac{\partial}{\partial \xi_i}[X\sigma\alpha \frac{\partial N_j^{(2)}}{\partial \xi_i} + (X\sigma\alpha^2 + \kappa)\frac{\partial M_j^{(2)}}{\partial \xi_i}] = 0, \tag{7.31}$$

$\widetilde{T}_0\frac{\partial \phi_0}{\partial x_j}$:

$$\frac{\partial}{\partial \xi_i}[\sigma\alpha \frac{\partial (N_j^{(3)} + \xi_j)}{\partial \xi_i} + \sigma\alpha^2 \frac{\partial M_j^{(3)}}{\partial \xi_i}] = 0, \tag{7.32}$$

$\widetilde{T}_0\frac{\partial \widetilde{T}_0}{\partial x_j}$:

$$\frac{\partial}{\partial \xi_i}[\sigma\alpha \frac{\partial N_j^{(4)}}{\partial \xi_i} + \sigma\alpha^2 \frac{\partial (M_j^{(4)} + \xi_j)}{\partial \xi_i}] = 0, \tag{7.33}$$

$\frac{\partial \phi_0}{\partial x_j}$:

$$\frac{\partial}{\partial \xi_i}[\sigma \frac{\partial (N_j^{(3)} + \xi_j)}{\partial \xi_i} + \sigma\alpha \frac{\partial M_j^{(3)}}{\partial \xi_i}] = 0, \tag{7.34}$$

$$\frac{\partial}{\partial \xi_i}[\sigma\alpha \frac{\partial N_j^{(1)}}{\partial \xi_i} + \sigma\alpha^2 \frac{\partial M_j^{(1)}}{\partial \xi_i} + \kappa \frac{\partial M_j^{(3)}}{\partial \xi_i}] = 0, \tag{7.35}$$

$\frac{\partial \widetilde{T}_0}{\partial x_j}$:

$$\frac{\partial}{\partial \xi_i}[\sigma \frac{\partial N_j^{(4)}}{\partial \xi_i} + \sigma\alpha \frac{\partial (M_j^{(4)} + \xi_j)}{\partial \xi_i}] = 0, \tag{7.36}$$

$$\frac{\partial}{\partial \xi_i}[\sigma\alpha \frac{\partial N_j^{(2)}}{\partial \xi_i} + \sigma\alpha^2 \frac{\partial M_j^{(2)}}{\partial \xi_i} + \kappa \frac{\partial (M_j^{(4)} + \xi_j)}{\partial \xi_i}] = 0. \tag{7.37}$$

Note we have replaced $T^{(0)} - X$ by $\widetilde{T}^{(0)}$ for convenience. These ten equations are our governing equations for unit cell problem.

As a side note, the reason why we guess such structures of (7.26-7.27) is partly due to the one-dimensional (1D) results that we obtained in previous chapter. In 1D, from the governing equations it can be derived that

$$\begin{aligned}\phi^{(1)} &= N^{(1)}(\xi)\frac{1}{T^{(0)}-X}\frac{d\phi^{(0)}}{dx}+N^{(2)}(\xi)\frac{1}{T^{(0)}-X}\frac{dT^{(0)}}{dx}\\ &+ N^{(3)}(\xi)\frac{d\phi^{(0)}}{dx}+N^{(4)}(\xi)\frac{dT^{(0)}}{dx}, \qquad (7.38)\\ T^{(1)} &= M^{(1)}(\xi)\frac{1}{T^{(0)}-X}\frac{d\phi^{(0)}}{dx}+M^{(2)}(\xi)\frac{1}{T^{(0)}-X}\frac{dT^{(0)}}{dx}\\ &+ M^{(3)}(\xi)\frac{d\phi^{(0)}}{dx}+M^{(4)}(\xi)\frac{dT^{(0)}}{dx}, \qquad (7.39)\end{aligned}$$

where

$$\begin{aligned}N^{(1)}(\xi) &= \frac{V_2}{V_1^2}\int_0^\xi(V_3\frac{\alpha}{\kappa}-\frac{\alpha^2}{\kappa})d\xi-\frac{1}{V_1}\int_0^\xi\frac{1}{\sigma}d\xi, \qquad (7.40)\\ N^{(2)}(\xi) &= \frac{V_2V_3}{V_1^2}\int_0^\xi(V_3\frac{\alpha}{\kappa}-\frac{\alpha^2}{\kappa})d\xi-\frac{V_3}{V_1}\int_0^\xi\frac{1}{\sigma}d\xi, \qquad (7.41)\\ N^{(3)}(\xi) &= \frac{1}{V_1}\int_0^\xi(V_3\frac{\alpha}{\kappa}-\frac{\alpha^2}{\kappa})d\xi-\xi, \qquad (7.42)\\ N^{(4)}(\xi) &= \frac{V_3}{V_1}\int_0^\xi(V_3\frac{\alpha}{\kappa}-\frac{\alpha^2}{\kappa})d\xi-\int_0^\xi\langle\frac{1}{\kappa}\rangle^{-1}\frac{\alpha}{\kappa}d\xi, \qquad (7.43)\\ M^{(1)}(\xi) &= -\frac{V_2}{V_1^2}\int_0^\xi(V_3\frac{1}{\kappa}-\frac{\alpha}{\kappa})d\xi, \qquad (7.44)\\ M^{(2)}(\xi) &= -\frac{V_2V_3}{V_1^2}\int_0^\xi(V_3\frac{1}{\kappa}-\frac{\alpha}{\kappa})d\xi, \qquad (7.45)\\ M^{(3)}(\xi) &= -\frac{1}{V_1}\int_0^\xi(V_3\frac{1}{\kappa}-\frac{\alpha}{\kappa})d\xi, \qquad (7.46)\\ M^{(4)}(\xi) &= -\frac{V_3}{V_1}\int_0^\xi(V_3\frac{1}{\kappa}-\frac{\alpha}{\kappa})d\xi+\int_0^\xi(\langle\frac{1}{\kappa}\rangle^{-1}\frac{1}{\kappa}-1)d\xi, \qquad (7.47)\\ X &= \frac{V_2}{V_1}, \qquad (7.48)\\ V_1 &= \langle\frac{\alpha}{\kappa}\rangle^2\langle\frac{1}{\kappa}\rangle^{-1}-\langle\frac{\alpha^2}{\kappa}\rangle, \qquad (7.49)\\ V_2 &= \langle\frac{1}{\sigma}\rangle, \qquad (7.50)\\ V_3 &= \langle\frac{\alpha}{\kappa}\rangle\langle\frac{1}{\kappa}\rangle^{-1}. \qquad (7.51)\end{aligned}$$

Comparing with 1D results, the guess of (7.26-7.27) is significantly more complex, and by

confining to 1D calculation, it can be degenerated to (7.38-7.39) satisfactorily. So equations (7.26-7.27) look like a very plausible guess to try with.

The perspective of Green's function method[98] also suggests the guess of (7.26-7.27). To that end, we look at equation (7.25). Clearly by Green's function,

$$\mathbf{v}^{(1)} = \int_{\Omega'} \mathbf{G}(\boldsymbol{\xi}, \boldsymbol{\xi}', \mathbf{v}^{(0)}) \mathbf{f}(\boldsymbol{\xi}', \mathbf{v}^{(0)}) d\boldsymbol{\xi}' + \textit{boundary terms}, \tag{7.52}$$

given that $\mathbf{G}(\boldsymbol{\xi}, \boldsymbol{\xi}', \mathbf{v}^{(0)})$ is a Green's function and satisfy

$$\frac{\partial}{\partial \xi_i}[\widetilde{\mathbf{D}}(\boldsymbol{\xi}, \mathbf{v}^{(0)}) \frac{\partial}{\partial \xi_i} \mathbf{G}(\boldsymbol{\xi}, \boldsymbol{\xi}', \mathbf{v}^{(0)})] = \delta(\boldsymbol{\xi} - \boldsymbol{\xi}'), \tag{7.53}$$

together with some boundary condition. That is to say the $\mathbf{v}^{(0)}$, $\frac{\partial \mathbf{v}^{(0)}}{\partial x_i}$ terms in (7.25) that are only functions of $\mathbf{x}$ will most likely stay untouched in the expression of $\mathbf{v}^{(1)}$, and thus prompt us the guess of (7.26-7.27).

7.2.2 Interface conditions for piece-wise smooth material properties

The foregoing discussion is applicable to the region that is off the interfaces of neighbouring phases. At the interfaces, however, due to the discontinuity of the material property matrices $D_{\rho\theta}$ and $E_{\rho\theta\zeta}$, it is expected $\frac{\partial v_\theta}{\partial x_i}$ will be discontinuous. As a result, some interface conditions need to be applied. Specifically, we require

$$[v_\theta]|_\Sigma = 0, \quad [q_{i\rho} n_i]|_\Sigma = 0, \tag{7.54}$$

to hold, where $[.]|_\Sigma$ denotes the jump of values across the interfaces Σ and

$$q_{i\rho} = D_{\rho\theta} \frac{\partial v_\theta}{\partial x_i} + E_{\rho\theta\zeta} v_\theta \frac{\partial v_\zeta}{\partial x_i}, \tag{7.55}$$

is the current density and heat flux with

$$q_{i1} = J_i, \tag{7.56}$$

$$q_{i2} = J_{Ui}. \tag{7.57}$$

n_i is the outward vector normal at the interface. We apply the asymptotic expansion of (7.11) into (7.54). For the first part of (7.54), we have

$$[v_\theta]|_\Sigma = \eta^0 [v_\theta^{(0)}]|_\Sigma + \eta^1 [v_\theta^{(1)}]|_\Sigma + \eta^2 [v_\theta^{(2)}]|_\Sigma + ..., \tag{7.58}$$

where terms with different orders of η are required to be zero individually. Especially, if we require η^1 term to be zero, and by plugging the guess of (7.26-7.27), we have

$$\begin{aligned}[N_i^{(1)}(\boldsymbol{\xi})]|_\Sigma = [N_i^{(2)}(\boldsymbol{\xi})]|_\Sigma = [N_i^{(3)}(\boldsymbol{\xi})]|_\Sigma = [N_i^{(4)}(\boldsymbol{\xi})]|_\Sigma \\ = [M_i^{(1)}(\boldsymbol{\xi})]|_\Sigma = [M_i^{(2)}(\boldsymbol{\xi})]|_\Sigma = [M_i^{(3)}(\boldsymbol{\xi})]|_\Sigma = [M_i^{(4)}(\boldsymbol{\xi})]|_\Sigma = 0, \end{aligned} \tag{7.59}$$

because all the terms have different factoring functions of $\mathbf{x}$, and as a result, are required to equal zero individually. Similarly, for the second part of (7.54), we have

$$\begin{aligned}[q_{i\rho}n_i]|_\Sigma &= \eta^{-1}[q_{i\rho}^{(-1)}n_i]|_\Sigma + \eta^0[q_{i\rho}^{(0)}n_i]|_\Sigma + ... \\ &= \eta^{-1}[D_{\rho\theta}\frac{\partial v_\theta^{(0)}}{\partial \xi_i}n_i + E_{\rho\theta\zeta}v_\theta^{(0)}\frac{\partial v_\zeta^{(0)}}{\partial \xi_i}n_i]|_\Sigma \\ +\eta^0[D_{\rho\theta}(\frac{\partial v_\theta^{(1)}}{\partial \xi_i} + \frac{\partial v_\theta^{(0)}}{\partial x_i})n_i + E_{\rho\theta\zeta}(v_\theta^{(0)}\frac{\partial v_\zeta^{(1)}}{\partial \xi_i} + v_\theta^{(0)}\frac{\partial v_\zeta^{(0)}}{\partial x_i} + v_\theta^{(1)}\frac{\partial v_\zeta^{(0)}}{\partial \xi_i})n_i]|_\Sigma \\ &+..., \end{aligned} \tag{7.60}$$

and terms of different orders of η are required to be zero individually. Especially, if we require η^0 term to be zero, and by plugging the guess of (7.26-7.27), we have

$$[(\sigma\frac{\partial N_j^{(1)}}{\partial \xi_i} + \sigma\alpha\frac{\partial M_j^{(1)}}{\partial \xi_i})n_i]|_\Sigma = 0, \tag{7.61}$$

$$[(X\sigma\alpha\frac{\partial N_j^{(1)}}{\partial \xi_i} + (X\sigma\alpha^2+\kappa)\frac{\partial M_j^{(1)}}{\partial \xi_i})n_i]|_\Sigma = 0, \tag{7.62}$$

$$[(\sigma\frac{\partial N_j^{(2)}}{\partial \xi_i} + \sigma\alpha\frac{\partial M_j^{(2)}}{\partial \xi_i})n_i]|_\Sigma = 0, \tag{7.63}$$

$$[(X\sigma\alpha\frac{\partial N_j^{(2)}}{\partial \xi_i} + (X\sigma\alpha^2+\kappa)\frac{\partial M_j^{(2)}}{\partial \xi_i})n_i]|_\Sigma = 0, \tag{7.64}$$

$$[(\sigma\alpha\frac{\partial (N_j^{(3)}+\xi_j)}{\partial \xi_i} + \sigma\alpha^2\frac{\partial M_j^{(3)}}{\partial \xi_i})n_i]|_\Sigma = 0, \tag{7.65}$$

$$[(\sigma\alpha\frac{\partial N_j^{(4)}}{\partial \xi_i} + \sigma\alpha^2\frac{\partial (M_j^{(4)}+\xi_j)}{\partial \xi_i})n_i]|_\Sigma = 0, \tag{7.66}$$

$$[(\sigma\frac{\partial (N_j^{(3)}+\xi_j)}{\partial \xi_i} + \sigma\alpha\frac{\partial M_j^{(3)}}{\partial \xi_i})n_i]|_\Sigma = 0, \tag{7.67}$$

$$[(\sigma\alpha\frac{\partial N_j^{(1)}}{\partial \xi_i} + \sigma\alpha^2\frac{\partial M_j^{(1)}}{\partial \xi_i} + \kappa\frac{\partial M_j^{(3)}}{\partial \xi_i})n_i]|_\Sigma = 0, \tag{7.68}$$

$$[(\sigma\frac{\partial N_j^{(4)}}{\partial \xi_i}+\sigma\alpha\frac{\partial(M_j^{(4)}+\xi_j)}{\partial \xi_i})n_i]|_\Sigma=0, \tag{7.69}$$

$$[(\sigma\alpha\frac{\partial N_j^{(2)}}{\partial \xi_i}+\sigma\alpha^2\frac{\partial M_j^{(2)}}{\partial \xi_i}+\kappa\frac{\partial(M_j^{(4)}+\xi_j)}{\partial \xi_i})n_i]|_\Sigma=0. \tag{7.70}$$

A striking correspondence is observed between these interface conditions and the governing equations (7.28-7.37). As a matter of fact, the same interface conditions can be derived by simply applying divergence theorem on (7.28-7.37) across the interface.

7.2.3 Boundary conditions

The boundary conditions of the unit cell problem are considered in the following way. Suppose on the macroscopic material, the following boundary conditions are applied

$$\phi(0,x_2,x_3)=h_1(x_2,x_3), \tag{7.71}$$

$$\phi(L_1,x_2,x_3)=h_2(x_2,x_3), \tag{7.72}$$

where 0 and L_1 are considered as the two ends along x_1 of the macroscopic material, h_1 and h_1 are given distributions of potential on the corresponding boundary. For (7.71), if we use asymptotic expansion of $\phi(0,x_2,x_3)$, we have

$$\begin{aligned}\phi^{(0)}(0,x_2,x_3)+\eta N_i^{(1)}(0,\xi_2,\xi_3)\frac{1}{\widetilde{T}^{(0)}(0,x_2,x_3)}\frac{\partial\phi^{(0)}}{\partial x_i}|_{(0,x_2,x_3)}\\ +\eta N_i^{(2)}(0,\xi_2,\xi_3)\frac{1}{\widetilde{T}^{(0)}(0,x_2,x_3)}\frac{\partial\widetilde{T}^{(0)}}{\partial x_i}|_{(0,x_2,x_3)}+\eta N_i^{(3)}(0,\xi_2,\xi_3)\frac{\partial\phi^{(0)}}{\partial x_i}|_{(0,x_2,x_3)}\\ +\eta N_i^{(4)}(0,\xi_2,\xi_3)\frac{\partial\widetilde{T}^{(0)}}{\partial x_i}|_{(0,x_2,x_3)}+...\\ \sim h_1(x_2,x_3),\end{aligned} \tag{7.73}$$

meaning h_1 are asymptotically approached by the series. For (7.72), similarly we have

$$\begin{aligned}
&\phi^{(0)}(L_1,x_2,x_3)+\eta N_i^{(1)}(\frac{L_1}{\eta},\xi_2,\xi_3)\frac{1}{\widetilde{T}^{(0)}(L_1,x_2,x_3)}\frac{\partial\phi^{(0)}}{\partial x_i}|_{(L_1,x_2,x_3)}\\
&+\eta N_i^{(2)}(\frac{L_1}{\eta},\xi_2,\xi_3)\frac{1}{\widetilde{T}^{(0)}(L_1,x_2,x_3)}\frac{\partial\widetilde{T}^{(0)}}{\partial x_i}|_{(L_1,x_2,x_3)}\\
&+\eta N_i^{(3)}(\frac{L_1}{\eta},\xi_2,\xi_3)\frac{\partial\phi^{(0)}}{\partial x_i}|_{(L_1,x_2,x_3)}\\
&+\eta N_i^{(4)}(\frac{L_1}{\eta},\xi_2,\xi_3)\frac{\partial\widetilde{T}^{(0)}}{\partial x_i}|_{(L_1,x_2,x_3)}+...\\
=\ &\phi^{(0)}(L_1,x_2,x_3)+\eta N_i^{(1)}(0,\xi_2,\xi_3)\frac{1}{\widetilde{T}^{(0)}(L_1,x_2,x_3)}\frac{\partial\phi^{(0)}}{\partial x_i}|_{(L_1,x_2,x_3)}\\
&+\eta N_i^{(2)}(0,\xi_2,\xi_3)\frac{1}{\widetilde{T}^{(0)}(L_1,x_2,x_3)}\frac{\partial\widetilde{T}^{(0)}}{\partial x_i}|_{(L_1,x_2,x_3)}\\
&+\eta N_i^{(3)}(0,\xi_2,\xi_3)\frac{\partial\phi^{(0)}}{\partial x_i}|_{(L_1,x_2,x_3)}\\
&+\eta N_i^{(4)}(0,\xi_2,\xi_3)\frac{\partial\widetilde{T}^{(0)}}{\partial x_i}|_{(L_1,x_2,x_3)}+...\\
&\sim h_2(x_2,x_3),
\end{aligned}\tag{7.74}$$

because $N_i^{(j)}(\frac{L_1}{\eta},\xi_2,\xi_3)=N_i^{(j)}(n_1,\xi_2,\xi_3)=N_i^{(j)}(0,\xi_2,\xi_3)$ due to the periodicity of $N_i^{(j)}$, where $j=1,2,3,4$, and n_1 being integer number. So if we require

$$N_i^{(j)}(0,\xi_2,\xi_3)=0,\tag{7.75}$$

the macroscopic boundary conditions are streamlined as

$$\phi^{(0)}(0,x_2,x_3)\sim h_1(x_2,x_3),\tag{7.76}$$

$$\phi^{(0)}(L_1,x_2,x_3)\sim h_2(x_2,x_3).\tag{7.77}$$

For the same reason, we also require

$$N_i^{(j)}(\xi_1,0,\xi_3)=0,\tag{7.78}$$

$$N_i^{(j)}(\xi_1,\xi_2,0)=0.\tag{7.79}$$

For the boundary conditions on temperature, we can similarly obtain

$$M_i^{(j)}(0,\xi_2,\xi_3)=0, \tag{7.80}$$

$$M_i^{(j)}(\xi_1,0,\xi_3)=0, \tag{7.81}$$

$$M_i^{(j)}(\xi_1,\xi_2,0)=0. \tag{7.82}$$

Thus, we have equations (7.75) and (7.78-7.82) as the boundary conditions for our unit cell problem.

7.3 Homogenized governing equations of thermoelectricity

With the governing equations, interface conditions and boundary conditions, the unit cell problem is fully formulated and if it is a correct formulation, $N_i^{(1)} \sim N_i^{(4)}, M_i^{(1)} \sim M_i^{(4)}$ can be solved together, and (7.26-7.27) will give us the right expression for $\mathbf{v}^{(1)}$. From the Existence and Uniqueness theorem, a $\mathbf{v}^{(1)}$ that satisfies equation (7.16) is the real solution of the equation. We will save the detail of numerical solution of the unit cell problem for the next section. Here we assume that the problem is correctly formulated and the solutions are obtained, so that we are ready to derive the homogenized governing equations that determine the macroscopic distribution of fields of temperature and electric potential.

To this end, we substitute (7.26-7.27) into (7.17) while also apply $\langle . \rangle$ operation on the two sides. Attention is called into the fact that

$$\langle \frac{\partial f}{\partial \xi_i} \rangle = \int_0^1 \frac{\partial f}{\partial \xi_i} d\xi_i = f|_0^1 = 0, \tag{7.83}$$

for some 1-periodic f, so that from (7.17) we have

$$\langle \frac{\partial}{\partial x_i}[D_{\rho\theta}(\frac{\partial v_\theta^{(1)}}{\partial \xi_i} + \frac{\partial v_\theta^{(0)}}{\partial x_i})] \rangle + \langle \frac{\partial}{\partial x_i}[E_{\rho\theta\zeta} v_\theta^{(0)}(\frac{\partial v_\zeta^{(1)}}{\partial \xi_i} + \frac{\partial v_\zeta^{(0)}}{\partial x_i})] \rangle = 0. \tag{7.84}$$

We then plug in (7.26-7.27). For simplicity, at the moment we only consider $\rho = 1$ such

that we have

$$\begin{aligned}
\frac{\partial}{\partial x_i}[\langle\sigma\frac{\partial N_j^{(1)}}{\partial \xi_i}+\sigma\alpha\frac{\partial M_j^{(1)}}{\partial \xi_i}\rangle\frac{1}{\widetilde{T}^{(0)}}\frac{\partial \phi^{(0)}}{\partial x_j} \\
+\langle\sigma\frac{\partial N_j^{(2)}}{\partial \xi_i}+\sigma\alpha\frac{\partial M_j^{(2)}}{\partial \xi_i}\rangle\frac{1}{\widetilde{T}^{(0)}}\frac{\partial \widetilde{T}^{(0)}}{\partial x_j} \\
+\langle\sigma\frac{\partial (N_j^{(3)}+\xi_j)}{\partial \xi_i}+\sigma\alpha\frac{\partial M_j^{(3)}}{\partial \xi_i}\rangle\frac{\partial \phi^{(0)}}{\partial x_j} \\
+\langle\sigma\frac{\partial N_j^{(4)}}{\partial \xi_i}+\sigma\alpha\frac{\partial (M_j^{(4)}+\xi_j)}{\partial \xi_i}\rangle\frac{\partial \widetilde{T}^{(0)}}{\partial x_j}]=0. \qquad (7.85)
\end{aligned}$$

In the above equation, the terms in the angular bracket are recognized as constants, and $\mathbf{x}$ is the only spatial variable remaining, so we have actually derived a homogenized governing equation that governs the macroscopic field $\phi^{(0)}$ and $\widetilde{T}^{(0)}$. And the terms in the angular bracket are interpreted as effective properties for the composite material. With organization, (7.85) becomes

$$\frac{\partial}{\partial x_i}\langle q_{i1}^{(0)}\rangle=0, \qquad (7.86)$$

where

$$\langle q_{i1}^{(0)}\rangle=\frac{G_{ij}^{(1)}+G_{ij}^{(3)}\widetilde{T}^{(0)}}{\widetilde{T}^{(0)}}\frac{\partial \phi^{(0)}}{\partial x_j}+\frac{G_{ij}^{(2)}+G_{ij}^{(4)}\widetilde{T}^{(0)}}{\widetilde{T}^{(0)}}\frac{\partial \widetilde{T}^{(0)}}{\partial x_j}, \qquad (7.87)$$

is the macroscopic current density with effective properties

$$G_{ij}^{(1)} = \langle\sigma\frac{\partial N_j^{(1)}}{\partial \xi_i}+\sigma\alpha\frac{\partial M_j^{(1)}}{\partial \xi_i}\rangle, \qquad (7.88)$$

$$G_{ij}^{(2)} = \langle\sigma\frac{\partial N_j^{(2)}}{\partial \xi_i}+\sigma\alpha\frac{\partial M_j^{(2)}}{\partial \xi_i}\rangle, \qquad (7.89)$$

$$G_{ij}^{(3)} = \langle\sigma\frac{\partial (N_j^{(3)}+\xi_j)}{\partial \xi_i}+\sigma\alpha\frac{\partial M_j^{(3)}}{\partial \xi_i}\rangle, \qquad (7.90)$$

$$G_{ij}^{(4)} = \langle\sigma\frac{\partial N_j^{(4)}}{\partial \xi_i}+\sigma\alpha\frac{\partial (M_j^{(4)}+\xi_j)}{\partial \xi_i}\rangle. \qquad (7.91)$$

Plugging (7.26-7.27) in (7.84), and considering $j=2$, we get

$$\frac{\partial}{\partial x_i}\langle q_{i2}^{(0)}\rangle=0, \qquad (7.92)$$

which is the other homogenized governing equation, and

$$\begin{aligned}\langle q_{i2}^{(0)}\rangle &= (H_{ij}^{(3)}\widetilde{T}^{(0)} + G_{ij}^{(3)}\phi^{(0)} + H_{ij}^{(1)} + XH_{ij}^{(3)} + K_{ij}^{(3)})\frac{\partial\phi^{(0)}}{\partial x_j} \\ &+ \frac{G_{ij}^{(1)}\phi^{(0)} + XH_{ij}^{(1)} + K_{ij}^{(1)}}{\widetilde{T}^{(0)}}\frac{\partial\phi^{(0)}}{\partial x_j} \\ &+ (H_{ij}^{(4)}\widetilde{T}^{(0)} + G_{ij}^{(4)}\phi^{(0)} + H_{ij}^{(2)} + XH_{ij}^{(4)} + K_{ij}^{(4)})\frac{\partial\widetilde{T}^{(0)}}{\partial x_j} \\ &+ \frac{G_{ij}^{(2)}\phi^{(0)} + XH_{ij}^{(2)} + K_{ij}^{(2)}}{\widetilde{T}^{(0)}}\frac{\partial\widetilde{T}^{(0)}}{\partial x_j}, \end{aligned} \tag{7.93}$$

is the macroscopic energy flux with more effective properties

$$H_{ij}^{(1)} = \langle\sigma\alpha\frac{\partial N_j^{(1)}}{\partial\xi_i} + \sigma\alpha^2\frac{\partial M_j^{(1)}}{\partial\xi_i}\rangle, \tag{7.94}$$

$$H_{ij}^{(2)} = \langle\sigma\alpha\frac{\partial N_j^{(2)}}{\partial\xi_i} + \sigma\alpha^2\frac{\partial M_j^{(2)}}{\partial\xi_i}\rangle, \tag{7.95}$$

$$H_{ij}^{(3)} = \langle\sigma\alpha\frac{\partial(N_j^{(3)} + \xi_j)}{\partial\xi_i} + \sigma\alpha^2\frac{\partial M_j^{(3)}}{\partial\xi_i}\rangle, \tag{7.96}$$

$$H_{ij}^{(4)} = \langle\sigma\alpha\frac{\partial N_j^{(4)}}{\partial\xi_i} + \sigma\alpha^2\frac{\partial(M_j^{(4)} + \xi_j)}{\partial\xi_i}\rangle, \tag{7.97}$$

$$K_{ij}^{(1)} = \langle\kappa\frac{\partial M_j^{(1)}}{\partial\xi_i}\rangle, \tag{7.98}$$

$$K_{ij}^{(2)} = \langle\kappa\frac{\partial M_j^{(2)}}{\partial\xi_i}\rangle, \tag{7.99}$$

$$K_{ij}^{(3)} = \langle\kappa\frac{\partial M_j^{(3)}}{\partial\xi_i}\rangle, \tag{7.100}$$

$$K_{ij}^{(4)} = \langle\kappa\frac{\partial(M_j^{(4)} + \xi_j)}{\partial\xi_i}\rangle. \tag{7.101}$$

7.4 A variation of unit cell problem: pseudo 2D/3D case

So above we have discussed the way of applying asymptotic method to thermoelectrics mainly in a general sense. There is one special case that is probably of more practical importance, which is the so-called pseudo 2D/3D case, shown in Figure 7.2, in which, a macroscopically homogeneous composite material is subjected to temperature and potential differences on the two ends along x_1, whereas along x_2 and x_3, no macroscopic difference

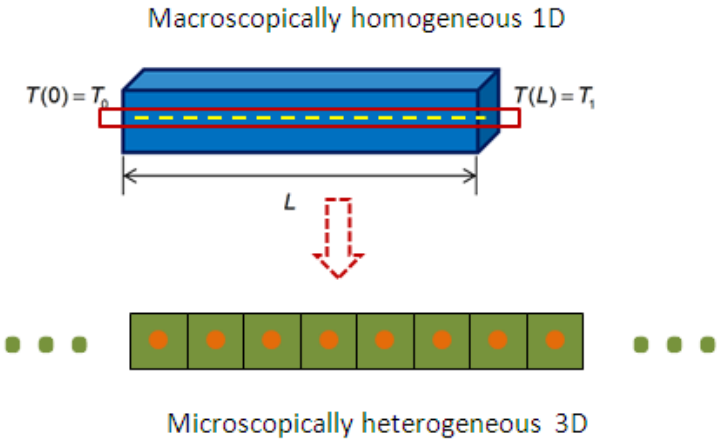

Figure 7.2: The schematics of the pseudo 3D case.

can be observed.

With pseudo 3D, it is not hard to see for macroscopic current density and energy flux, there is

$$\langle q_{i\rho}^{(0)} \rangle = 0, \tag{7.102}$$

for $i = 2, 3$, which suggests there is no overall exchange between neighboring cells in lateral directions. As for $q_{i\rho}^{(0)}$ (without averaging), which depends on $\boldsymbol{\xi}$ in addition to $\mathbf{x}$, we have, for instance,

$$q_{i\rho}^{(0)}(\xi_1, 0, \xi_3, \mathbf{x}) = q_{i\rho}^{(0)}(\xi_1, 1, \xi_3, \mathbf{x}), \tag{7.103}$$

by periodicity, then the flux normal to the boundary will be $q_{2\rho}^{(0)}(\xi_1, 1, \xi_3, \mathbf{x})$ and $-q_{2\rho}^{(0)}(\xi_1, 0, \xi_3, \mathbf{x})$, meaning one flowing-in, and the other flowing-out. Assuming symmetry is present such that fluxes on the opposite boundaries mirror each other, due to symmetry in the unit cell structure, then the only possibility is

$$q_{2\rho}^{(0)}(\xi_1, 0, \xi_3, \mathbf{x}) = q_{2\rho}^{(0)}(\xi_1, 1, \xi_3, \mathbf{x}) = 0. \tag{7.104}$$

So we see by periodicity and symmetry, the condition (7.102) can get to point-wise

$$q_{i\rho}^{(0)}(\boldsymbol{\xi}, \mathbf{x}) n_i = 0, \tag{7.105}$$

for $\boldsymbol{\xi}$ at the lateral boundary of unit cell, where $\mathbf{n}$ is the outward unit vector normal to the unit cell boundary. That means a chain of cells along x_1 can be treated individually.

Due to the particularity of pseudo 3D analysis, the asymptotic expansion of v_θ is modified as

$$v_\theta(x_1,\xi_i) = v_\theta^{(0)}(x_1)+\eta v_\theta^{(1)}(x_1,\xi_i)+\eta^2 v_\theta^{(2)}(x_1,\xi_i)+..., \tag{7.106}$$

and (7.16-7.17) become

$$\frac{\partial}{\partial\xi_i}[D_{\rho\theta}\frac{\partial v_\theta^{(1)}}{\partial\xi_i}]+\frac{\partial}{\partial\xi_i}[E_{\rho\theta\zeta}v_\theta^{(0)}\frac{\partial v_\zeta^{(1)}}{\partial\xi_i}] = -\frac{\partial D_{\rho\theta}}{\partial\xi_1}\frac{\partial v_\theta^{(0)}}{\partial x_1}-\frac{\partial E_{\rho\theta\zeta}}{\partial\xi_1}v_\theta^{(0)}\frac{\partial v_\zeta^{(0)}}{\partial x_1}, \tag{7.107}$$

$$\begin{aligned}\frac{\partial}{\partial\xi_i}[D_{\rho\theta}\frac{\partial v_\theta^{(2)}}{\partial\xi_i}]+\frac{\partial}{\partial\xi_i}[E_{\rho\theta\zeta}v_\theta^{(0)}\frac{\partial v_\zeta^{(2)}}{\partial\xi_i}] &= -\frac{\partial}{\partial\xi_1}[D_{\rho\theta}\frac{\partial v_\theta^{(1)}}{\partial x_1}]\\ &-\frac{\partial}{\partial x_1}[D_{\rho\theta}(\frac{\partial v_\theta^{(1)}}{\partial\xi_1}+\frac{\partial v_\theta^{(0)}}{\partial x_1})]-\frac{\partial}{\partial\xi_i}[E_{\rho\theta\zeta}v_\theta^{(1)}\frac{\partial v_\zeta^{(1)}}{\partial\xi_i}]\\ -\frac{\partial}{\partial\xi_1}[E_{\rho\theta\zeta}(v_\theta^{(1)}\frac{\partial v_\zeta^{(0)}}{\partial x_1}+v_\theta^{(0)}\frac{\partial v_\zeta^{(1)}}{\partial x_1})]-\frac{\partial}{\partial x_1}[E_{\rho\theta\zeta}v_\theta^{(0)}(\frac{\partial v_\zeta^{(1)}}{\partial\xi_1}+\frac{\partial v_\zeta^{(0)}}{\partial x_1})].\end{aligned} \tag{7.108}$$

So the hypothesized $\mathbf{v}^{(1)}$ are accordingly modified to

$$\begin{aligned}v_1^{(1)} &= N_1^{(1)}(\boldsymbol{\xi})\frac{1}{T^{(0)}-X}\frac{\partial\phi^{(0)}}{\partial x_1}+N_1^{(2)}(\boldsymbol{\xi})\frac{1}{T^{(0)}-X}\frac{\partial T^{(0)}}{\partial x_1}\\ &+ N_1^{(3)}(\boldsymbol{\xi})\frac{\partial\phi^{(0)}}{\partial x_1}+N_1^{(4)}(\boldsymbol{\xi})\frac{\partial T^{(0)}}{\partial x_1},\end{aligned} \tag{7.109}$$

$$\begin{aligned}v_2^{(1)} &= M_1^{(1)}(\boldsymbol{\xi})\frac{1}{T^{(0)}-X}\frac{\partial\phi^{(0)}}{\partial x_1}+M_1^{(2)}(\boldsymbol{\xi})\frac{1}{T^{(0)}-X}\frac{\partial T^{(0)}}{\partial x_1}\\ &+ M_1^{(3)}(\boldsymbol{\xi})\frac{\partial\phi^{(0)}}{\partial x_1}+M_1^{(4)}(\boldsymbol{\xi})\frac{\partial T^{(0)}}{\partial x_1}.\end{aligned} \tag{7.110}$$

And then we have the governing equations of the unit cell problem

$$\frac{\partial}{\partial \xi_i}[\sigma \frac{\partial N_1^{(1)}}{\partial \xi_i} + \sigma\alpha \frac{\partial M_1^{(1)}}{\partial \xi_i}] = 0, \tag{7.111}$$

$$\frac{\partial}{\partial \xi_i}[X\sigma\alpha \frac{\partial N_1^{(1)}}{\partial \xi_i} + (X\sigma\alpha^2 + \kappa) \frac{\partial M_1^{(1)}}{\partial \xi_i}] = 0, \tag{7.112}$$

$$\frac{\partial}{\partial \xi_i}[\sigma \frac{\partial N_1^{(2)}}{\partial \xi_i} + \sigma\alpha \frac{\partial M_1^{(2)}}{\partial \xi_i}] = 0, \tag{7.113}$$

$$\frac{\partial}{\partial \xi_i}[X\sigma\alpha \frac{\partial N_1^{(2)}}{\partial \xi_i} + (X\sigma\alpha^2 + \kappa) \frac{\partial M_1^{(2)}}{\partial \xi_i}] = 0, \tag{7.114}$$

$$\frac{\partial}{\partial \xi_i}[\sigma\alpha \frac{\partial (N_1^{(3)} + \xi_1)}{\partial \xi_i} + \sigma\alpha^2 \frac{\partial M_1^{(3)}}{\partial \xi_i}] = 0, \tag{7.115}$$

$$\frac{\partial}{\partial \xi_i}[\sigma\alpha \frac{\partial N_1^{(4)}}{\partial \xi_i} + \sigma\alpha^2 \frac{\partial (M_1^{(4)} + \xi_1)}{\partial \xi_i}] = 0, \tag{7.116}$$

$$\frac{\partial}{\partial \xi_i}[\sigma \frac{\partial (N_1^{(3)} + \xi_1)}{\partial \xi_i} + \sigma\alpha \frac{\partial M_1^{(3)}}{\partial \xi_i}] = 0, \tag{7.117}$$

$$\frac{\partial}{\partial \xi_i}[\sigma\alpha \frac{\partial N_1^{(1)}}{\partial \xi_i} + \sigma\alpha^2 \frac{\partial M_1^{(1)}}{\partial \xi_i} + \kappa \frac{\partial M_1^{(3)}}{\partial \xi_i}] = 0, \tag{7.118}$$

$$\frac{\partial}{\partial \xi_i}[\sigma \frac{\partial N_1^{(4)}}{\partial \xi_i} + \sigma\alpha \frac{\partial (M_1^{(4)} + \xi_1)}{\partial \xi_i}] = 0, \tag{7.119}$$

$$\frac{\partial}{\partial \xi_i}[\sigma\alpha \frac{\partial N_1^{(2)}}{\partial \xi_i} + \sigma\alpha^2 \frac{\partial M_1^{(2)}}{\partial \xi_i} + \kappa \frac{\partial (M_1^{(4)} + \xi_1)}{\partial \xi_i}] = 0, \tag{7.120}$$

and interface conditions

$$[N_1^{(1)}]|_\Sigma = [N_1^{(2)}]|_\Sigma = [N_1^{(3)}]|_\Sigma = [N_1^{(4)}]|_\Sigma$$
$$= [M_1^{(1)}]|_\Sigma = [M_1^{(2)}]|_\Sigma = [M_1^{(3)}]|_\Sigma = [M_1^{(4)}]|_\Sigma = 0, \tag{7.121}$$

$$[(\sigma \frac{\partial N_1^{(1)}}{\partial \xi_i} + \sigma\alpha \frac{\partial M_1^{(1)}}{\partial \xi_i}) n_i]|_\Sigma = 0, \tag{7.122}$$

$$[(X\sigma\alpha \frac{\partial N_1^{(1)}}{\partial \xi_i} + (X\sigma\alpha^2 + \kappa) \frac{\partial M_1^{(1)}}{\partial \xi_i}) n_i]|_\Sigma = 0, \tag{7.123}$$

$$[(\sigma \frac{\partial N_1^{(2)}}{\partial \xi_i} + \sigma\alpha \frac{\partial M_1^{(2)}}{\partial \xi_i}) n_i]|_\Sigma = 0, \tag{7.124}$$

$$[(X\sigma\alpha \frac{\partial N_1^{(2)}}{\partial \xi_i} + (X\sigma\alpha^2 + \kappa) \frac{\partial M_1^{(2)}}{\partial \xi_i}) n_i]|_\Sigma = 0, \tag{7.125}$$

$$[(\sigma\alpha \frac{\partial (N_1^{(3)} + \xi_1)}{\partial \xi_i} + \sigma\alpha^2 \frac{\partial M_1^{(3)}}{\partial \xi_i}) n_i]|_\Sigma = 0, \tag{7.126}$$

$$[(\sigma\alpha\frac{\partial N_1^{(4)}}{\partial \xi_i}+\sigma\alpha^2\frac{\partial(M_1^{(4)}+\xi_1)}{\partial \xi_i})n_i]|_\Sigma=0, \tag{7.127}$$

$$[(\sigma\frac{\partial(N_1^{(3)}+\xi_1)}{\partial \xi_i}+\sigma\alpha\frac{\partial M_1^{(3)}}{\partial \xi_i})n_i]|_\Sigma=0, \tag{7.128}$$

$$[(\sigma\alpha\frac{\partial N_1^{(1)}}{\partial \xi_i}+\sigma\alpha^2\frac{\partial M_1^{(1)}}{\partial \xi_i}+\kappa\frac{\partial M_1^{(3)}}{\partial \xi_i})n_i]|_\Sigma=0, \tag{7.129}$$

$$[(\sigma\frac{\partial N_1^{(4)}}{\partial \xi_i}+\sigma\alpha\frac{\partial(M_1^{(4)}+\xi_1)}{\partial \xi_i})n_i]|_\Sigma=0, \tag{7.130}$$

$$[(\sigma\alpha\frac{\partial N_1^{(2)}}{\partial \xi_i}+\sigma\alpha^2\frac{\partial M_1^{(2)}}{\partial \xi_i}+\kappa\frac{\partial(M_1^{(4)}+\xi_1)}{\partial \xi_i})n_i]|_\Sigma=0. \tag{7.131}$$

For the consideration of boundary conditions of the unit cell problem, we suppose on the macroscopic material the following boundary conditions are applied

$$\phi(0)=h_1, \tag{7.132}$$

$$\phi(L_1)=h_2, \tag{7.133}$$

where h_1 and h_2 are specified electric potentials on the two ends of the macroscopic material 0 and L_1 along x_1. As what has been done previously, we will still get

$$N_1^{(j)}(0,\xi_2,\xi_3)=0, \tag{7.134}$$

where $j=1,2,3,4$. Similarly, for the boundary condition of temperature, there is

$$M_1^{(j)}(0,\xi_2,\xi_3)=0. \tag{7.135}$$

On the lateral directions, we have the Neumann type boundary condition of (7.105). To be specific, we have

$$\begin{aligned} q_{i1}^{(0)} &= (\sigma\frac{\partial N_1^{(1)}}{\partial \xi_i}+\sigma\alpha\frac{\partial M_1^{(1)}}{\partial \xi_i})\frac{1}{\widetilde{T}^{(0)}}\frac{\partial \phi^{(0)}}{\partial x_1} \\ &+(\sigma\frac{\partial N_1^{(2)}}{\partial \xi_i}+\sigma\alpha\frac{\partial M_1^{(2)}}{\partial \xi_i})\frac{1}{\widetilde{T}^{(0)}}\frac{\partial \widetilde{T}^{(0)}}{\partial x_1}+[\sigma\frac{\partial(N_1^{(3)}+\xi_1)}{\partial \xi_i}+\sigma\alpha\frac{\partial M_1^{(3)}}{\partial \xi_i}]\frac{\partial \phi^{(0)}}{\partial x_1} \\ &+[\sigma\frac{\partial N_1^{(4)}}{\partial \xi_i}+\sigma\alpha\frac{\partial(M_1^{(4)}+\xi_1)}{\partial \xi_i}]\frac{\partial \widetilde{T}^{(0)}}{\partial x_1}. \end{aligned} \tag{7.136}$$

Then due to (7.105), the following boundary conditions

$$
\begin{aligned}
&(\sigma\frac{\partial N_1^{(1)}}{\partial \xi_2}+\sigma\alpha\frac{\partial M_1^{(1)}}{\partial \xi_2})n_2|_{(\xi_1,0,\xi_3)}\\
&=(\sigma\frac{\partial N_1^{(1)}}{\partial \xi_3}+\sigma\alpha\frac{\partial M_1^{(1)}}{\partial \xi_3})n_3|_{(\xi_1,\xi_2,0)}=0, \qquad (7.137)\\
&(\sigma\frac{\partial N_1^{(2)}}{\partial \xi_2}+\sigma\alpha\frac{\partial M_1^{(2)}}{\partial \xi_2})n_2|_{(\xi_1,0,\xi_3)}\\
&=(\sigma\frac{\partial N_1^{(2)}}{\partial \xi_3}+\sigma\alpha\frac{\partial M_1^{(2)}}{\partial \xi_3})n_3|_{(\xi_1,\xi_2,0)}=0, \qquad (7.138)\\
&(\sigma\frac{\partial (N_1^{(3)}+\xi_1)}{\partial \xi_2}+\sigma\alpha\frac{\partial M_1^{(3)}}{\partial \xi_2})n_2|_{(\xi_1,0,\xi_3)}\\
&=(\sigma\frac{\partial (N_1^{(3)}+\xi_1)}{\partial \xi_3}+\sigma\alpha\frac{\partial M_1^{(3)}}{\partial \xi_3})n_3|_{(\xi_1,\xi_2,0)}=0, \qquad (7.139)\\
&(\sigma\frac{\partial N_1^{(4)}}{\partial \xi_2}+\sigma\alpha\frac{\partial (M_1^{(4)}+\xi_1)}{\partial \xi_2})n_2|_{(\xi_1,0,\xi_3)}\\
&=(\sigma\frac{\partial N_1^{(4)}}{\partial \xi_3}+\sigma\alpha\frac{\partial (M_1^{(4)}+\xi_1)}{\partial \xi_3})n_3|_{(\xi_1,\xi_2,0)}=0, \qquad (7.140)
\end{aligned}
$$

are required on the lateral directions. Similarly, from $q_{i2}^{(0)}$ we have

$$
\begin{aligned}
(\kappa\frac{\partial M_1^{(1)}}{\partial \xi_2})n_2|_{(\xi_1,0,\xi_3)}&=(\kappa\frac{\partial M_1^{(1)}}{\partial \xi_3})n_3|_{(\xi_1,\xi_2,0)}=0, \qquad (7.141)\\
(\kappa\frac{\partial M_1^{(2)}}{\partial \xi_2})n_2|_{(\xi_1,0,\xi_3)}&=(\kappa\frac{\partial M_1^{(2)}}{\partial \xi_3})n_3|_{(\xi_1,\xi_2,0)}=0, \qquad (7.142)\\
(\kappa\frac{\partial M_1^{(3)}}{\partial \xi_2})n_2|_{(\xi_1,0,\xi_3)}&=(\kappa\frac{\partial M_1^{(3)}}{\partial \xi_3})n_3|_{(\xi_1,\xi_2,0)}=0, \qquad (7.143)\\
(\kappa\frac{\partial (M_1^{(4)}+\xi_1)}{\partial \xi_2})n_2|_{(\xi_1,0,\xi_3)}&=(\kappa\frac{\partial (M_1^{(4)}+\xi_1)}{\partial \xi_3})n_3|_{(\xi_1,\xi_2,0)}=0. \qquad (7.144)
\end{aligned}
$$

Considering (7.137-7.144) altogether, it is required

$$\frac{\partial M_1^{(1)}}{\partial \xi_2}|_{(\xi_1,0,\xi_3)} = \frac{\partial M_1^{(2)}}{\partial \xi_2}|_{(\xi_1,0,\xi_3)} = \frac{\partial M_1^{(3)}}{\partial \xi_2}|_{(\xi_1,0,\xi_3)}$$
$$= \frac{\partial (M_1^{(4)} + \xi_1)}{\partial \xi_2}|_{(\xi_1,0,\xi_3)} = \frac{\partial N_1^{(1)}}{\partial \xi_2}|_{(\xi_1,0,\xi_3)} = \frac{\partial N_1^{(2)}}{\partial \xi_2}|_{(\xi_1,0,\xi_3)}$$
$$= \frac{\partial (N_1^{(3)} + \xi_1)}{\partial \xi_2}|_{(\xi_1,0,\xi_3)} = \frac{\partial N_1^{(4)}}{\partial \xi_2}|_{(\xi_1,0,\xi_3)} = 0, \tag{7.145}$$

$$\frac{\partial M_1^{(1)}}{\partial \xi_3}|_{(\xi_1,\xi_2,0)} = \frac{\partial M_1^{(2)}}{\partial \xi_3}|_{(\xi_1,\xi_2,0)} = \frac{\partial M_1^{(3)}}{\partial \xi_3}|_{(\xi_1,\xi_2,0)}$$
$$= \frac{\partial (M_1^{(4)} + \xi_1)}{\partial \xi_3}|_{(\xi_1,\xi_2,0)} = \frac{\partial N_1^{(1)}}{\partial \xi_3}|_{(\xi_1,\xi_2,0)} = \frac{\partial N_1^{(2)}}{\partial \xi_3}|_{(\xi_1,\xi_2,0)}$$
$$= \frac{\partial (N_1^{(3)} + \xi_1)}{\partial \xi_3}|_{(\xi_1,\xi_2,0)} = \frac{\partial N_1^{(4)}}{\partial \xi_3}|_{(\xi_1,\xi_2,0)} = 0, \tag{7.146}$$

or in short,

$$\frac{\partial \mathbf{V}}{\partial \xi_i} n_i = \mathbf{0}, \tag{7.147}$$

is required at the lateral boundaries, where

$$\mathbf{V} = \left[\begin{array}{cccccccc} M_1^{(1)} & M_1^{(2)} & M_1^{(3)} & M_1^{(4)} + \xi_1 & N_1^{(1)} & N_1^{(2)} & N_1^{(3)} + \xi_1 & N_1^{(4)} \end{array} \right]^T. \tag{7.148}$$

Finally, the homogenized governing equations in pseudo 3D are

$$\frac{d}{dx_1} \langle q_{11}^{(0)} \rangle = 0, \tag{7.149}$$

$$\frac{d}{dx_1} \langle q_{12}^{(0)} \rangle = 0, \tag{7.150}$$

where

$$\langle q_{11}^{(0)} \rangle = \frac{G^{(1)} + G^{(3)} \widetilde{T}^{(0)}}{\widetilde{T}^{(0)}} \frac{d\phi^{(0)}}{dx_1} + \frac{G^{(2)} + G^{(4)} \widetilde{T}^{(0)}}{\widetilde{T}^{(0)}} \frac{d\widetilde{T}^{(0)}}{dx_1}, \tag{7.151}$$

$$\begin{aligned} \langle q_{12}^{(0)} \rangle &= (H^{(3)} \widetilde{T}^{(0)} + G^{(3)} \phi^{(0)} + H^{(1)} + X H^{(3)} + K^{(3)}) \frac{d\phi^{(0)}}{dx_1} \\ &+ \frac{G^{(1)} \phi^{(0)} + X H^{(1)} + K^{(1)}}{\widetilde{T}^{(0)}} \frac{d\phi^{(0)}}{dx_1} \\ &+ (H^{(4)} \widetilde{T}^{(0)} + G^{(4)} \phi^{(0)} + H^{(2)} + X H^{(4)} + K^{(4)}) \frac{d\widetilde{T}^{(0)}}{dx_1} \\ &+ \frac{G^{(2)} \phi^{(0)} + X H^{(2)} + K^{(2)}}{\widetilde{T}^{(0)}} \frac{d\widetilde{T}^{(0)}}{dx_1}, \end{aligned} \tag{7.152}$$

with effective properties

$$G^{(1)} = \langle \sigma \frac{\partial N_1^{(1)}}{\partial \xi_1} + \sigma\alpha \frac{\partial M_1^{(1)}}{\partial \xi_1} \rangle, \tag{7.153}$$

$$G^{(2)} = \langle \sigma \frac{\partial N_1^{(2)}}{\partial \xi_1} + \sigma\alpha \frac{\partial M_1^{(2)}}{\partial \xi_1} \rangle, \tag{7.154}$$

$$G^{(3)} = \langle \sigma \frac{\partial (N_1^{(3)} + \xi_1)}{\partial \xi_1} + \sigma\alpha \frac{\partial M_1^{(3)}}{\partial \xi_1} \rangle, \tag{7.155}$$

$$G^{(4)} = \langle \sigma \frac{\partial N_1^{(4)}}{\partial \xi_1} + \sigma\alpha \frac{\partial (M_1^{(4)} + \xi_1)}{\partial \xi_1} \rangle, \tag{7.156}$$

$$H^{(1)} = \langle \sigma\alpha \frac{\partial N_1^{(1)}}{\partial \xi_1} + \sigma\alpha^2 \frac{\partial M_1^{(1)}}{\partial \xi_1} \rangle, \tag{7.157}$$

$$H^{(2)} = \langle \sigma\alpha \frac{\partial N_1^{(2)}}{\partial \xi_1} + \sigma\alpha^2 \frac{\partial M_1^{(2)}}{\partial \xi_1} \rangle, \tag{7.158}$$

$$H^{(3)} = \langle \sigma\alpha \frac{\partial (N_1^{(3)} + \xi_1)}{\partial \xi_1} + \sigma\alpha^2 \frac{\partial M_1^{(3)}}{\partial \xi_1} \rangle, \tag{7.159}$$

$$H^{(4)} = \langle \sigma\alpha \frac{\partial N_1^{(4)}}{\partial \xi_1} + \sigma\alpha^2 \frac{\partial (M_1^{(4)} + \xi_1)}{\partial \xi_1} \rangle, \tag{7.160}$$

$$K^{(1)} = \langle \kappa \frac{\partial M_1^{(1)}}{\partial \xi_1} \rangle, \tag{7.161}$$

$$K^{(2)} = \langle \kappa \frac{\partial M_1^{(2)}}{\partial \xi_1} \rangle, \tag{7.162}$$

$$K^{(3)} = \langle \kappa \frac{\partial M_1^{(3)}}{\partial \xi_1} \rangle, \tag{7.163}$$

$$K^{(4)} = \langle \kappa \frac{\partial (M_1^{(4)} + \xi_1)}{\partial \xi_1} \rangle. \tag{7.164}$$

It is worth comparing (7.151-7.152) with the macroscopic current density and heat flux in 1D, which are

$$J = \frac{1}{V_1} \frac{1}{\widetilde{T}^{(0)}} \frac{d\phi^{(0)}}{dx} + \frac{V_3}{V_1} \frac{1}{\widetilde{T}^{(0)}} \frac{d\widetilde{T}^{(0)}}{dx}, \tag{7.165}$$

$$\begin{aligned} J_U &= \frac{\frac{1}{V_1}\phi^{(0)} + \frac{V_3}{V_1}\widetilde{T}^{(0)} + \frac{V_3}{V_1} X}{\widetilde{T}^{(0)}} \frac{d\phi^{(0)}}{dx} \\ &+ \frac{\frac{V_3}{V_1}\phi^{(0)} + (\frac{V_3^2}{V_1} - < \frac{1}{\kappa} >^{-1})\widetilde{T}^{(0)} + \frac{V_3^2}{V_1} X}{\widetilde{T}^{(0)}} \frac{d\widetilde{T}^{(0)}}{dx}, \end{aligned} \tag{7.166}$$

where V_1, V_3, X are constants, and can be calculated by (7.48-7.51). Clearly pseudo 3D results are significantly more complex. By using 1D equations (7.40-7.47) for $N^{(1)}$ etc. for

the calculation of effective properties, it is verified that (7.151-7.152) will recover (7.165-7.166).

Compared to 3D problem, pseudo 3D can be understood as a simplified version where the subscription of $N_i^{(j)}$ and $M_i^{(j)}$ is limited to $i = 1$. There is virtually no difference between 3D and pseudo 3D in unit cell problem formulation, except that on lateral boundary pseudo 3D has Neumann type boundary condition (7.147).

7.5 Summary

In this chapter, we applied asymptotic homogenization method on 2D/3D thermoelectric composite with nonlinearly coupled transport of heat and electricity. The unit cell problems, both for general and pseudo 2D/3D cases, are established, which are to be solved numerically. The 2D/3D homogenized thermoelectric governing equation that governs the distributions of macroscopic temperature and electric potential are also established.

Chapter 8

ASYMPTOTIC ANALYSIS OF TWO-DIMENSIONAL THERMOELECTRIC MEDIUM II: NUMERICAL SOLUTION

8.1 Introductory remarks

For the unit cell problem represented by the governing differential equations (7.28-7.37), interface conditions of (7.59, 7.61-7.70), and boundary conditions (7.75, 7.78-7.82), or the pseudo 2D/3D problem presented in Section 7.4, it is generally difficult to find analytical solutions due to the complexity of the 2D/3D multi-phase structure. As a result, we applied Finite Element method[99–101] to find the numerical solutions.

In Section 2, the concept and general knowledge of Finite Element method is introduced, with more details for 2D triangular element given. In Section 3, the particularity of our problem presents more difficulty, and the strategy is discussed. In Section 4, numerical results are provided, both for verification case and for 2D calculations. In Section 5, the summary for this chapter is given.

8.2 Finite Element method

8.2.1 General knowledge

Let's consider a problem formulated with the following differential equations and boundary conditions

$$\frac{\partial}{\partial x_i}[\mathbf{A}_{ij}(\mathbf{x})\frac{\partial \mathbf{u}}{\partial x_j}] = \mathbf{f}(\mathbf{x}),\ \mathbf{x} \in \Omega, \tag{8.1}$$

$$\mathbf{u} = \overline{\mathbf{u}},\ \mathbf{x} \in \Gamma_1, \tag{8.2}$$

$$\mathbf{A}_{ij}\frac{\partial \mathbf{u}}{\partial x_j}n_i = \overline{\mathbf{q}},\ \mathbf{x} \in \Gamma_2, \tag{8.3}$$

where $\mathbf{A}_{ij}$ $(i, j = 1, 2, 3)$ are given $n \times n$ matrix-valued functions of material properties, $\mathbf{f}$ is a given n-dimensional vector function. The required n-dimensional variable $\mathbf{u}$ needs to satisfy equation (8.1) inside the domain Ω, and on boundary Γ_1 the Dirichlet boundary

condition (8.2), and on Γ_2 the Neumann boundary condition (8.3), where $\overline{\mathbf{u}}$ and $\overline{\mathbf{q}}$ are given n-dimensional vector functions, and $\partial\Omega = \Gamma_1 + \Gamma_2$ is the whole boundary of Ω.

We can equivalently formulate the problem using the following integral form,

$$\int_\Omega \mathbf{V}_1^T(\mathbf{x})[\frac{\partial}{\partial x_i}(\mathbf{A}_{ij}\frac{\partial \mathbf{u}}{\partial x_j}) - \mathbf{f}]d\Omega + \int_{\Gamma_2} \mathbf{V}_2^T(\mathbf{x})(\mathbf{A}_{ij}\frac{\partial \mathbf{u}}{\partial x_j}n_i - \overline{\mathbf{q}})d\Gamma + \int_{\Gamma_1} \mathbf{V}_3^T(\mathbf{x})(\mathbf{u} - \overline{\mathbf{u}})d\Gamma = 0, \tag{8.4}$$

(8.4) should be valid for any arbitrary n-dimensional functions of $\mathbf{V}_1$, $\mathbf{V}_2$, $\mathbf{V}_3$, here the superscript T denotes transpose of the vectors. By divergence theorem, the first term of (8.4) can transformed

$$\begin{aligned}
&\int_\Omega \mathbf{V}_1^T[\frac{\partial}{\partial x_i}(\mathbf{A}_{ij}\frac{\partial \mathbf{u}}{\partial x_j}) - \mathbf{f}]d\Omega \\
&= \int_\Omega \frac{\partial}{\partial x_i}(\mathbf{V}_1^T\mathbf{A}_{ij}\frac{\partial \mathbf{u}}{\partial x_j})d\Omega - \int_\Omega \frac{\partial \mathbf{V}_1^T}{\partial x_i}\mathbf{A}_{ij}\frac{\partial \mathbf{u}}{\partial x_j}d\Omega - \int_\Omega \mathbf{V}_1^T\mathbf{f}d\Omega \\
&= \int_{\partial\Omega} \mathbf{V}_1^T\mathbf{A}_{ij}\frac{\partial \mathbf{u}}{\partial x_j}n_i d\Gamma - \int_\Omega \frac{\partial \mathbf{V}_1^T}{\partial x_i}\mathbf{A}_{ij}\frac{\partial \mathbf{u}}{\partial x_j}d\Omega - \int_\Omega \mathbf{V}_1^T\mathbf{f}d\Omega.
\end{aligned} \tag{8.5}$$

Plugging (8.5) into (8.4), and using $\mathbf{V}_2 = -\mathbf{V}_1$ without loss of generality, we have

$$-\int_\Omega \frac{\partial \mathbf{V}_1^T}{\partial x_i}\mathbf{A}_{ij}\frac{\partial \mathbf{u}}{\partial x_j}d\Omega - \int_\Omega \mathbf{V}_1^T\mathbf{f}d\Omega + \int_{\Gamma_1} \mathbf{V}_1^T\mathbf{A}_{ij}\frac{\partial \mathbf{u}}{\partial x_j}n_i d\Gamma + \int_{\Gamma_2} \mathbf{V}_1^T\overline{\mathbf{q}}d\Gamma + \int_{\Gamma_1} \mathbf{V}_3^T(\mathbf{u} - \overline{\mathbf{u}})d\Gamma = 0, \tag{8.6}$$

which is the weak form of (8.1-8.3).

Suppose the field variable is to be approximated by the following

$$\mathbf{u} \approx \mathbf{u}^* = \sum_{i=1}^{m} \mathbf{N}_i a_i, \tag{8.7}$$

where a_i are parameters to be determined, $\mathbf{N}_i$ $(i = 1, 2, ..., m)$ are some given complete and linearly independent function series. Suppose (8.2) on Γ_1 is strictly satisfied when we do the approximation, whereas for (8.1) and (8.3) we have

$$\frac{\partial}{\partial x_i}[\mathbf{A}_{ij}\frac{\partial(\mathbf{N}_k a_k)}{\partial x_j}] - \mathbf{f} = \mathbf{R},\ \mathbf{x} \in \Omega, \tag{8.8}$$

$$\mathbf{A}_{ij}\frac{\partial(\mathbf{N}_k a_k)}{\partial x_j}n_i - \overline{\mathbf{q}} = \overline{\mathbf{R}},\ \mathbf{x} \in \Gamma_2, \tag{8.9}$$

where $\mathbf{R}$ and $\overline{\mathbf{R}}$ are known as residuals. We use the approximation (8.7) in (8.4) and choose

$$\mathbf{V}_1 = \mathbf{W}_k, \tag{8.10}$$

$$\mathbf{V}_2 = \overline{\mathbf{W}}_k, \tag{8.11}$$

where $\mathbf{W}_k$ and $\overline{\mathbf{W}}_k$ $(k = 1, 2, ..., m)$ are some specially chosen functions, we have

$$\int_\Omega \mathbf{W}_l^T(\mathbf{x})[\frac{\partial}{\partial x_i}(\mathbf{A}_{ij}\frac{\partial(\mathbf{N}_k a_k)}{\partial x_j}) - \mathbf{f}]d\Omega$$
$$+ \int_{\Gamma_2} \overline{\mathbf{W}}_l^T(\mathbf{x})(\mathbf{A}_{ij}\frac{\partial(\mathbf{N}_k a_k)}{\partial x_j}n_i - \overline{\mathbf{q}})d\Gamma = 0,\ l = 1, 2, ..., m \tag{8.12}$$

which gives us a system of m equations to solve for a_k. (8.12) can be interpreted as averaging out the residuals over the domain, and this method is known as Weighted Residuals method. Especially, if we choose

$$\mathbf{W}_k = \mathbf{N}_k, \tag{8.13}$$

$$\overline{\mathbf{W}}_k = -\mathbf{N}_k,\ k = 1, 2, ..., m \tag{8.14}$$

we have Galerkin's method. So the idea is to establish a mechanism to approximate the field variable using the description of (8.7).

The finite element method can also be formulated equivalently from variational point of view, where a functional

$$\Pi = \int_\Omega F(\mathbf{u}, \frac{\partial \mathbf{u}}{\partial x_i}, ...)d\Omega + \int_\Gamma E(\mathbf{u}, \frac{\partial \mathbf{u}}{\partial x_i}, ...)d\Gamma, \tag{8.15}$$

is defined, in which $\mathbf{u}$ is field variable, F and E are some operators. The functional Π is so defined such that the value of $\mathbf{u}$ that satisfies (8.1-8.3) corresponds to the stationary value of Π with respect to small variation of $\delta\mathbf{u}$. By invoking the stationarity of Π, from the approximation of (8.7), we have

$$\delta\Pi = \frac{\partial \Pi}{\partial a_1}\delta a_1 + \frac{\partial \Pi}{\partial a_2}\delta a_2 + ... + \frac{\partial \Pi}{\partial a_m}\delta a_m = 0. \tag{8.16}$$

Because the arbitrariness of δa_i, we have

$$\frac{\partial \Pi}{\partial a_i} = 0,\ i = 1, 2, ..., m, \tag{8.17}$$

which constitutes a system of equations that we can use to solve for a_i. This is called Ritz method.

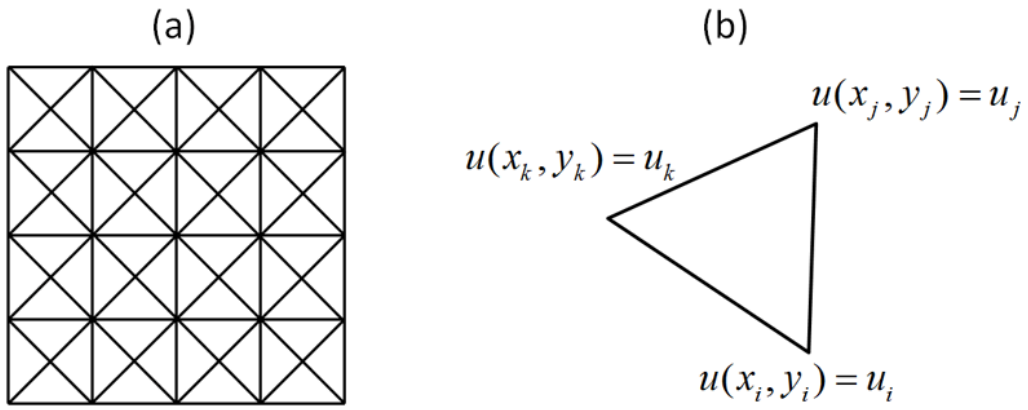

Figure 8.1: An example of (a) a 2D finite element mesh, (b) a 3-node triangular element.

8.2.2 2D triangular element together with Galerkin method

The foregoing descriptions on the asymptotic analysis and numeric calculation are so general such that it is applicable to both 2D (spacial indices taking values of 1, 2) and 3D (spacial indices taking values of 1, 2, 3). But from here on, we are confining our finite element calculation into 2D due to the relatively simple implementation. The extension of finite element method implementation from 2D to 3D should be straightforward, and conceptually they should be the same.

Specifically we consider 2D triangular 3-node element as shown in Figure 8.1(b), where the value of some field variable u on the element is assumed to be linear with respect to the spacial coordinates

$$u = \beta_1 + \beta_2 x + \beta_3 y, \tag{8.18}$$

in which, β_1, β_2, β_3 are coefficients that will be determined later. With the values of u at the three nodes, and their coordinates, the coefficients can be calculated as

$$\beta_1 = \frac{1}{2S}(a_i u_i + a_j u_j + a_k u_k), \tag{8.19}$$

$$\beta_2 = \frac{1}{2S}(b_i u_i + b_j u_j + b_k u_k), \tag{8.20}$$

$$\beta_3 = \frac{1}{2S}(c_i u_i + c_j u_j + c_k u_k), \tag{8.21}$$

where S is the area of the element with

$$2S = \begin{vmatrix} 1 & x_i & y_i \\ 1 & x_j & y_j \\ 1 & x_k & y_k \end{vmatrix}, \tag{8.22}$$

and

$$a_i = x_j y_k - x_k y_j, \tag{8.23}$$

$$b_i = y_j - y_k, \tag{8.24}$$

$$c_i = -x_j + x_k, \ (i,j,k), \tag{8.25}$$

where (i,j,k) denotes the index permutation of $i \to j$, $j \to k$, $k \to i$, so that (8.23-8.25) apply to all the coefficients. By substituting (8.19-8.21) into (8.18), we have

$$u = N_i^e u_i + N_j^e u_j + N_k^e u_k, \tag{8.26}$$

where

$$N_i^e = \frac{1}{2S}(a_i + b_i x + c_i y), \ (i,j,k). \tag{8.27}$$

N_i^e, N_j^e, N_k^e are known as shape functions, and they satisfy

$$N_i^e(x_i, y_i) = 1, \quad N_i^e(x_j, y_j) = 0, \quad N_i^e(x_k, y_k) = 0, \quad (i,j,k). \tag{8.28}$$

Also at every point on the element, there is

$$N_i^e + N_j^e + N_k^e = 1. \tag{8.29}$$

If we replace scalar field variable u with n-dimensional vector $\mathbf{u}$, the foregoing procedure still applies, and (8.26) becomes

$$\mathbf{u} = N_i^e \mathbf{u}_i + N_j^e \mathbf{u}_j + N_k^e \mathbf{u}_k, \tag{8.30}$$

or

$$\mathbf{u} = \mathbf{N}^{eT} \mathbf{u}^e, \tag{8.31}$$

where

$$\mathbf{u}^e = \begin{bmatrix} \mathbf{u}_i^T & \mathbf{u}_j^T & \mathbf{u}_k^T \end{bmatrix}^T, \tag{8.32}$$

$$\mathbf{N}^e = \begin{bmatrix} \mathbf{N}_i^e & \mathbf{N}_j^e & \mathbf{N}_k^e \end{bmatrix}^T, \tag{8.33}$$

and

$$\mathbf{N}_i^e = N_i^e \underbrace{\begin{bmatrix} 1 & 0 & 0 & \dots & 0 \\ 0 & 1 & 0 & \dots & 0 \\ 0 & 0 & 1 & \dots & 0 \\ \vdots & \vdots & \vdots & \ddots & \vdots \\ 0 & 0 & 0 & \dots & 1 \end{bmatrix}}_{n} = N_i^e \mathbf{I}, \quad (i,j,k), \tag{8.34}$$

the superscript T denotes transpose of the matrix.

For a domain that has been discretized into pieces of such triangular elements with a total of m nodes, similar to what Figure 8.1(a) shows, we organize all the node values as

$$\mathbf{u}^a = \begin{bmatrix} \mathbf{u}_1^T & \mathbf{u}_2^T & \cdots & \mathbf{u}_m^T \end{bmatrix}^T, \tag{8.35}$$

analogous to (8.31), we have

$$\mathbf{u} = \mathbf{N}^{aT}\mathbf{u}^a, \tag{8.36}$$

where

$$\mathbf{N}^a = \begin{bmatrix} \mathbf{N}_1 & \mathbf{N}_2 & \cdots & \mathbf{N}_m \end{bmatrix}^T, \tag{8.37}$$

here $\mathbf{N}_1$ etc. are values defined on the whole domain, they have different formulae inside different elements. Inside the element with nodes of i, j, k, $\mathbf{u}^e$ can be converted from $\mathbf{u}^a$ by

$$\mathbf{u}^e = \mathbf{G}\mathbf{u}^a, \tag{8.38}$$

where

$$\mathbf{G} = \begin{array}{c} \begin{array}{ccccccccc} 1 & \cdots & i & \cdots & j & \cdots & k & \cdots & m \end{array} \\ \begin{bmatrix} \mathbf{0} & \cdots & \mathbf{I} & \cdots & \mathbf{0} & \cdots & \mathbf{0} & \cdots & \mathbf{0} \\ \mathbf{0} & \cdots & \mathbf{0} & \cdots & \mathbf{I} & \cdots & \mathbf{0} & \cdots & \mathbf{0} \\ \mathbf{0} & \cdots & \mathbf{0} & \cdots & \mathbf{0} & \cdots & \mathbf{I} & \cdots & \mathbf{0} \end{bmatrix} \end{array}. \tag{8.39}$$

From (8.31), we have

$$\mathbf{u} = \mathbf{N}^{eT}\mathbf{G}\mathbf{u}^a = \widetilde{\mathbf{N}}^{aT}\mathbf{u}^a, \tag{8.40}$$

with

$$\widetilde{\mathbf{N}}^a = \mathbf{G}^T\mathbf{N}^e = \begin{array}{c} \begin{array}{ccccccccc} 1 & \cdots & i & \cdots & j & \cdots & k & \cdots & m \end{array} \\ \begin{bmatrix} \mathbf{0} & \cdots & \mathbf{N}_i^e & \cdots & \mathbf{N}_j^e & \cdots & \mathbf{N}_k^e & \cdots & \mathbf{0} \end{bmatrix}^T \end{array}. \tag{8.41}$$

Here in contrast with $\mathbf{N}^a$, $\widetilde{\mathbf{N}}^a$ is defined on the element of ijk. The definition of $\widetilde{\mathbf{N}}^a$ for all elements inside the domain constitutes the definition of $\mathbf{N}^a$. We use $\mathbf{u}$ of (8.36) defined on the whole domain, in place of the approximation $\mathbf{u}^*$ in Galerkin's method. From (8.12), we have

$$-\int_\Omega \frac{\partial \mathbf{N}_l^T}{\partial x_i}\mathbf{A}_{ij}\frac{\partial(\mathbf{N}^{aT}\mathbf{u}^a)}{\partial x_j}d\Omega - \int_\Omega \mathbf{N}_l^T\mathbf{f}d\Omega + \int_{\Gamma_1}\mathbf{N}_l^T\mathbf{A}_{ij}\frac{\partial(\mathbf{N}^{aT}\mathbf{u}^a)}{\partial x_j}n_i d\Gamma + \int_{\Gamma_2}\mathbf{N}_l^T\overline{\mathbf{q}}d\Gamma = 0,\ l = 1, 2, ..., m \tag{8.42}$$

or

$$-\int_\Omega \frac{\partial \mathbf{N}^a}{\partial x_i}\mathbf{A}_{ij}\frac{\partial \mathbf{N}^{aT}}{\partial x_j}\mathbf{u}^a d\Omega - \int_\Omega \mathbf{N}^a\mathbf{f}d\Omega + \int_{\Gamma_2}\mathbf{N}^a\overline{\mathbf{q}}d\Gamma = 0. \tag{8.43}$$

In the latter equation, we have chosen $\mathbf{N}^a|_{\Gamma_1} = 0$ so that

$$\int_{\Gamma_1}\mathbf{N}_l^T\mathbf{A}_{ij}\frac{\partial(\mathbf{N}^{aT}\mathbf{u}^a)}{\partial x_j}n_i d\Gamma$$

term disappears. We can do this because on the boundary Γ_1, the Dirichlet type boundary condition $\mathbf{u} = \overline{\mathbf{u}}$ has already been strictly satisfied. Equation (8.43) are reorganized as

$$\mathbf{K}^a\mathbf{u}^a = \mathbf{P}^a, \tag{8.44}$$

with

$$\mathbf{K}^a = \int_\Omega \frac{\partial \mathbf{N}^a}{\partial x_i} \mathbf{A}_{ij} \frac{\partial \mathbf{N}^{aT}}{\partial x_j} d\Omega, \tag{8.45}$$

and

$$\mathbf{P}^a = \int_{\Gamma_2} \mathbf{N}^a \overline{\mathbf{q}} d\Gamma - \int_\Omega \mathbf{N}^a \mathbf{f} d\Omega. \tag{8.46}$$

(8.45) is simplified as

$$\begin{aligned} \mathbf{K}^a &= \sum_e \int_{\Omega^e} \frac{\partial \widetilde{\mathbf{N}}^a}{\partial x_i} \mathbf{A}_{ij} \frac{\partial \widetilde{\mathbf{N}}^{aT}}{\partial x_j} d\Omega, \\ &= \sum_e \int_{\Omega^e} \mathbf{G}^T \frac{\partial \mathbf{N}^e}{\partial x_i} \mathbf{A}_{ij} \frac{\partial \mathbf{N}^{eT}}{\partial x_j} \mathbf{G} d\Omega, \\ &= \sum_e \mathbf{G}^T \mathbf{K}^e \mathbf{G}, \end{aligned} \tag{8.47}$$

with

$$\mathbf{K}^e = \int_{\Omega^e} \frac{\partial \mathbf{N}^e}{\partial x_i} \mathbf{A}_{ij} \frac{\partial \mathbf{N}^{eT}}{\partial x_j} d\Omega. \tag{8.48}$$

So the overall matrix $\mathbf{K}^a$ is assembled by combining all the elemental matrices $\mathbf{K}^e$. From (8.33), we have

$$\frac{\partial \mathbf{N}^e}{\partial x} = \left[\begin{array}{ccc} \frac{\partial \mathbf{N}_i^e}{\partial x} & \frac{\partial \mathbf{N}_j^e}{\partial x} & \frac{\partial \mathbf{N}_k^e}{\partial x} \end{array} \right]^T. \tag{8.49}$$

From (8.34), we have

$$\frac{\partial \mathbf{N}_i^e}{\partial x} = \frac{\partial N_i^e}{\partial x} \mathbf{I} = \frac{b_i}{2S} \mathbf{I}, \quad (i, j, k). \tag{8.50}$$

Similarly, we have

$$\frac{\partial \mathbf{N}_i^e}{\partial y} = \frac{\partial N_i^e}{\partial y} \mathbf{I} = \frac{c_i}{2S} \mathbf{I}, \quad (i, j, k). \tag{8.51}$$

If we assume isotropic materials such that $\mathbf{A}_{ij} = \mathbf{A}\delta_{ij}$, from (8.33, 8.50, 8.51), (8.48) becomes

$$\mathbf{K}^e = \left[\begin{array}{ccc} \mathbf{K}_{ii}^e & \mathbf{K}_{ij}^e & \mathbf{K}_{ik}^e \\ \mathbf{K}_{ji}^e & \mathbf{K}_{jj}^e & \mathbf{K}_{jk}^e \\ \mathbf{K}_{ki}^e & \mathbf{K}_{kj}^e & \mathbf{K}_{kk}^e \end{array} \right], \tag{8.52}$$

where

$$\begin{aligned}\mathbf{K}^e_{pq} &= \int_{\Omega^e} (\frac{\partial \mathbf{N}^e_p}{\partial x}\mathbf{A}\frac{\partial \mathbf{N}^e_q}{\partial x} + \frac{\partial \mathbf{N}^e_p}{\partial y}\mathbf{A}\frac{\partial \mathbf{N}^e_q}{\partial y})d\Omega \\ &= \frac{b_p b_q + c_p c_q}{4S}\mathbf{A}, \quad p,q = i,j,k. \end{aligned} \tag{8.53}$$

From (8.46), $\mathbf{P}^a$ has two components, one inside the body, the other from the boundary condition. Especially, if we have $\mathbf{f} = \mathbf{0}$, (8.46) becomes

$$\begin{aligned}\mathbf{P}^a &= \sum_e \int_{\Gamma^e_2} \widetilde{\mathbf{N}}^a \overline{\mathbf{q}} d\Gamma \\ &= \sum_e \mathbf{G}^T \int_{\Gamma^e_2} \mathbf{N}^e \overline{\mathbf{q}} d\Gamma \\ &= \sum_e \mathbf{G}^T \mathbf{P}^e, \end{aligned} \tag{8.54}$$

where

$$\mathbf{P}^e = \int_{\Gamma^e_2} \mathbf{N}^e \overline{\mathbf{q}} d\Gamma. \tag{8.55}$$

So like $\mathbf{K}^a$, $\mathbf{P}^a$ is obtained through the calculation of the element values of $\mathbf{P}^e$. From (8.33), (8.55) becomes

$$\mathbf{P}^e = \begin{bmatrix} \mathbf{P}^e_i \\ \mathbf{P}^e_j \\ \mathbf{P}^e_k \end{bmatrix}, \tag{8.56}$$

where

$$\begin{aligned}\mathbf{P}^e_i &= \int_{\Gamma^e_2} \mathbf{N}^e_i \overline{\mathbf{q}} d\Gamma \\ &= \int_{\Gamma^e_2} N^e_i \overline{\mathbf{q}} d\Gamma, \quad (i,j,k). \end{aligned} \tag{8.57}$$

For the purpose of illustration, suppose the element ijk has the edge ij on the Γ_2 boundary, as shown in the Figure 8.2, where the length of edge ij is l. We use the local coordinate s that is measured from node i, and along ij. It can be determined that

$$N^e_i = 1 - \frac{s}{l}, \quad N^e_j = \frac{s}{l}, \quad N^e_k = 0. \tag{8.58}$$

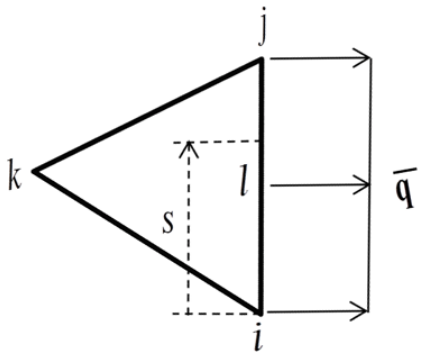

Figure 8.2: An example of an element ijk with its edge ij on the boundary where Neumann boundary condition is applied.

Based on (8.58), we have

$$\mathbf{P}_i^e = \mathbf{P}_j^e = \frac{l}{2}\overline{\mathbf{q}}, \quad \mathbf{P}_k^e = \mathbf{0}. \tag{8.59}$$

Conceptually, we have assumed that the Dirichlet boundary condition $\mathbf{u} = \overline{\mathbf{u}}$ was strictly satisfied by choosing the appropriate $\mathbf{N}^a$ to start with. Practically, this is not necessarily the case. Rather we normally apply the $\mathbf{u} = \overline{\mathbf{u}}$ boundary condition directly onto the overall equation system (8.44), and there are two cases. First, supposed we have $u_l^a = 0$ as boundary condition, we update (8.44) by modifying the l-th row and l-th column of $\mathbf{K}^a$ and l-th row of $\mathbf{P}^a$ as the following

$$\begin{array}{c} 1 \quad 2 \quad \cdots \quad l \quad \cdots \quad m \\ \begin{bmatrix} K_{11}^a & K_{12}^a & \cdots & 0 & \cdots & K_{1m}^a \\ K_{21}^a & K_{22}^a & \cdots & 0 & \cdots & K_{2m}^a \\ \vdots & \vdots & \vdots & \vdots & \vdots & \vdots \\ 0 & 0 & \cdots & 1 & \cdots & 0 \\ \vdots & \vdots & \vdots & \vdots & \vdots & \vdots \\ K_{m1}^a & K_{m2}^a & \cdots & 0 & \cdots & K_{mm}^a \end{bmatrix} \end{array} \begin{bmatrix} u_1^a \\ u_2^a \\ \vdots \\ u_l^a \\ \vdots \\ u_m^a \end{bmatrix} = \begin{bmatrix} P_1^a \\ P_2^a \\ \vdots \\ 0 \\ \vdots \\ P_m^a \end{bmatrix}. \tag{8.60}$$

On the other hand, if we have $u_l^a = \overline{u}_l^a$ as boundary condition, we update (8.44) by modifying

the l-th row of $\mathbf{K}^a$ and $\mathbf{P}^a$ as the following

$$\begin{array}{cccccc} 1 & 2 & \cdots & l & \cdots & m \end{array}$$
$$\begin{bmatrix} K^a_{11} & K^a_{12} & \cdots & K^a_{1l} & \cdots & K^a_{1m} \\ K^a_{21} & K^a_{22} & \cdots & K^a_{2l} & \cdots & K^a_{2m} \\ \vdots & \vdots & \vdots & \vdots & \vdots & \vdots \\ K^a_{l1} & K^a_{l2} & \cdots & \mu K^a_{ll} & \cdots & K^a_{lm} \\ \vdots & \vdots & \vdots & \vdots & \vdots & \vdots \\ K^a_{m1} & K^a_{m2} & \cdots & K^a_{ml} & \cdots & K^a_{mm} \end{bmatrix} \begin{bmatrix} u^a_1 \\ u^a_2 \\ \vdots \\ u^a_l \\ \vdots \\ u^a_m \end{bmatrix} = \begin{bmatrix} P^a_1 \\ P^a_2 \\ \vdots \\ \mu K^a_{ll} \overline{u}^a_l \\ \vdots \\ P^a_m \end{bmatrix}, \tag{8.61}$$

where μ is a giant number. So the l-th row is approximately

$$\mu K^a_{ll} u^a_l \approx \mu K^a_{ll} \overline{u}^a_l, \tag{8.62}$$

or

$$u^a_l \approx \overline{u}^a_l. \tag{8.63}$$

So we have the linear system (8.44), and have updated it using the $\mathbf{u} = \overline{\mathbf{u}}$ boundary condition. It is ready to be solved to give us the nodal result of $\mathbf{u}^a$. From there, according to (8.36), the field of $\mathbf{u}$ can be determined, and then $\frac{\partial \mathbf{u}}{\partial x_i}$ if it is required. The solving of the linear system can be carried out by Gauss elimination or other optimized algorithms such as LU decomposition.

8.3 Solving four fields from five equations

We are ready to solve the problem represented by the governing differential equations (7.28-7.37), together with corresponding continuity and boundary conditions, or the pseudo 2D/3D problem presented in Section 7.4. Further examination of the problem reveals two sub-problems that can be solved individually, and each sub-problem consists of five equa-

tions, and the corresponding interfacial and boundary conditions. To be specific, we define

$$\mathbf{A} = \begin{bmatrix} \sigma & \sigma\alpha & 0 & 0 \\ X\sigma\alpha & X\sigma\alpha^2+\kappa & 0 & 0 \\ 0 & 0 & \sigma & \sigma\alpha \\ 0 & 0 & \sigma\alpha & \sigma\alpha^2 \\ \sigma\alpha & \sigma\alpha^2 & 0 & \kappa \end{bmatrix}, \quad \mathbf{u} = \begin{bmatrix} N_1^{(1)} \\ M_1^{(1)} \\ \widetilde{N}_1^{(3)} \\ M_1^{(3)} \end{bmatrix}, \tag{8.64}$$

where

$$\widetilde{N}_1^{(3)} = N_1^{(3)} + \xi_1, \tag{8.65}$$

and we are confining the calculation as to the case where the subscription $j = 1$, for $j = 2$ calculation can be similarly carried out. So one of the sub-problem can be characterized as

$$\begin{cases} \frac{\partial}{\partial \xi_i}(\mathbf{A}\frac{\partial \mathbf{u}}{\partial \xi_i}) = \mathbf{0}, \quad \boldsymbol{\xi} \in \Omega, \\ [\mathbf{u}]|_\Sigma = \mathbf{0}, \quad [\mathbf{A}\frac{\partial \mathbf{u}}{\partial \xi_i} n_i]|_\Sigma = \mathbf{0}, \\ \mathbf{u}(0,\xi_2) = \begin{bmatrix} 0 & 0 & 0 & 0 \end{bmatrix}^T, \\ \mathbf{u}(1,\xi_2) = \begin{bmatrix} 0 & 0 & 1 & 0 \end{bmatrix}^T, \\ \mathbf{u}(\xi_1,0) = \mathbf{u}(\xi_1,1) = \begin{bmatrix} 0 & 0 & \xi_1 & 0 \end{bmatrix}^T. \end{cases} \tag{8.66}$$

Similarly, we define

$$\widetilde{\mathbf{u}} = \begin{bmatrix} N_1^{(2)} \\ M_1^{(2)} \\ N_1^{(4)} \\ \widetilde{M}_1^{(4)} \end{bmatrix}, \tag{8.67}$$

where

$$\widetilde{M}_1^{(4)} = M_1^{(4)} + \xi_1. \tag{8.68}$$

So the other sub-problem is characterized as

$$\begin{cases} \frac{\partial}{\partial \xi_i}(\mathbf{A}\frac{\partial \widetilde{\mathbf{u}}}{\partial \xi_i}) = \mathbf{0}, \quad \boldsymbol{\xi} \in \Omega, \\ [\widetilde{\mathbf{u}}]|_\Sigma = \mathbf{0}, \quad [\mathbf{A}\frac{\partial \widetilde{\mathbf{u}}}{\partial \xi_i} n_i]|_\Sigma = \mathbf{0}, \\ \widetilde{\mathbf{u}}(0, \xi_2) = \begin{bmatrix} 0 & 0 & 0 & 0 \end{bmatrix}^T, \\ \widetilde{\mathbf{u}}(1, \xi_2) = \begin{bmatrix} 0 & 0 & 0 & 1 \end{bmatrix}^T, \\ \widetilde{\mathbf{u}}(\xi_1, 0) = \widetilde{\mathbf{u}}(\xi_1, 1) = \begin{bmatrix} 0 & 0 & 0 & \xi_1 \end{bmatrix}^T. \end{cases} \tag{8.69}$$

The two sub-problems are so similar to each other that if we can solve one of them, we can solve the other. Thus for the following calculation, we only consider the first sub-problem.

One strange thing about our sub-problem (8.66) is that in the governing equation, $\mathbf{A}$ is a 5×4 matrix, and $\mathbf{u}$ is a four-dimensional vector, which means we have more equations than unknown variables. But on the other hand, we have X inside $\mathbf{A}$, which is an unknown constant. So no equation is really redundant. Further, we notice that we could have grouped $N_1^{(1)}$, $M_1^{(1)}$ together such as

$$\mathbf{u} = \begin{bmatrix} N_1^{(1)} \\ M_1^{(1)} \end{bmatrix}, \tag{8.70}$$

and accordingly modified

$$\mathbf{A} = \begin{bmatrix} \sigma & \sigma\alpha \\ X\sigma\alpha & X\sigma\alpha^2 + \kappa \end{bmatrix}. \tag{8.71}$$

Notice that the boundary condition is now $\mathbf{u}|_{\partial\Omega} = \mathbf{0}$, it is immediate that $\mathbf{u} = \mathbf{0}$ is the solution, unless the problem is singular. In the latter case, no solution can be determined. But we know that $N_1^{(1)}$, $M_1^{(1)}$ are not uniformly zero from 1D results (7.40-7.47), so it must be that there is a special value of X that makes the problem singular, and as a result, the choice of (8.70-8.71) makes an incomplete description of problem. Furthermore, we can see anything less than (8.64) is an incomplete description of the problem.

Another thing worth noting is that the third and fourth rows of $\mathbf{A}$ are different only by a factor of α. In fact, they mean the same thing inside individual phases because material

properties are uniform inside any phases, such that α can be pulled out and then canceled. They do differ across the interface, being respectively

$$[(\sigma\frac{\partial\widetilde{N}_1^{(3)}}{\partial\xi_i}+\sigma\alpha\frac{\partial M_1^{(3)}}{\partial\xi_i})n_i]|_\Sigma=0, \tag{8.72}$$

and

$$[(\sigma\alpha\frac{\partial\widetilde{N}_1^{(3)}}{\partial\xi_i}+\sigma\alpha^2\frac{\partial M_1^{(3)}}{\partial\xi_i})n_i]|_\Sigma=0. \tag{8.73}$$

But generally, α has different values for the two phases across the interface. For (8.72) and (8.73) to be valid simultaneously, it has to be that

$$(\sigma\frac{\partial\widetilde{N}_1^{(3)}}{\partial\xi_i}+\sigma\alpha\frac{\partial M_1^{(3)}}{\partial\xi_i})n_i|_{\boldsymbol{\xi}\in\Sigma}=0. \tag{8.74}$$

Thus (8.74) imposes a strong interface condition on our problem. Considering all the special features of our problem, a two-step approach is proposed as follows for solving the problem.

8.3.1 Step one: finding X

The grouping of (8.70) and (8.71) provides us the following problem

$$\begin{cases}\frac{\partial}{\partial\xi_i}(\mathbf{A}\frac{\partial\mathbf{u}}{\partial\xi_i})=\mathbf{0}, \quad \boldsymbol{\xi}\in\Omega,\\ [\mathbf{u}]|_\Sigma=\mathbf{0}, \quad [\mathbf{A}\frac{\partial\mathbf{u}}{\partial\xi_i}n_i]|_\Sigma=\mathbf{0},\\ \mathbf{u}|_{\partial\Omega}=\mathbf{0}.\end{cases} \tag{8.75}$$

We have argued in the above that this problem has to be incompletely defined, because otherwise we would have $\mathbf{u}=\mathbf{0}$, which is an impossible result. So for this to be an incomplete description of the problem, we should have $\mathbf{K}^a$ as in

$$\mathbf{K}^a\mathbf{u}^a=\mathbf{0}, \tag{8.76}$$

to be a singular matrix, where (8.76) represents the overall linear system of the problem (8.75) using Finite Element method. Or X in (8.71) should be so chosen such that

$$f(X)=|\mathbf{K}^a|=0. \tag{8.77}$$

Instead of using the determinant of a matrix, we actually use

$$f(X)=\frac{1}{cond(\mathbf{K}^a)}=0, \tag{8.78}$$

for finding X, where $cond(\mathbf{K}^a)$ denotes the condition number of $\mathbf{K}^a$. Due to the numerical nature of the result, we want to choose a function that can directly correlate with the closeness of the calculated result X_C towards the precise value X, some relationship such as

$$||f(X_{C1})|| \leq ||f(X_{C2})||, \quad if\ and\ only\ if\ ||X_{C1} - X|| \leq ||X_{C2} - X||, \tag{8.79}$$

where $||.||$ means a norm, of the enclosed values. For that matter, condition number makes a better candidate than determinant. Condition number of a matrix $\mathbf{A}$ is defined by[102]

$$cond(\mathbf{A}) = ||\mathbf{A}^{-1}||\ ||\mathbf{A}||, \tag{8.80}$$

where $||.||$ means norm of the enclosed matrix. Especially, the matrix norm subordinate to the two-norm of vectors is

$$||\mathbf{A}||_2 = \sigma_1(\mathbf{A}), \tag{8.81}$$

in which, $\sigma_1(\mathbf{A})$ is the largest singular value of $\mathbf{A}$. For any matrix, there is $cond(\mathbf{A}) \geq 1$. A well conditioned matrix has a condition number of order unity. A bigger condition number generally means a more ill-conditioned matrix. From (8.80-8.81), $cond(\mathbf{A})$ can be calculated as

$$cond(\mathbf{A}) = \frac{\sigma_1(\mathbf{A})}{\sigma_p(\mathbf{A})}, \tag{8.82}$$

where $\sigma_p(\mathbf{A})$ is the smallest singular value of $\mathbf{A}$. We can use the algorithm of singular value decomposition for the calculation of $\sigma_1(\mathbf{A})$ and $\sigma_p(\mathbf{A})$.

8.3.2 Step two: solving field variables

In the second step, we modify (8.64) as

$$\mathbf{A} = \begin{bmatrix} \sigma & \sigma\alpha & 0 & 0 \\ X\sigma\alpha & X\sigma\alpha^2 + \kappa & 0 & 0 \\ 0 & 0 & \sigma & \sigma\alpha \\ \sigma\alpha & \sigma\alpha^2 & 0 & \kappa \end{bmatrix}, \quad \mathbf{u} = \begin{bmatrix} N_1^{(1)} \\ M_1^{(1)} \\ \widetilde{N}_1^{(3)} \\ M_1^{(3)} \end{bmatrix}. \tag{8.83}$$

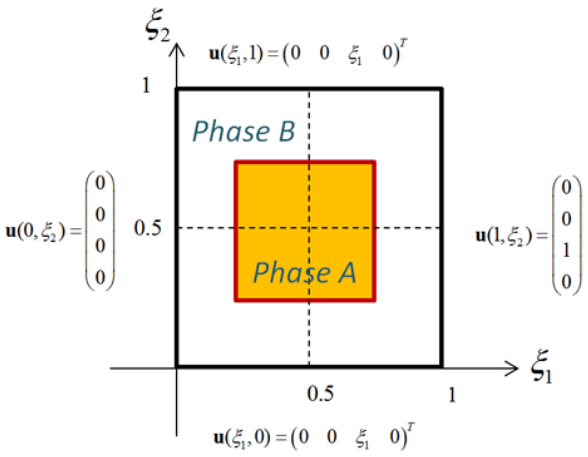

Figure 8.3: An example of a unit cell problem defined on the full unit cell.

Essentially, we removed the fourth row of (8.64) to make $\mathbf{A}$ as a square matrix. The value of X calculated in the first step is used here. So the Finite Element method can be applied to the problem represented by (8.66), see Figure 8.3. It is expected in the overall linear system of the problem

$$\mathbf{K}^a\mathbf{u}^a = \mathbf{P}^a, \tag{8.84}$$

there is $|\mathbf{K}^a| = 0$, because of the way we have chosen X in step one. We then extend (8.84) to get

$$\begin{bmatrix} \mathbf{K}^a \\ \mathbf{K}^a_{int} \end{bmatrix} \mathbf{u}^a = \begin{bmatrix} \mathbf{P}^a \\ \mathbf{P}^a_{int} \end{bmatrix}, \tag{8.85}$$

where $\mathbf{K}^a_{int}\mathbf{u}^a = \mathbf{P}^a_{int}$ are equations derived using the interface condition (8.74). The inclusion of these interface condition equations would make the problem complete, and $\mathbf{u}^a$ solvable from (8.85). Note that in (8.85), we have more equations than variables. For the solution of such over-determined system, we would need the least square method to minimize the sum of the squares of the errors made in the results of every single equations.

Depending on the structure of the unit cell, the problem of (8.66) can be reduced to simpler problems. Suppose the unit cell has symmetry in the structure similar to Figure 8.3, we can simply do a translation on the coordinate system to get Figure 8.4(a), where the

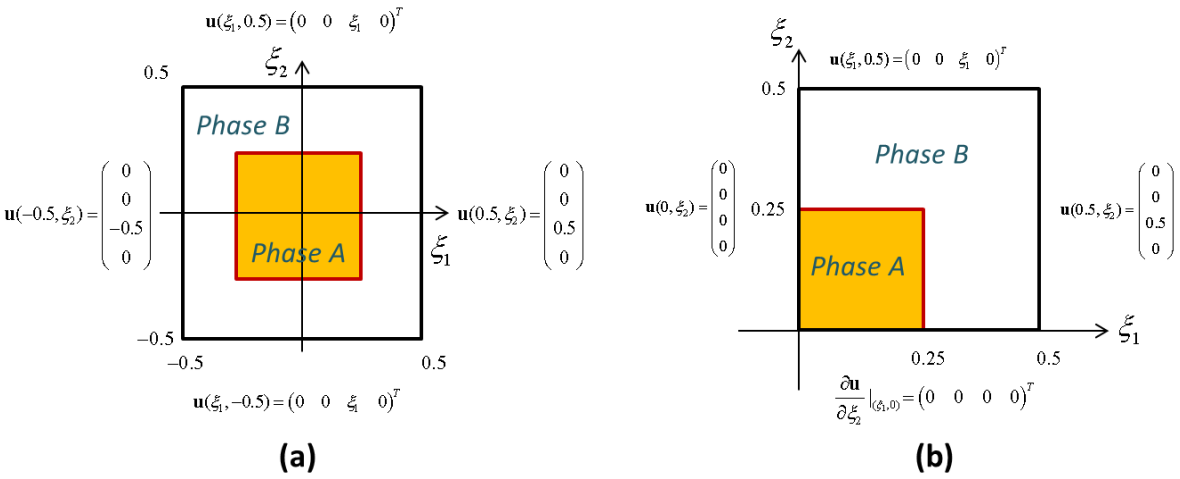

Figure 8.4: An example of a unit cell problem defined on (a) a full unit cell which is symmetric in structure and has the coordinate system offset to its center, and equivalently on (b) a quarter of the unit cell due to the symmetry of the system.

coordinate system is offset to the center of the unit cell. From the symmetry in the system, we can conclude that the field $\mathbf{u}$ is symmetric with respect to ξ_1 axis, and anti-symmetric with respect to ξ_2 axis. Thus, we can replace the original problem by an equivalent problem on a quarter of the domain. For example, we can use the upper right quarter of the domain, and re-define the problem as

$$\begin{cases} \frac{\partial}{\partial \xi_i}(\mathbf{A}\frac{\partial \mathbf{u}}{\partial \xi_i}) = \mathbf{0}, \quad \boldsymbol{\xi} \in \Omega, \\ [\mathbf{u}]|_\Sigma = \mathbf{0}, \quad [\mathbf{A}\frac{\partial \mathbf{u}}{\partial \xi_i} n_i]|_\Sigma = \mathbf{0}, \\ \mathbf{u}(0, \xi_2) = \begin{bmatrix} 0 & 0 & 0 & 0 \end{bmatrix}^T, \\ \mathbf{u}(0.5, \xi_2) = \begin{bmatrix} 0 & 0 & 0.5 & 0 \end{bmatrix}^T, \\ \frac{\partial \mathbf{u}}{\partial \xi_2}|_{(\xi_1, 0)} = \begin{bmatrix} 0 & 0 & 0 & 0 \end{bmatrix}^T, \\ \mathbf{u}(\xi_1, 0.5) = \begin{bmatrix} 0 & 0 & \xi_1 & 0 \end{bmatrix}^T, \end{cases} \tag{8.86}$$

see Figure 8.4(b).

8.3.3 Modification on step one

We have described the way of solving equation of (8.78) to find X in a somewhat simplified fashion. There is actually more intricacy such as whether the X that satisfies (8.78) is unique, and how to determine the correct X if it is not. To fully understand it, we return to (8.75). This time, by exposing X, we get

$$\mathbf{K}^a\mathbf{u}^a = (\mathbf{K}_1^a + X\mathbf{K}_2^a)\mathbf{u}^a = \mathbf{0}, \tag{8.87}$$

as the overall linear system of the problem. Since the idea is to find X that makes

$$|\mathbf{K}_1^a + X\mathbf{K}_2^a| = 0, \tag{8.88}$$

this is actually equivalent to the generalized eigenvalue problem

$$\mathbf{K}_1^a\mathbf{x} = -X\mathbf{K}_2^a\mathbf{x}, \tag{8.89}$$

where $\mathbf{K}_1^a$ and $\mathbf{K}_2^a$ are matrices, $-X$ and $\mathbf{x}$ are eigenvalue and eigenvector that make the equation hold. For such a generalized eigenvalue problem, we know that there are n eigenvalues (including duplicates) in total, given that $\mathbf{K}_1^a$ and $\mathbf{K}_2^a$ are $n \times n$ matrices. (8.89) can be transformed into

$$\mathbf{K}_2^a\mathbf{x} = -X^{-1}\mathbf{K}_1^a\mathbf{x}. \tag{8.90}$$

These two forms are equivalent theoretically, however, numerically one form may be more favorable than the other in terms of convergence of the results.

As part of the guess of the expression of $\mathbf{v}^{(1)}$, see equations (7.26-7.27), our Existence and Uniqueness theorem requires the correct X should be unique. Imaginably, wrong pick of X, after plugging in (8.83), would make (8.84) unsolvable (we are relaxing ourself by assuming that (8.84) is a complete system). But again, because we use least square method to solve the over-determined system of (8.85), no matter what choice of X, least square method will always converge at a result. The best we can do is to compare the residual

$$\mathbf{R} = \begin{bmatrix} \mathbf{P}^a \\ \mathbf{P}_{int}^a \end{bmatrix} - \begin{bmatrix} \mathbf{K}^a \\ \mathbf{K}_{int}^a \end{bmatrix} \mathbf{u}^a. \tag{8.91}$$

Conceptually, out of all the plausible X, the correct choice should result in the minimum residual, quantified by comparing the norms of vector $\mathbf{R}$.

8.3.4 Normalization of values

In numerical calculations, it is sometimes beneficial to normalize the parameters. For example, instead of α, we may want to use the normalized value of $\widehat{\alpha} = \frac{\alpha}{\dot{\alpha}}$, where $\dot{\alpha}$ is characteristic value of α. To put forward a proper scheme for keeping track of the normalized values and units, we need to look into the governing equations. We first look at equation (7.34), which, using normalized values, becomes

$$\frac{\partial}{\partial \xi_i}[\widehat{\sigma}\dot{\sigma}\frac{\partial(N_j^{(3)}+\xi_j)}{\partial \xi_i} + \widehat{\sigma}\dot{\sigma}\widehat{\alpha}\dot{\alpha}\frac{\partial M_j^{(3)}}{\partial \xi_i}] = 0. \tag{8.92}$$

(7.34) is special because $N_j^{(3)} + \xi_j$ is dimensionless and thus cannot be altered. As such, the normalized version of (7.34) must be

$$\frac{\partial}{\partial \xi_i}[\widehat{\sigma}\frac{\partial(\widehat{N}_j^{(3)}+\xi_j)}{\partial \xi_i} + \widehat{\sigma}\widehat{\alpha}\frac{\partial \widehat{M}_j^{(3)}}{\partial \xi_i}] = 0, \tag{8.93}$$

where

$$\widehat{N}_j^{(3)} = N_j^{(3)}, \tag{8.94}$$

$$\widehat{M}_j^{(3)} = \dot{\alpha} M_j^{(3)}, \tag{8.95}$$

are normalized field variables. The normalization of (7.32), (7.35), (7.28) are carried out with respect to (8.93)

$$\frac{\partial}{\partial \xi_i}[\widehat{\sigma}\widehat{\alpha}\frac{\partial(\widehat{N}_j^{(3)}+\xi_j)}{\partial \xi_i} + \widehat{\sigma}\widehat{\alpha}^2\frac{\partial \widehat{M}_j^{(3)}}{\partial \xi_i}] = 0, \tag{8.96}$$

$$\frac{\partial}{\partial \xi_i}[\widehat{\sigma}\widehat{\alpha}\frac{\partial \widehat{N}_j^{(1)}}{\partial \xi_i} + \widehat{\sigma}\widehat{\alpha}^2\frac{\partial \widehat{M}_j^{(1)}}{\partial \xi_i} + \widehat{\kappa}\frac{\partial \widehat{M}_j^{(3)}}{\partial \xi_i}] = 0, \tag{8.97}$$

$$\frac{\partial}{\partial \xi_i}[\widehat{\sigma}\frac{\partial \widehat{N}_j^{(1)}}{\partial \xi_i} + \widehat{\sigma}\widehat{\alpha}\frac{\partial \widehat{M}_j^{(1)}}{\partial \xi_i}] = 0, \tag{8.98}$$

where

$$\widehat{N}_j^{(1)} = \frac{\dot{\sigma}\dot{\alpha}^2}{\dot{\kappa}} N_j^{(1)}, \tag{8.99}$$

$$\widehat{M}_j^{(1)} = \frac{\dot{\sigma}\dot{\alpha}^3}{\dot{\kappa}} M_j^{(1)}. \tag{8.100}$$

From (7.29), we get

$$\frac{\partial}{\partial \xi_i}[\widehat{X}\widehat{\sigma}\widehat{\alpha}\frac{\partial(\dot{X}\dot{\sigma}\dot{\alpha}N_j^{(1)})}{\partial \xi_i} + \widehat{X}\widehat{\sigma}\widehat{\alpha}^2\frac{\partial(\dot{X}\dot{\sigma}\dot{\alpha}^2 M_j^{(1)})}{\partial \xi_i} + \widehat{\kappa}\frac{\partial(\dot{\kappa}M_j^{(1)})}{\partial \xi_i}] = 0, \tag{8.101}$$

where $\dot{X}\dot{\sigma}\dot{\alpha}^2 M_j^{(1)}$ and $\dot{\kappa}M_j^{(1)}$ must be the same value, thus we have

$$\dot{X} = \frac{\dot{\kappa}}{\dot{\sigma}\dot{\alpha}^2}, \tag{8.102}$$

and we obtain the normalized (7.29)

$$\frac{\partial}{\partial \xi_i}[\widehat{X}\widehat{\sigma}\widehat{\alpha}\frac{\partial \widehat{N}_j^{(1)}}{\partial \xi_i} + (\widehat{X}\widehat{\sigma}\widehat{\alpha}^2 + \widehat{\kappa})\frac{\partial \widehat{M}_j^{(1)}}{\partial \xi_i}] = 0. \tag{8.103}$$

By the same token, we can immediately find the normalized version of (7.30-7.31), (7.33), (7.36-7.37) as

$$\frac{\partial}{\partial \xi_i}[\widehat{\sigma}\frac{\partial \widehat{N}_j^{(2)}}{\partial \xi_i} + \widehat{\sigma}\widehat{\alpha}\frac{\partial \widehat{M}_j^{(2)}}{\partial \xi_i}] = 0, \tag{8.104}$$

$$\frac{\partial}{\partial \xi_i}[\widehat{X}\widehat{\sigma}\widehat{\alpha}\frac{\partial \widehat{N}_j^{(2)}}{\partial \xi_i} + (\widehat{X}\widehat{\sigma}\widehat{\alpha}^2 + \widehat{\kappa})\frac{\partial \widehat{M}_j^{(2)}}{\partial \xi_i}] = 0, \tag{8.105}$$

$$\frac{\partial}{\partial \xi_i}[\widehat{\sigma}\widehat{\alpha}\frac{\partial \widehat{N}_j^{(4)}}{\partial \xi_i} + \widehat{\sigma}\widehat{\alpha}^2\frac{\partial (\widehat{M}_j^{(4)} + \xi_j)}{\partial \xi_i}] = 0, \tag{8.106}$$

$$\frac{\partial}{\partial \xi_i}[\widehat{\sigma}\frac{\partial \widehat{N}_j^{(4)}}{\partial \xi_i} + \widehat{\sigma}\widehat{\alpha}\frac{\partial (\widehat{M}_j^{(4)} + \xi_j)}{\partial \xi_i}] = 0, \tag{8.107}$$

$$\frac{\partial}{\partial \xi_i}[\widehat{\sigma}\widehat{\alpha}\frac{\partial \widehat{N}_j^{(2)}}{\partial \xi_i} + \widehat{\sigma}\widehat{\alpha}^2\frac{\partial \widehat{M}_j^{(2)}}{\partial \xi_i} + \widehat{\kappa}\frac{\partial (\widehat{M}_j^{(4)} + \xi_j)}{\partial \xi_i}] = 0, \tag{8.108}$$

where

$$\widehat{N}_j^{(2)} = \frac{\dot{\sigma}\dot{\alpha}}{\dot{\kappa}}N_j^{(2)}, \tag{8.109}$$

$$\widehat{M}_j^{(2)} = \frac{\dot{\sigma}\dot{\alpha}^2}{\dot{\kappa}}M_j^{(2)}, \tag{8.110}$$

$$\widehat{N}_j^{(4)} = \frac{1}{\dot{\alpha}}N_j^{(4)}, \tag{8.111}$$

$$\widehat{M}_j^{(4)} = M_j^{(4)}. \tag{8.112}$$

So when we use the normalized version of governing equations (8.93), (8.96-8.98), (8.103-8.108) for solving the problem, after obtaining the normalized field variable, we turn to (8.94-8.95), (8.99-8.100), (8.109-8.112) to transform them to the real field values.

8.4 Numerical results

Instead of a square, our simulation is mostly carried out using a polygon as phase A, see Figure 8.5, the main reason is that we tend to have singularity at the sharp angles. For

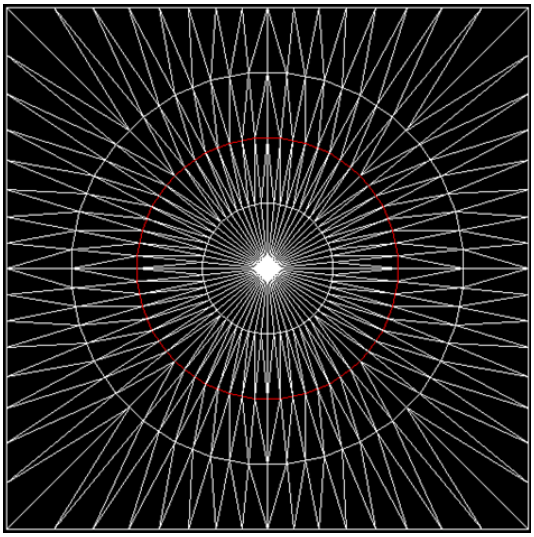

Figure 8.5: An example of mesh structure for unit cell with polygon as phase A. The red lines mark the interface between phases A and B.

that reason, fillets are preferred to sharp angles. Also fine mesh at angles is more favorable for increased accuracy. The phase A polygon is a regular polygon with 32 sides and 32 vertices. We can change the relative size of phase A with the unit cell to have different volume fraction of phase A. We use $Ag(Pb_{1-y}Sn_y)_mSbTe_{2+m}$ as phase A and Bi_2Te_3 as phase B, with their thermoelectric properties tabulated in Table 3.1.

8.4.1 Verification with 1D analytical results

Table 8.1: Numerically calculated values of X ($\times 10^4 K$) for different unit cell structures. For polygons, the number in brackets denotes its volume fraction of phase A.

1D laminar	polygon (0.126)	polygon (0.197)	polygon (0.284)
-2.638	-3.272	-3.527	-4.056

Calculation is first carried out on a unit cell problem with 1D laminar structure as show

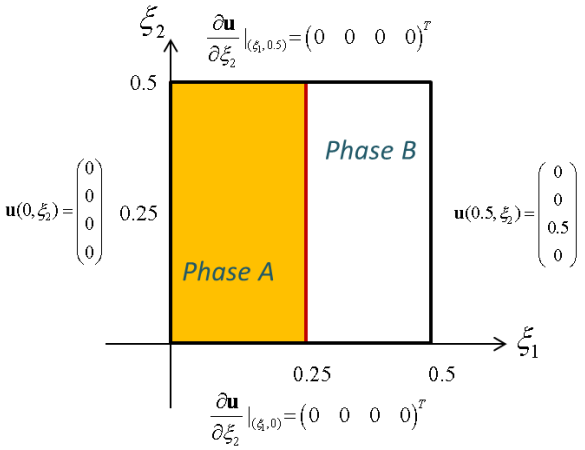

Figure 8.6: The unit cell problem with 1D domain structure, symmetry is present so that only a quarter of the domain is considered.

in Fig. 8.6, for the purpose of verification because analytical results are available for such 1D problem. Note on lateral boundaries, Neumann type of boundary condition is applied. Calculation of X shows an error of as small as 10^{-7}, compared with analytical value by (7.48). The exact value of X can be found in Table 8.1. Through Finite Element method, $N_1^{(1)}$, $M_1^{(1)}$, $N_1^{(3)}$, $M_1^{(3)}$, (and $N_1^{(2)}$, $M_1^{(2)}$, $N_1^{(4)}$, $M_1^{(4)}$ by grouping their corresponding governing equations and boundary conditions) are calculated, and the error compared with analytical result (7.40-7.47) can be evaluated. Due to the similarity of the results, only a figure of $N_1^{(1)}$ is included, see Figure 8.7. With field variables solved, we can also calculate the effective properties through (7.153-7.164). Table 8.2 lists all the effective properties, both numerically and analytically obtained. By comparing all the numerical and analytical results, we can conclude that our Finite Element method is sufficiently accurate.

8.4.2 Values of X

We now turn to the problem of unit cell with polygon phase A. As described earlier, the X value that make matrix $\mathbf{K}^a$ singular is not unique, but the right X should make the system have the smallest residual $\mathbf{R}$, and we use norms for the purpose of comparison. For all the calculation carried out, it is observed that all of one-norm, two-norm, infinity-norm

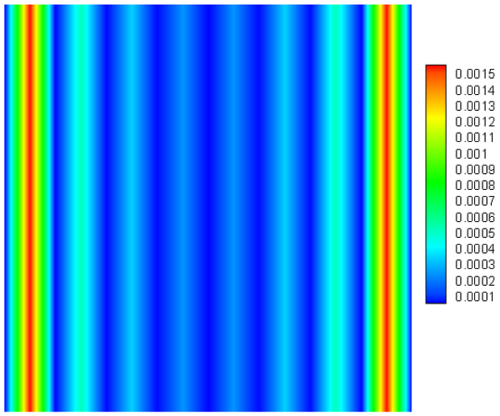

Figure 8.7: The error of numerical $N_1^{(1)}$ value compared with analytical result, for the calculation of 1D laminar unit cell. The error results of $N_1^{(2)}$, $N_1^{(3)}$, $N_1^{(4)}$, $M_1^{(1)}$, $M_1^{(2)}$, $M_1^{(3)}$, $M_1^{(4)}$ are similar to this, and are not reproduced. The maximum error for all field variables are around 0.16%.

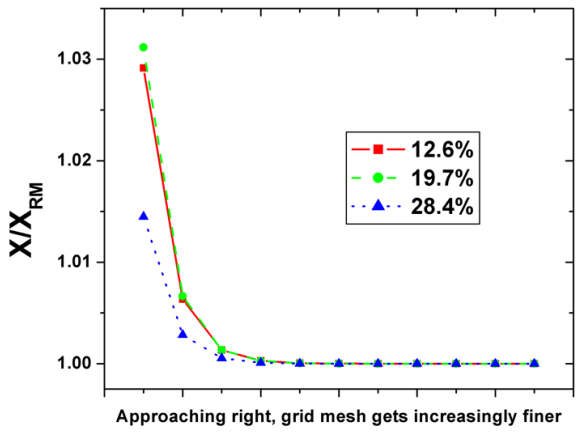

Figure 8.8: The X value calculated for polygon unit cell structure, for volume fraction of 12.6%, 19.7%, 28.4%. As the mesh grid gets finer, X converges. X is normalized with the right-most value X_{RM}.

Table 8.2: Effective properties for 1D unit cell structure, both Finite Element method results and analytical results are included.

	$G^{(1)}(\times 10^8 KS/m)$	$H^{(1)}(\times 10^5 W/m/V)$	$K^{(1)}(\times 10^8 WK/m/V)$
Numeric	9.67	2.27	-3.13
Analytic	9.67	2.27	-3.13
	$G^{(3)}(S/m)$	$H^{(3)}(W/m/V/K)$	$K^{(3)}(\times 10^4 W/m/V)$
Numeric	4.8×10^{-13}	7.4×10^{-13}	1.19
Analytic	0.0	0.0	1.19
	$G^{(2)}(\times 10^5 W/m/V)$	$H^{(2)}(W/m/K)$	$K^{(2)}(\times 10^4 W/m)$
Numeric	2.39	56.2	-7.73
Analytic	2.39	56.2	-7.73
	$G^{(4)}(W/m/V/K)$	$H^{(4)}(W/m/K^2)$	$K^{(4)}(W/m/K)$
Numeric	-3.2×10^{-12}	-6.9×10^{-12}	3.97
Analytic	0.0	0.0	3.97

consistently point to a value of X as having the smallest residual. As we use increasingly finer mesh, this X converges satisfactorily, as can be seen in Figure 8.8. The value X_{RM} for the finest mesh can be found in Table 8.1 for different volume fractions.

8.4.3 Distributions of field variables

Use the X value obtained in step one, the field variables are calculated by solving unit cell problem. Figures 8.9-8.10 show the field result for a general 2D unit cell problem with volume fraction of 19.7%. For pseudo 2D problem, the result is in Figures 8.11-8.12. Note only the top-right quarter of the unit cell is shown, due to symmetry, the bottom half is symmetric to the top, and the left half is anti-symmetric to the right. All fields in both figures have zero values on the left and right boundaries. Compared with general 2D, the boundary constraint on pseudo 2D is less strict as there could be non-zero value on the

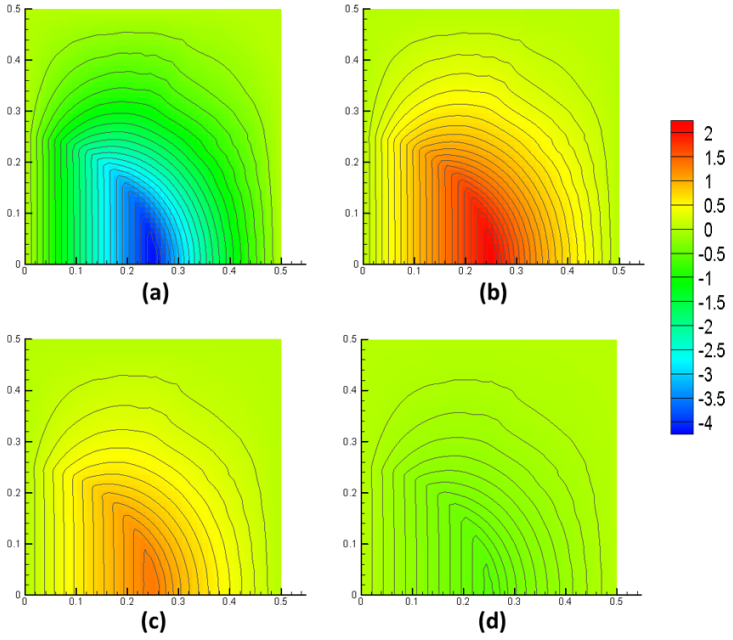

Figure 8.9: The field distributions for (a) $N_1^{(1)}$, (b) $M_1^{(1)}$, (c) $N_1^{(3)}$, (d) $M_1^{(3)}$ for a general 2D calculation with volume fraction of 19.7%. Due to symmetry, only a quarter of the unit cell is shown. Values are normalized, and should take the unit of 10^4K for $N_1^{(1)}$, $10^8K^2/V$ for $M_1^{(1)}$, 1 for $N_1^{(3)}$, $10^4K/V$ for $M_1^{(3)}$.

top boundary, which can be observed in the pseudo 2D result. The field results are for subscription of $j = 1$, the results for $j = 2$ are obtained by exchanging the coordinate axes of ξ_1 and ξ_2.

8.4.4 Effective properties

With field variables solved, we use (7.88-7.91), (7.94-7.101) to evaluate the effective properties. Figure 8.13 shows, as we use increasingly finer mesh, there is convergence in the values of the effective properties. We carried out calculation for general 2D case for volume fraction of 12.6%, 19.7%, 28.4%, the effective properties results are organized in Table 8.3. The similar results for pseudo 2D are also obtained in Table 8.4. Note due to symmetry, there is, for example, $G_{ij}^{(1)} = G^{(1)}\delta_{ij}$ for $G_{ij}^{(1)}$. So only moduli such as $G^{(1)}$ need to be

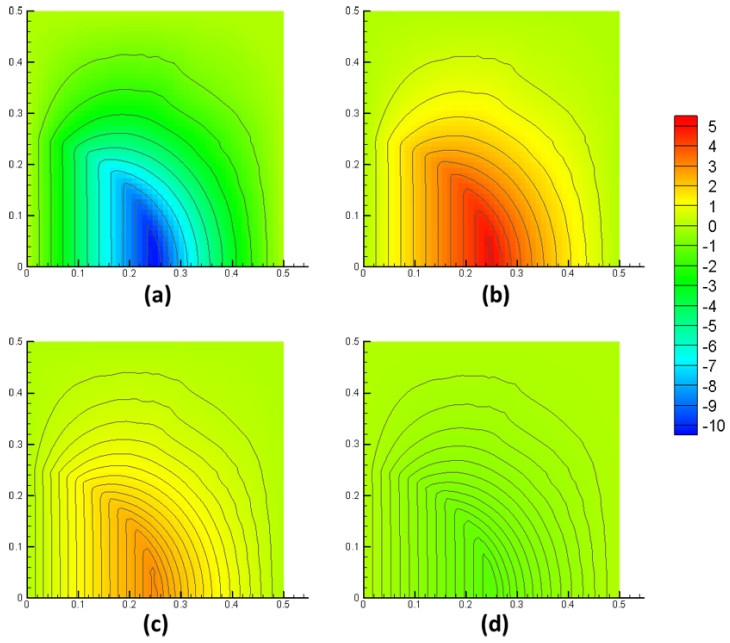

Figure 8.10: The field distributions for (a) $N_1^{(2)}$, (b) $M_1^{(2)}$, (c) $N_1^{(4)}$, (d) $M_1^{(4)}$ for a general 2D calculation with volume fraction of 19.7%. Due to symmetry, only a quarter of the unit cell is shown. Values are normalized, and should take the unit of $1V$ for $N_1^{(2)}$, 10^4K for $M_1^{(2)}$, $10^{-4}V/K$ for $N_1^{(4)}$, 1 for $M_1^{(4)}$.

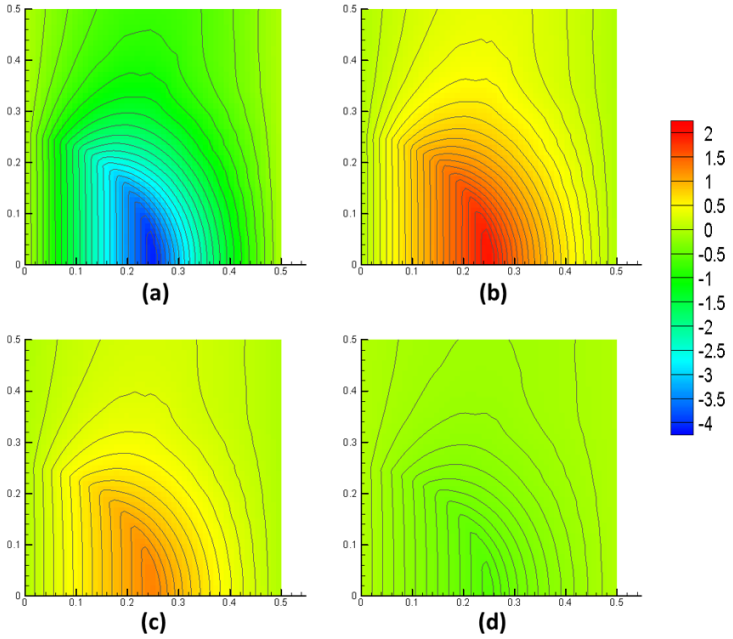

Figure 8.11: The field distributions for (a) $N_1^{(1)}$, (b) $M_1^{(1)}$, (c) $N_1^{(3)}$, (d) $M_1^{(3)}$ for a pseudo 2D calculation with volume fraction of 19.7%. Due to symmetry, only a quarter of the unit cell is shown. Values are normalized, and should take the unit of 10^4K for $N_1^{(1)}$, $10^8K^2/V$ for $M_1^{(1)}$, 1 for $N_1^{(3)}$, $10^4K/V$ for $M_1^{(3)}$.

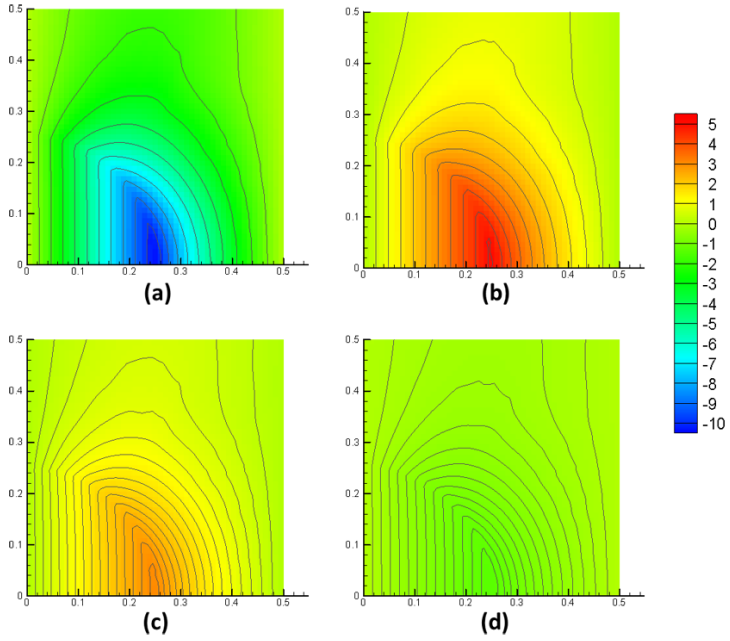

Figure 8.12: The field distributions for (a) $N_1^{(2)}$, (b) $M_1^{(2)}$, (c) $N_1^{(4)}$, (d) $M_1^{(4)}$ for a pseudo 2D calculation with volume fraction of 19.7%. Due to symmetry, only a quarter of the unit cell is shown. Values are normalized, and should take the unit of $1V$ for $N_1^{(2)}$, 10^4K for $M_1^{(2)}$, $10^{-4}V/K$ for $N_1^{(4)}$, 1 for $M_1^{(4)}$.

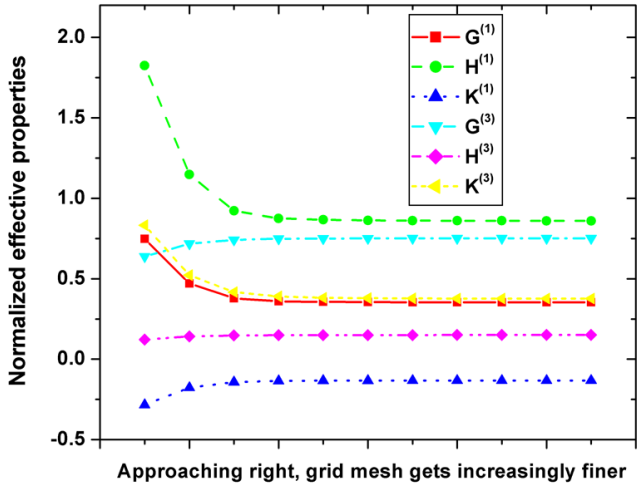

Figure 8.13: The effective properties calculated for polygon unit cell structure, for general 2D calculation and volume fraction of 19.7%. As the mesh grid gets finer, effective properties converge. Effective properties are normalized, and should take the unit of $10^9 KS/m$ for $G^{(1)}$, $10^5 W/m/V$ for $H^{(1)}$, $10^9 WK/m/V$ for $K^{(1)}$, $10^5 S/m$ for $G^{(3)}$, $10^2 W/m/V/K$ for $H^{(3)}$, $10^4 W/m/V$ for $K^{(3)}$.

considered.

8.5 Summary

In this chapter, the unit cell problems derived in the previous chapter for 2D asymptotic analysis of thermoelectric composites are solved numerically by Finite Element method. With the satisfactory convergence of the results of the field variables, the 2D homogenized thermoelectric governing equation is validated, with its effective properties determined.

Table 8.3: Effective properties for polygon unit cell structure and general 2D calculation, for volume fractions of 12.6%, 19.7%, 28.4%.

	$G^{(1)}(\times 10^8 KS/m)$	$H^{(1)}(\times 10^5 W/m/V)$	$K^{(1)}(\times 10^8 WK/m/V)$
12.6%	2.26	0.547	-0.822
19.7%	3.53	0.860	-1.33
28.4%	5.17	1.28	-2.04
	$G^{(3)}(\times 10^4 S/m)$	$H^{(3)}(W/m/V/K)$	$K^{(3)}(\times 10^4 W/m/V)$
12.6%	8.67	17.3	0.252
19.7%	7.52	15.0	0.377
28.4%	6.33	12.7	0.506
	$G^{(2)}(\times 10^5 W/m/V)$	$H^{(2)}(W/m/K)$	$K^{(2)}(\times 10^4 W/m)$
12.6%	0.572	13.8	-2.08
19.7%	0.897	21.8	-3.37
28.4%	1.33	32.7	-5.24
	$G^{(4)}(W/m/V/K)$	$H^{(4)}(\times 10^{-4} W/m/K^2)$	$K^{(4)}(W/m/K)$
12.6%	17.3	34.7	2.10
19.7%	15.0	30.1	2.35
28.4%	12.7	25.3	2.61

Table 8.4: Effective properties for polygon unit cell structure and pseudo 2D calculation, for volume fractions of 12.6%, 19.7%, 28.4%.

	$G^{(1)}(\times 10^8 KS/m)$	$H^{(1)}(\times 10^5 W/m/V)$	$K^{(1)}(\times 10^8 WK/m/V)$
12.6%	2.30	0.554	-0.825
19.7%	3.59	0.871	-1.33
28.4%	5.24	1.29	-2.03
	$G^{(3)}(\times 10^4 S/m)$	$H^{(3)}(W/m/V/K)$	$K^{(3)}(\times 10^4 W/m/V)$
12.6%	8.63	17.3	0.256
19.7%	7.45	14.9	0.385
28.4%	6.20	12.4	0.520
	$G^{(2)}(\times 10^5 W/m/V)$	$H^{(2)}(W/m/K)$	$K^{(2)}(\times 10^4 W/m)$
12.6%	0.580	14.0	-2.08
19.7%	0.910	22.1	-3.36
28.4%	1.34	32.9	-5.18
	$G^{(4)}(W/m/V/K)$	$H^{(4)}(\times 10^{-4} W/m/K^2)$	$K^{(4)}(W/m/K)$
12.6%	17.3	34.5	2.11
19.7%	14.9	29.8	2.37
28.4%	12.4	24.8	2.64

Chapter 9

CONCLUSIONS AND FUTURE WORKS

9.1 Conclusions

We have developed in Chapter 3 a rigorous 1D analysis of bi-layered thermoelectric composite. From the established effective thermoelectric properties through equivalency principle, an enhanced thermoelectric figure of merit of layered medium is achieved, demonstrating that in the absence of size and interfacial effects, higher figure of merit of thermoelectric composite than any of its constituents is indeed possible.

Through the analysis and calculations in Chapter 4, we conclude that (1) thermoelectric figure of merit ZT as we know it is ill-defined for layered thermoelectrics, and is irrelevant to their conversion efficiency; (2) thermoelectric conversion efficiency of a composite is not bounded by its constituents, and can be higher than all its constituents; and (3) requirements on constituent phases for enhanced conversion efficiency in layered composites are identified, and the upper bound on their conversion efficiency is established. This thus points to a new route for high efficiency thermoelectric materials that does not rely on either size or interfacial effects.

Motivated by the potential application in automobile waste heat recovery, we carried out an analysis on axially-symmetric thermoelectric problem in Chapter 5. We show that higher thermoelectric conversion efficiency can be achieved in core-shell composites, while the effective figure of merit is not well defined.

We developed a non-linear asymptotic homogenization theory for studying thermoelectric composite with periodic microstructure in 1D in Chapter 6, and in 2D in Chapter 7. In Chapter 6, the 1D homogenized governing equations of macroscopic temperature and potential distribution smeared out of microscopic fluctuation are established and solved with temperature and potential boundary condition. The macroscopic field distributions are observed to be drastically different from those in homogeneous materials. With an idealized

thermoelectric module, we analyzed the overall conversion efficiency, and showed that the effective thermoelectric figure of merit does not directly correlate with the thermoelectric conversion efficiency. In Chapter 7, we applied asymptotic homogenization method to establish the unit cell problem for both 2D and 3D. The unit cell problem is later solved by using 2D Finite Element method. The obtained 2D homogenized governing equations of macroscopic temperature and potential distribution are significantly more complex compared with 1D homogenized equations, and their effective properties are evaluated from the results of unit cell problem.

9.2 Future works

Our asymptotic analysis shows drastically different governing equations and functional distribution of thermoelectric fields in the composite from those of homogenous materials, and thus provides us with a new route to optimize the conversion efficiency of thermoelectric materials, especially for those with 2D or 3D micro-structures.

We have demonstrated a Finite Element method for solving 2D unit cell problem for asymptotic analysis. This method can be extended to 3D in a straightforward way. The 3D asymptotic analysis will provide with us more insight into the effective behavior of thermoelectric composites for their design and optimization.

BIBLIOGRAPHY

[1] F. J. DiSalvo, Science **285**, 703 (1999).

[2] T. C. Harman and J. M. Honig, 1967. Thermoelectric and thermomagnetic effects and applications, McGraw-Hill, New York.

[3] T. M. Tritt, H. Boettner, and L. Chen, MRS Bulletin **33**, 366 (2008).

[4] J. H. Yang, and T. Caillat, MRS Bulletin **31**, 224 (2006).

[5] D. Narducci, Appl. Phys. Lett. **99**, 102104 (2011).

[6] T. M. Tritt, and M. A. Subramanian, MRS Bulletin **31**, 188 (2006).

[7] D. Kraemer, B. Poudel, H. P. Feng, J. C. Caylor, B. Yu, X. Yan, Y. Ma, X. W. Wang, D. Z. Wang, A. Muto, K. McEnaney, M. Chiesa, Z. F. Ren, and G. Chen, Nature Materials **10**, 532 (2011).

[8] H. X. Xi, L. G. Luo, and G. Fraisse, Renewable and Sustainable Energy Reviews **11**, 923-936 (2007).

[9] Y. Vorobiev, J. Gonzalez-Hernandez, P. Vorobiev, and L. Bulat, Solar Energy **80**, 170-176 (2006).

[10] L. E. Bell, Science **321**, 1457 (2008).

[11] S. B. Riffat, S. A. Omer, and X. Ma, Renewable Energy **23**, 313-323 (2001).

[12] J. F. Li, W. S. Liu, L. D. Zhao, and M. Zhou, Npg Asia Materials **2**, 152-158 (2010).

[13] P. Pichanusakorn, and P. Bandaru, Materials Science and Engineering R-Reports **67**, 19-63 (2010).

[14] K. Koumoto, Y. F. Wang, R. Z. Zhang, A. Kosuga, and R. Funahashi, Annual Review of Materials Research **40**, 363-394 (2010).

[15] T. M. Tritt, and M. A. Subramanian, MRS Bulletin **31**, 188-229 (2006).

[16] K. Koumoto, I. Terasaki, and R. Funahashi, MRS Bulletin **31**, 206-210 (2006).

[17] G. J. Snyder, and E. S. Toberer, Nature Materials **7**, 105-114 (2008).

[18] G. S. Nolas, D. T. Morelli, and T. M. Tritt, Annual Review of Materials Science **29**, 89 (1999).

[19] Q. Yao, L. D. Chen, W. Q. Zhang, S. C. Liufu, and X. H. Chen, Acs Nano **4**, 2445-2451 (2010).

[20] X. B. Zhao, S. H. Hu, M. J. Zhao, and T. J. Zhu, Materials Letters **52**, 147-149 (2002).

[21] N. Toshima, M. Imai, and S. Ichikawa, Journal of Electronic Materials **40**, 898-902 (2011).

[22] A. M. Rao, X. H. Ji, and T. M. Tritt, Mrs Bulletin **31**, 218-223 (2006).

[23] S. N. Girard, J. Q. He, X. Y. Zhou, D. Shoemaker, C. M. Jaworski, C. Uher, V. P. Dravid, J. P. Heremans, and M. G. Kanatzidis, Journal of the American Chemical Society **133**, 16588-16597 (2011).

[24] A. Shakouri, Annual Review of Materials Research **41**, 399-431 (2011).

[25] J. Y. Tang, H. T. Wang, D. H. Lee, M. Fardy, Z. Y. Huo, T. P. Russell, and P. D. Yang, Nano Letters **10**, 4279-4283 (2010).

[26] K. C. See, J. P. Feser, C. E. Chen, A. Majumdar, J. J. Urban, and R. A. Segalman, Nano Letters **10**, 4664-4667 (2010).

[27] Y. Q. Cao, X. B. Zhao, T. J. Zhu, X. B. Zhang, and J. P. Tu, Applied Physics Letters **92**, 143106 (2008).

[28] J. S. Son, M. K. Choi, M. K. Han, K. Park, J. Y. Kim, S. J. Lim, M. Oh, Y. Kuk, C. Park, S. J. Kim, and T. Hyeon, Nano Letters **12**, 640-647 (2012).

[29] G. Joshi, H. Lee, Y. C. Lan, X. W. Wang, G. H. Zhu, D. Z. Wang, R. W. Gould, D. C. Cuff, M. Y. Tang, M. S. Dresselhaus, G. Chen, and Z. F. Ren, Nano Letters **8**, 4670-4674 (2008).

[30] A. J. Minnich, M. S. Dresselhaus, Z. F. Ren, and G. Chen, Energy and Environmental Science **2**, 466-479 (2009).

[31] Y. K. Koh, C. J. Vineis, S. D. Calawa, M. P. Walsh, and D. G. Cahill, Applied Physics Letters **94**, 153101 (2009).

[32] J. P. Heremans, C. M. Thrush, D. T. Morelli, and M. C. Wu, Physical Review Letters **88**, 216801 (2002).

[33] P. F. P. Poudeu, A. Gueguen, C. I. Wu, T. Hogan, and M. G. Kanatzidis, Chemistry of Materials **22**, 1046 (2010).

[34] Y. Z. Pei, J. Lensch-Falk, E. S. Toberer, D. L. Medlin, and G. J. Snyder, Advanced Functional Materials **21**, 241 (2011).

[35] W. J. Xie, X. F. Tang, Y. G. Yan, Q. J. Zhang, and T. M. Tritt, Applied Physics Letters **94**, 102111 (2009).

[36] W. J. Xie, J. He, H. J. Kang, X. F. Tang, S. Zhu, M. Laver, S. Y. Wang, J. R. D. Copley, C. M. Brown, Q. J. Zhang, and T. M. Tritt, Nano Letters **10**, 3283 (2010).

[37] M. Zhou, J. F. Li, and T. Kita, Journal of the American Chemical Society **130**, 4527 (2008).

[38] M. Ohtaki, Journal of the Ceramic Society of Japan **119**, 770-775 (2011).

[39] J. W. Fergus, Journal of the European Ceramic Society **32**, 525-540 (2012).

[40] J. He, Y. F. Liu, and R. Funahashi, Journal of Materials Research **26**, 1762-1772 (2011).

[41] X. Shi, S. Q. Bai, L. L. Xi, J. Yang, W. Q. Zhang, L. D. Chen, and J. H. Yang, Journal of Materials Research **26**, 1745-1754 (2011).

[42] J. Yang, Q. Hao, H. Wang, Y. C. Lan, Q. Y. He, A. Minnich, D. Z. Wang, J. A. Harriman, V. M. Varki, M. S. Dresselhaus, G. Chen, and Z. F. Ren, Physical Review B **80**, 115329 (2009).

[43] Y. Z. Pei, A. F. May, and G. J. Snyder, Advanced Energy Materials **1**, 291-296 (2011).

[44] H. Wang, A. Charoenphakdee, K. Kurosaki, S. Yamanaka, and G. J. Snyder, Physical Review B **83**, 024303 (2011).

[45] K. F. Hsu, S. Loo, F. Guo, W. Chen, J. S. Dyck, C. Uher, T. Hogan, E. K. Polychroniadis, and M. G. Kanatzidis, Science **303**, 818-821 (2004).

[46] B. Poudel, Q. Hao, Y. Ma, Y. C. Lan, A. Minnich, B. Yu, X. A. Yan, D. Z. Wang, A. Muto, D. Vashaee, X. Y. Chen, J. M. Liu, M. S. Dresselhaus, G. Chen, and Z. F. Ren, Science **320**, 634 (2008).

[47] G. H. Zhu, H. Lee, Y. C. Lan, X. W. Wang, G. Joshi, D. Z. Wang, J. Yang, D. Vashaee, H. Guilbert, A. Pillitteri, M. S. Dresselhaus, G. Chen, and Z. F. Ren, Physical Review Letters **102**, 196803 (2009).

[48] H. J. Kim, E. S. Bozin, S. M. Haile, G. J. Snyder, and S. J. L. Billinge, Physical Review B **75**, 134103 (2007).

[49] H. Lin, E. S. Bozin, S. J. L. Billinge, E. Quarez, and M. G. Kanatzidis, Physical Review B **72**, 174113 (2005).

[50] N. Gothard, X. Ji, J. He, and T. M. Tritta, Journal of Applied Physics **103**, 054314 (2008).

[51] L. P. Liu, International Journal of Engineering Science **55**, 35-53 (2012).

[52] F. Hao, D. N. Fang, and J. Y. Li, European Physical Journal-Applied Physics **58**, 58:30901 (2012).

[53] G. D. Mahan, Physical Review B **87**, 045415 (2013).

[54] R. G. Yang, and G. Chen, Physical Review B **69**, 195316 (2004).

[55] A. J. Minnich, H. Lee, X. W. Wang, G. Joshi, M. S. Dresselhaus, Z. F. Ren, G. Chen, and D. Vashaee, Physical Review B **80**, 155327 (2009).

[56] A. Minnich, and G. Chen, Applied Physics Letters **91**, 073105 (2007).

[57] R. G. Yang, G. Chen, and M. S. Dresselhaus, Nano Letters **5**, 1111 (2005).

[58] R. G. Yang, G. Chen, and M. S. Dresselhaus, Physical Review B **72**, 125418 (2005).

[59] R. G. Yang, and G. Chen, Physical Review B **69**, 195316 (2004).

[60] M. Zebarjadi, K. Esfarjani, J. A. Yang, Z. F. Ren, and G. Chen, Physical Review B **82**, 195207 (2010).

[61] J. Zhou, X. B. Li, G. Chen, and R. G. Yang, Physical Review B **82**, 115308 (2010).

[62] F. Yang, T. Ikeda, G. J. Snyder, and C. Dames, Journal of Applied Physics **108**, 034310 (2010).

[63] D. J. Bergman, and O. Levy, Journal of Applied Physics **70**, 6821 (1991).

[64] D. J. Bergman, and L. G. Fel, Journal of Applied Physics **85**, 8205 (1999).

[65] Z. Hashin, and S. Shtrikman, Journal of Applied Physics **33**, 3125 (1962).

[66] I. Webman, J. Jortner, and M. H. Cohen, Physical Review B **16**, 2959 (1977).

[67] J. Martin, T. Tritt, and C. Uher, Journal of Applied Physics **108**, 121101 (2010).

[68] H. B. Callen, 1960. Thermodynamics; an introduction to the physical theories of equilibrium thermostatics and irreversible thermodynamics, Wiley, New York.

[69] G. W. Milton, 2002. The theory of composites, Cambridge University Press.

[70] C. Goupil, W. Seifert, K. Zabrocki, E. Muller, and G. J. Snyder, Entropy **13**, 1481–1517 (2011).

[71] Y. Yang, S. H. Xie, F. Y. Ma, and J. Y. Li, J. Appl. Phys. **111**, 013510 (2012).

[72] E. E. Antonova, and D. C. Looman, Thermoelectrics, 2005. ICT 2005. 24th International Conference on , 215 (2005).

[73] J. Androulakis, K. F. Hsu, R. Pcionek, H. Kong, C. Uher, J. J. DAngelo, A. Downey, T. Hogan, and M. G. Kanatzidis, Advanced Materials **18**, 1170 (2006).

[74] Y. Yang, F. Y. Ma, C. H. Lei, Y. Y. Liu, and J. Y. Li, Appl.Phys. Lett. **102**, 053905 (2013).

[75] G. J. Snyder, and T. S. Ursell, Physical Review Letters **91**, 148301 (2003).

[76] D. M. Rowe, 1995. CRC handbook of thermoelectrics, CRC Press, Dordrecht; Boca Raton.

[77] G. J. Snyder, and T. Caillat, MRS Proceedings **793**, S2.1 (2003).

[78] G. J. Snyder, Applied Physics Letters **84**, 2436-2438 (2004).

[79] B. Sherman, R. R. Heikes, and R. W. Ure, J. Appl. Phys. **31**, 1 (1960).

[80] E. Muller, C. Drasar, J. Schilz, and W. A. Kaysser, Materials Science and Engineering **A362**, 17 (2003).

[81] L. J. Ybarrondo, Solid State Electronics **10**, 620-622 (1967).

[82] W. Seifert, V. Pluschke, C. Goupil, K. Zabrocki, E. Muller, and G. J. Snyder, Journal of Materials Research **26**, 1933-1939 (2011).

[83] W. Seifert, K. Zabrocki, G. J. Snyder, and E. Muller, Phys. Status Solidi A **207**, 760-765 (2010).

[84] Y. Yang, C. F. Gao, and J. Y. Li, Acta Mechanica , 10.1007/s00707-013-1063-3 (2014).

[85] M. Milgrom, and S. Shtrikman, Physical Review A **40**, 1568–1575 (1989).

[86] N. S. Bakhvalov and G. P. Panasenko, 1989. Homogenisation: averaging processes in periodic media : mathematical problems in the mechanics of composite materials, Kluwer Academic Publishers, Dordrecht; Boston.

[87] A. Bensoussan, J. L. Lions and G. Papanicolaou, 1978. Asymptotic analysis for periodic structures, North-Holland Pub. Co. ; sole distributors for the U.S.A. and Canada, Elsevier North-Holland, Amsterdam ; New York New York.

[88] J. F. Bourgat, Computing Methods in Applied Sciences and Engineering, 1977, I Lecture Notes in Mathematics **704**, 330-356 (1979).

[89] A. L. Kalamkarov, E. M. Hassan, A. V. Georgiades, and M. A. Savi, Composite Structures **89**, 186 (2009).

[90] J. Q. Tarn, Journal of the Mechanics and Physics of Solids **45**, 1105–1120 (1997).

[91] N. Triantafyllidis, and S. Bardenhagen, Journal of the Mechanics and Physics of Solids **44**, 1891–1928 (1996).

[92] D. Homentcovschi, and C. Dascalu, Journal of the Mechanics and Physics of Solids **48**, 153–173 (2000).

[93] Y. Yang, F. Y. Ma, C. H. Lei, Y. Y. Liu, and J. Y. Li, Journal of the Mechanics and Physics of Solids **61**, 1768-1783 (2013).

[94] M. Agoras, O. Lopez-Pamies, and P. P. Castaneda, Journal of the Mechanics and Physics of Solids **57**, 1828–1850 (2009).

[95] S. Ghosh, J. Bai, and D. Paquet, Journal of the Mechanics and Physics of Solids **57**, 1017–1044 (2009).

[96] L. C. Evans, 2010. Partial differential equations, American Mathematical Society, Providence.

[97] D. Gilbarg and N. S. Trudinger, 1983. Elliptic partial differential equations of second order, Springer-Verlag; Berlin; New York.

[98] T. Mura, 1982. Micromechanics of defects in solids, M. Nijhoff, Boston.

[99] K. J. Bathe and E. L. Wilson, 1976. Numerical methods in finite element analysis, Prentice-Hall; Englewood Cliffs.

[100] K. J. Bathe, 1982. Finite element procedures in engineering analysis, Prentice-Hall; Englewood Cliffs.

[101] C. S. Desai and J. F. Abel, 1971. Introduction to the finite element method; a numerical method for engineering analysis, Van Nostrand Reinhold Co.; New York.

[102] P. E. Gill, W. Murray and M. H. Wright, 1991. Numerical linear algebra and optimization, Addison-Wesley Pub. Co.; Redwood City.

VITA

Yang Yang was born in Yiyang, China. He received his Bachelor's degree in Engineering Mechanics from Tianjin University, and Master's degree in Engineering Mechanics from Tongji University. In 2014 he earned his Doctor of Philosophy degree at University of Washington in Mechanical Engineering.